ALMA MATER STUDIORUM
UNIVERSITÀ DI BOLOGNA

DEPARTMENT OF PHYSICS AND ASTRONOMY "A. RIGHI"

SECOND CYCLE DEGREE

PHYSICS

Probing Non-Gaussianity in the Stochastic Gravitational Wave Background with PTAs and Ground-Based Interferometers

Supervisor
Prof. Michele Lucente

Co-supervisor
Prof. Gianmassimo Tasinato

Defended by
Maria Lucia Marcelli

Graduation Session March 2026

Academic Year 2024/2025

Abstract

The discovery of gravitational waves (GWs) marked an essential moment in our understanding of the Universe, opening a new era in astronomy.
From the first direct detection to the observation of hundreds of such events, each observation has provided invaluable insights into the strong gravity regime. Yet, the quest to fully explore the GW spectrum is far from over. The next major breakthrough on the horizon is the detection of a stochastic gravitational wave background (SGWB), originating from hums of spacetime arising from a superposition of countless unresolved sources.
While standard searches assume SGWBs to be Gaussian, several early-Universe scenarios predict intrinsically non-Gaussian backgrounds.
In this thesis, we investigate how non-Gaussian signatures of a primordial SGWB manifest in the correlators of present and future gravitational-wave detectors, focusing on Pulsar Timing Arrays (PTAs) and ground-based interferometers.
In particular, we first review the theoretical framework for gravitational waves and stochastic backgrounds and then we study in detail the response of both detector families to a SGWB.
For PTAs, we analyse the Hellings-Downs curve and compute its variance. For ground-based interferometers, we derive the two-point correlation function between detector pairs.
Building on this foundation, we present the original results of this work. We compute for the first time the non-Gaussian contribution to the variance of the Hellings-Downs curve, showing that it carries a measurable imprint of primordial non-Gaussianity.
We further derive the four-point correlation function for four distinct ground-based interferometers interacting with a non-Gaussian SGWB, a quantity that has not previously appeared in the literature.
Our results demonstrate that non-Gaussian signatures of primordial SGWBs leave measurable signatures in detector correlators, opening a new observational window onto early-Universe physics beyond the standard Gaussian paradigm.

Contents

List of Figures

1 Introduction

This is an exciting time for the field of gravitational-wave astronomy. Since the first observation of gravitational waves in September 2015 [1], we have a new way of observing the Universe. The event, designated GW150914 , was observed by the two detectors of the Laser Interferometer Gravitational-Wave Observatory (LIGO). The observed gravitational waves originated from the inspiral and merger of a pair of black holes. This process radiated an astonishing amount of energy and the fact that this event was observed only in gravitational waves illustrates the complementarity and potential for new discoveries that come with the opening of the gravitational-wave window onto the universe.
This event has been the first of numerous gravitational-wave signals that have been observed by the global network of ground-based interferometers.
Gravitational-wave astronomy has expanded remarkably in recent years and not only on account of ground-based interferometers. In fact, by studying Pulsar Timing Arrays (PTAs) as galactic-scale gravitational-wave detectors, global collaborations have recently collected compelling evidence for a gravitational-wave background at nanohertz frequencies.
In 2023, four PTA collaborations (the North American Nanohertz Observatory for Gravitational Waves (NANOGrav) [2], the Parkes Pulsar Timing Array (PPTA)[3], the European Pulsar Timing Array (EPTA) [4] and the Chinese Pulsar Timing Array (CPTA) [5]) simultaneously reported evidence of a common-spectrum process consistent with a stochastic gravitational-wave background (SGWB).
These results therefore mark the first strong evidence for a nanohertz gravitational-wave background and inaugurate a truly multi-frequency gravitational-wave astronomy, spanning many orders of magnitude in frequency.
To date, direct detections of GWs have consisted of coherent measurements of resolved waveforms that can be attributed to individual, compact sources. This class of signals is characterized by a high signal-to-noise ratio [1] and the probability that these detections are due to noise alone is extremely small.
But for every loud event like GW150914, we expect many more quiet events that are too distant to be individually detected, since the associated signal-to-noise ratios are too low.
As an example, take into account the population of stellar-mass binary black holes to which GW150914 belongs: the total rate of merger events from such systems can be estimated to be around ~ 1 to a few per hour [6]. However, each signal remains in the sensitive band of ground-based detectors for at most ~ 1 second, meaning the duty cycle of the population is much smaller than unity.

[1] The signal-to-noise ratio (SNR) quantifies the relative strength of a signal compared to the background noise. It therefore indicates how easily the signal can be identified in the data.

Consequently, the combined signal from such a population of binary black holes will be "popcorn-like": a superposition of short, sparse bursts, most of which are too weak to be individually resolved.
Since the arrival times of the merger signals are randomly distributed, the combined signal from the population of binary black holes is itself random. This is an example of a stochastic background of gravitational radiation.
More generally, a stochastic background of gravitational radiation is any random gravitational-wave signal produced by a large number of weak, independent and unresolved sources.
The background does not necessarily have to be popcorn-like: in fact, it can be composed of individual deterministic signals that overlap in time, producing a "confusion" noise. Such a confusion noise is for example produced by the galactic population of compact white dwarf binaries.
Alternatively, the signal can be *intrinsically* random, associated with stochastic processes in the early Universe or with unmodeled sources.

The detection of a stochastic gravitational-wave background poses fundamental observational challenges. In a single detector, a SGWB is indistinguishable from instrumental noise: both manifest as random fluctuations in the data stream, with no obvious signature that would allow one to tell them apart.
The key problem is therefore how to disentangle gravitational-wave "noise" from detector noise. This is a crucial difference with respect to resolved signals like GW150914.
The solution to this problem lies in exploiting the fact that, unlike instrumental noise, a gravitational-wave background is a physical signal that permeates all of space. Two separated detectors will therefore share a common gravitational-wave component in their data streams, while their noise sources remain largely independent.
This is the core idea behind *cross-correlation methods*: by correlating the outputs of multiple detectors, we can isolate the common gravitational-wave contribution and suppress the uncorrelated noise.
This cross-correlation framework forms the backbone of standard searches for a stochastic background, which is typically assumed to be Gaussian, stationary, isotropic and unpolarized.
However, this framework can be extended to probe richer possibilities, including non-Gaussian, anisotropic and circularly-polarized backgrounds.
As we will discuss, these extensions open a window onto new physics phenomena and it is precisely in this extended framework that we have built our work.

The stochastic backgrounds that we expect to detect fall broadly into two categories, each with a distinct physical origin.

We can have *astrophysical backgrounds* (see [7] for a review on this matter) that arise, as we have said, from the superposition of a large number of individually unresolved sources such as compact binary mergers, supernovae or neutron stars. On the other hand, we also can have *cosmological backgrounds* (see [8]) generated by processes in the very early Universe.
Primordial stochastic gravitational-wave backgrounds offer a unique and powerful window onto the physics of the early Universe, whose investigation would be otherwise impossible. In fact, unlike electromagnetic radiation that cannot probe earlier than the time of last of scattering (roughly 4×10^5 years after the Big Bang), primordial gravitational waves can propagate from much earlier times and can give us information all the way back to the onset of inflation, around $\sim 10^{-32} s$ after the Big Bang (See [9] for a discussion of both cosmological and astrophysical sources of stochastic gravitational-wave backgrounds.)
Detecting such a signal would provide us with remarkably precious information about the first instants of our Universe.

At this point, we ask how we can actually distinguish between a cosmological background from an astrophysical one. The answer lies in the statistical properties of the signal.
Astrophysical backgrounds, being generated by the incoherent superposition of many independent sources, are expected to be nearly *Gaussian* by virtue of the central limit theorem [10, 11].
By contrast, cosmological backgrounds emerge from non-linear processes in the early-Universe, which generically break Gaussianity and give rise to non-vanishing higher-order correlators.
Non-Gaussianity is therefore a physically motivated, observable signature that can tell us whether a detected background has a primordial origin.
This expectation is concretely realized in numerous early-Universe models that aim to address open questions in physics: think about, for example, primordial black holes as dark matter candidates, primordial vector fields generating large-scale cosmic magnetism, or dark matter as dark photons [12, 13, 14]. These models induce the production of a gravitational-wave background at second order in fluctuations, as an unavoidable product of their non-linear generation mechanisms [15, 16].
The resulting backgrounds are therefore expected to carry *non-Gaussian signatures*, making non-Gaussianity not just a theoretical discriminator but a concrete observational target.

Motivated by this reason, this work investigates how primordial non-Gaussian SGWBs induced at second order by vector fluctuations can be detected with present and future gravitational-wave experiments.
In particular, we will make use of theoretical models that predict defined features of these GW backgrounds and we will analyse how Pulsar Timing Arrays (PTAs) and ground-based interferometers can detect these valuable signals from the early-Universe.
In order to do so, we will concentrate on studying the structure of correlators between detectors highlighting the non-Gaussian contributions to these quantities.

Executive Summary

This thesis explores observational prospects of non-Gaussian SGWBs by using PTAs and ground-based interferometers.
It is organized as follows: Chapter 2 provides a review of gravitational waves, deriving them from the linearized Einstein equations and discussing their energy and momentum content. After this, we focus on stochastic gravitational-wave backgrounds and how we can describe them.
We then introduce the response of detectors to a SGWB and define the key quantities that will be used throughout the thesis.
Building on this foundation, Chapter 3 explores the response of PTAs and ground-based interferometers to a SGWB.
In the PTA section, particular attention is given to the Hellings–Downs curve and to the statistical properties of its variance.
After this, we concentrate on ground-based interferometers and we explicitly compute the correlation function between the response of two interferometers interacting with a SGWB.
In Chapter 4 , we briefly introduce the physical features of a primordial non-Gaussian SGWB and then present the original contributions of this work.
We compute for the first time the non-Gaussian contribution to the variance of the Hellings-Downs curve.
Moreover, we calculate in a new way the two-point correlation function for interferometers, obtaining again the result previously found.
We conclude this chapter by computing for the first time the four-point correlation function for four distinct interferometers interacting with a SGWB.
Finally, we highlight the key findings and the open questions. We also present two technical appendices that support the main calculations.
Overall, the main goal of this project is to show that non-Gaussian features of a stochastic gravitational-wave backgrounds leave *measurable signatures* in detector correlators, opening the possibility of probing early-Universe physics beyond the standard Gaussian paradigm.

2 Gravitational Waves

In this chapter, we present a brief overview of gravitational waves and study how they naturally arise by studying Einstein's equations in the weak-field regime, where the spacetime metric is written as a small perturbation around flat Minkowski spacetime, following [17, 18] .
We then schematically obtain the energy and momentum carried by gravitational waves and review the quadrupole formula ([18]) .
After this, we introduce stochastic gravitational-wave backgrounds and describe their characteristics.
Finally, we investigate in detail how SGWBs can be observed and studied with detectors. In particular, we first illustrate how a single and two detectors interact with a SGWB and then analyse optimal filtering techniques.

2.1 Overview

Gravitational waves are propagating perturbations of spacetime generated by some of the most violent and energetic processes in the Universe.
General relativity predicts that accelerated massive systems (such as neutron stars or black holes orbiting each other) disrupt space-time, producing waves that propagate in all directions away from the source. These cosmic ripples travel at the speed of light, carrying with them information about their origins, as well as clues to the nature of gravity itself.

Albert Einstein first predicted the existence of gravitational waves in 1916 as a consequence of his general theory of relativity [19, 20]. However, their physical interpretation remained controversial for several decades, as it was unclear whether these solutions represented real propagating degrees of freedom or were merely artifacts of the coordinate description. Einstein himself revisited the issue more than once, at times expressing doubts during the development of the theory.

The first indirect evidence for the existence of gravitational waves came in 1974 with the discovery of the binary pulsar PSRB1913 + 16 by Russell Hulse and Joseph Taylor [21].
Precise timing measurements of this system revealed a gradual decay of its orbital period in exceptional agreement with the energy loss predicted by general relativity due to the emission of gravitational waves.
This result represented the first observation of physical reality of gravitational waves and earned Hulse and Taylor the Nobel Prize in Physics in 1993.

A direct detection was, as we have said, finally achieved in September 2015 with the observation of GW150914 [1]. This observation marked the beginning of gravitational-wave astronomy and confirmed the existence of propagating spacetime perturbations predicted by general relativity.

2.2 Waves from Geometry

2.2.1 Linearised theory

General Relativity is based on the gravitational action $S = S_E + S_M$, where :

$$S_E = \frac{1}{16\pi} \int d^4x \sqrt{-g}\, R \tag{1}$$

is the Einstein action and S_M is the matter action (see e.g. [18, 22, 23].
Notice that we are assuming natural units such that $G = c = 1$.
We know that $R_{\mu\nu} := R^{\lambda}_{\mu\lambda\nu}$ is the Ricci tensor obtained from the Riemann curvature tensor, $R = g^{\mu\nu} R_{\mu\nu}$ is the Ricci scalar, $g_{\mu\nu}$ is the metric and $g = \det g_{\mu\nu}$ is the metric's trace.
Moreover, the energy-momentum tensor $T_{\mu\nu}$ is defined from the variation of S_M under a change of the metric $g_{\mu\nu} \to g_{\mu\nu} + \delta g_{\mu\nu}$ according to:

$$\delta S_M = \frac{1}{2} \int d^4x \sqrt{-g}\, T^{\mu\nu}\, \delta g_{\mu\nu}. \tag{2}$$

Taking the variation of the total action with respect to $g_{\mu\nu}$, we find the Einstein field equations:

$$G_{\mu\nu} := R_{\mu\nu} - \frac{1}{2} g_{\mu\nu} R = 8\pi T_{\mu\nu}, \tag{3}$$

where $G_{\mu\nu}$ is the Einstein tensor.

To understand how gravitational waves are obtained, we need to consider the linearized theory: we take into account the spatially-flat 4-D Minkowski spacetime $\eta_{\mu\nu} = \mathrm{diag}(-1, 1, 1, 1)$ being perturbed by a tensor metric $h_{\mu\nu}$ such that $|h_{\mu\nu}| \ll 1$.
We then have:

$$g_{\mu\nu} = \eta_{\mu\nu} + h_{\mu\nu}. \tag{4}$$

This metric perturbation is assumed to be so small that we neglect all the terms at second order in $h_{\mu\nu}$ (this tells us, for example, that the usual index raising and lowering operations can be performed with $\eta_{\mu\nu}$) .
Expanding the Einstein tensor to linear order in $h_{\mu\nu}$ in this perturbed spacetime

gives ([17]),

$$G_{\mu\nu} = \frac{1}{2}\left(\partial_\mu\partial^\alpha h_{\alpha\nu} + \partial_\nu\partial^\alpha h_{\alpha\mu} - \partial_\mu\partial_\nu h - \Box h_{\mu\nu} + \eta_{\mu\nu}\Box h - \eta_{\mu\nu}\partial^\alpha\partial^\beta h_{\alpha\beta}\right), \quad (5)$$

where $\partial_\mu \equiv \partial/\partial x^\mu$, $\partial^\mu \equiv \eta^{\mu\nu}\partial_\nu$, $h = \eta^{\mu\nu}h_{\mu\nu}$ is the trace of $h_{\mu\nu}$ and $\Box = \eta^{\mu\nu}\partial_\mu\partial_\nu$ is the flat space d'Alembertian operator.
This expression can be simplified by defining the trace-reversed perturbation, $\bar{h}_{\mu\nu} = h_{\mu\nu} - n_{\mu\nu}h/2$, which also implies that $\bar{h} = \eta^{\mu\nu}\bar{h}_{\mu\nu} = h - 2h = -h$. Therefore, we have that $h_{\mu\nu} = \bar{h}_{\mu\nu} - n_{\mu\nu}\bar{h}/2$ and the Einstein tensor becomes

$$G_{\mu\nu} = \frac{1}{2}\left(\partial_\mu\partial^\alpha \bar{h}_{\alpha\nu} + \partial_\nu\partial^\alpha \bar{h}_{\alpha\mu} - \Box\bar{h}_{\mu\nu} - \eta_{\mu\nu}\partial^\alpha\partial^\beta \bar{h}_{\alpha\beta}\right). \quad (6)$$

We can now use that General Relativity is invariant under diffeomorphisms[2]. This means that physics doesn't change under, for example, the coordinate transformation $x^\alpha \mapsto x^\alpha + \xi^\alpha(x)$. Under this kind of action, the metric perturbation transforms as $h_{\mu\nu} \mapsto h_{\mu\nu} - (\partial_\mu\xi_\nu + \partial_\nu\xi_\mu)$ to first order.
Supposing that $\partial_\mu\xi_\nu$ is of the same order as $|h_{\mu\nu}|$, the transformed metric perturbation still satisfies the condition $|h_{\alpha\beta}| \ll 1$.
This symmetry allows us to select the *Lorenz Gauge*, where $\partial^\nu\bar{h}_{\mu\nu} = \partial^\nu(h_{\mu\nu} - \eta_{\mu\nu}h/2) = 0$, such that the Einstein tensor reduces to

$$G_{\mu\nu} = -\frac{1}{2}\Box\bar{h}_{\mu\nu}. \quad (9)$$

We notice that by selecting this gauge we have imposed 4 conditions that cut the degrees of freedom from 10 (symmetric 4×4 matrix) to 6.
Therefore, the field equations reduce to

$$\Box\bar{h}_{\mu\nu} = -16\pi T_{\mu\nu}. \quad (10)$$

For the moment, we focus on the region far from the source, where

$$\Box\bar{h}_{\mu\nu} = 0, \quad (11)$$

[2]Diffeomorphisms are coordinate transformations

$$x^\mu \to x'^\mu(x) \quad (7)$$

such that x'^μ is invertible, differentiable and with a differentiable inverse.
Under a diffeomorphism, the metric transforms as:

$$g_{\mu\nu}(x) \to g'_{\mu\nu}(x') = \frac{\partial x^\rho}{\partial x'^\mu}\frac{\partial x^\sigma}{\partial x'^\nu}g_{\rho\sigma}. \quad (8)$$

whose solution is clearly wave-like with propagation velocity equal to c.
At this point, we notice that the *Lorenz Gauge* is still preserved under another coordinate transformation $x^\mu \mapsto x^\mu + \xi^\mu$, provided that $\Box \xi_\mu = 0$.

This means that $\bar{h}_{\mu\nu}$ can have 4 of its independent components cut (since ξ_μ gives us 4 conditions), leaving it with only 2 degrees of freedom [24].
In particular, we can choose the components of ξ_μ such that $\bar{h} = 0$ (therefore $\bar{h}_{\mu\nu} = h_{\mu\nu}$) and $h^{0i} = 0$.
This leads to the definition of the *transverse-traceless* (TT) gauge, where:

$$h^{0\mu} = 0, \quad h^i{}_i = 0, \quad \partial^j h_{ij} = 0. \tag{12}$$

Finally, we obtain that the Einstein Field equations are given by:

$$\Box h_{ij}^{TT} = 0, \tag{13}$$

where we have considered only the spatial components, since in this gauge h_{00} is constant in time.

For later calculations, it is useful to define more accurately the solution to equation 10 outside the source: in the TT gauge we have $\Box h_{ij}^{TT} = 0$, therefore

$$h_{ij}^{\mathrm{TT}}(x) = \int \frac{d^3k}{(2\pi)^3} \left(A_{ij}(\mathbf{k}) e^{ikx} + A_{ij}^*(\mathbf{k}) e^{-ikx} \right). \tag{14}$$

Knowing that the four-vector $k^\mu = (\omega, \mathbf{k})$ has $|\mathbf{k}| = \omega = 2\pi f$ one can rewrite this expression using spherical coordinates:

$$h_{ij}^{\mathrm{TT}}(x) = \int_0^\infty df\, f^2 \int d^2\hat{\mathbf{n}} \left(A_{ij}(f, \hat{\mathbf{n}})\, e^{-2\pi i f(t - \hat{\mathbf{n}}\cdot\mathbf{x}/c)} + \text{c.c.}, \right) \tag{15}$$

where we consider $d^2\hat{\mathbf{n}} = d\cos\theta d\phi$ the integration over the solid angle.
From the TT gauge conditions 12 we see that $A^i{}_i(\mathbf{k}) = 0$ and that $k^i A_{ij}(\mathbf{k}) = 0$.

We can rewrite this plane wave expansion by introducing polarization tensors $e^+(\hat{\mathbf{n}})$ and $e^\times(\hat{\mathbf{n}})$. To do so, we first need to define:

$$\begin{aligned} \hat{\boldsymbol{\theta}} &= \cos\theta\cos\phi\,\hat{\mathbf{x}} + \cos\theta\sin\phi\,\hat{\mathbf{y}} - \sin\theta\,\hat{\mathbf{z}}, \\ \hat{\boldsymbol{\phi}} &= -\sin\phi\,\hat{\mathbf{x}} + \cos\phi\,\hat{\mathbf{y}}. \end{aligned} \tag{16}$$

and $\hat{\mathbf{n}}$ as pointing in the direction given by the standard angular coordinates (θ, ϕ) on the sphere:

$$\hat{\mathbf{n}} = \sin\theta\cos\phi\,\hat{\mathbf{x}} + \sin\theta\sin\phi\,\hat{\mathbf{y}} + \cos\theta\,\hat{\mathbf{z}}. \tag{17}$$

At this point we can write:

$$\begin{aligned} \mathbf{e}^{+}(\hat{\mathbf{n}}) &= \hat{\boldsymbol{\theta}} \otimes \hat{\boldsymbol{\theta}} - \hat{\boldsymbol{\phi}} \otimes \hat{\boldsymbol{\phi}}, \\ \mathbf{e}^{\times}(\hat{\mathbf{n}}) &= \hat{\boldsymbol{\theta}} \otimes \hat{\boldsymbol{\phi}} + \hat{\boldsymbol{\phi}} \otimes \hat{\boldsymbol{\theta}}. \end{aligned} \tag{18}$$

In a generic frame, we can define the amplitudes $\tilde{h}_P(f, \hat{\mathbf{n}})\, e_{ij}^P(\hat{\mathbf{n}})$ via:

$$f^2 A_{ij}(f, \hat{\mathbf{n}}) = \sum_{P=+,\times} \tilde{h}_P(f, \hat{\mathbf{n}})\, e_{ij}^P(\hat{\mathbf{n}}). \tag{19}$$

Therefore equation 15 becomes:

$$h_{ij}(t, \mathbf{x}) = \sum_{P=+,\times} \int_{-\infty}^{\infty} df \int d^2\hat{\mathbf{n}}\, \tilde{h}_P(f, \hat{\mathbf{n}})\, e_{ij}^P(\hat{\mathbf{n}})\, e^{-2\pi i f\,(t - \hat{\mathbf{n}}\cdot\mathbf{x})}. \tag{20}$$

We now study the physical effects of GWs by looking back at equation 13: from here, let us show that GWs affect distances.
Choosing a coordinate system where a plane GW propagates in the z-direction in the vacuum, we can write the solution to 13 as

$$h_{\mu\nu}^{\mathrm{TT}}(t, z) = \begin{pmatrix} 0 & 0 & 0 & 0 \\ 0 & h_+ & h_\times & 0 \\ 0 & h_\times & -h_+ & 0 \\ 0 & 0 & 0 & 0 \end{pmatrix} \cos\left[\omega(t - z)\right], \tag{21}$$

where h_+ and $h_\times$ are the amplitudes of the two distinct polarizations of GWs permitted within general relativity, denoted as "plus" $(+)$ and "cross" $(\times)$ modes. This perturbation of the metric will produce a new line element, given by:

$$\begin{aligned} ds^2 = &-dt^2 + dz^2 + \big(1 + h_+ \cos(\omega(t - z))\big)\, dx^2 + \big(1 - h_+ \cos(\omega(t - z))\big)\, dy^2 \\ &+ 2h_\times \cos(\omega(t - z))\, dx\, dy \end{aligned} \tag{22}$$

This tells us that proper distances get modified as a GW propagates: this can be clearly seen by, for example, computing the actual distance between a test mass located at $(t, L, 0, 0)$ and the origin $(0, 0, 0, 0)$:

$$S = \int_0^L \sqrt{g_{xx}}\, dx = L\sqrt{1 + h_+ \cos(\omega t)} \simeq L\left(1 + \frac{1}{2} h_+ \cos(\omega t)\right).$$

Therefore we see that there is a variation of the proper distance due to the presence of the gravitational-wave.

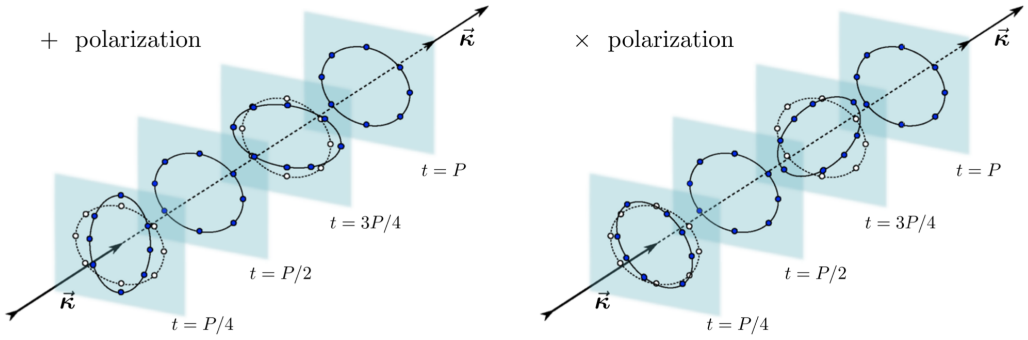

Figure 1: Deformations produced on a ring of freely-falling particles by gravitational waves that are linear polarized in the "+" ("plus") and "×" ("cross") modes. The continuous lines and the dark filled dots show the positions of the particles at different times, while the dashed lines and the open dots show the unperturbed positions. Figure taken by [25].

This effect is even more noticeable if we consider how a propagating GW affects a circular ring of test particles positioned in the plane perpendicular to the direction of propagation. What happens is shown in figure 1 .

From this we also understand the nomenclature behind the "plus" (+) and "cross" (×) modes: it is exactly related to how they tidally deform this ring.
This tidal deformation of spacetime caused by a propagating gravitational wave is the core of all the ground-based (LIGO, Virgo, KAGRA), galactic-scale (Pulsar Timing Arrays) and space-borne (LISA) detection efforts (see e.g. [26]).

2.2.2 Energy-momentum tensor of GWs

We now want to compute the energy and momentum carried by gravitational waves. In this section, we closely follow [18].
The fact that GWs carry energy and momentum is clear by their interaction with test masses: GWs can do work and the conservation of energy tells us that the kinetic energy acquired by the test masses must come from GWs' energy.
To obtain the expression of the energy-momentum tensor we can ask whether GWs curve space-time since they carry energy.
To answer this question, we need to change a little bit our setup: instead of considering GWs as a perturbation over a flat spacetime, we take into account a dynamical background. This must be done since if we consider GWs over a flat metric we exclude from the beginning the possibility of GWs bending space-time.

Therefore, we consider:

$$g_{\mu\nu} = \bar{g}_{\mu\nu} + h_{\mu\nu}, \tag{23}$$

with $|h_{\mu\nu}| \ll 1$.
However, we immediately see that we have an ambiguity in defining which part of $g_{\mu\nu}$ is the background and which is the fluctuations. In a general setting, there is no way to perform a clear separation of the type given by equation 23; however, there are some conditions that allow us to use this kind of description.
For example, a natural splitting between the space-time background and gravitational waves arises when we have a clear separation of scales.
Consider $\bar{g}_{\mu\nu}$ having a typical scale of variation L_B with small amplitude perturbations characterized by a wavelength λ such that $\lambda/(2\pi) \ll L_B$.
In this case, $h_{\mu\nu}$ can be seen as describing small ripples on a smooth background.
This idea can also be applied for the frequency space: considering the characteristic frequencies of $\bar{g}_{\mu\nu}$ (f_B) and $h_{\mu\nu}$ (f) as belonging to very different scales ($f_B \ll f$).
In this scenario, $h_{\mu\nu}$ is a high-frequency perturbation of a static or slowly varying background.
It should be pointed out that the latter case usually describes the case for GW detectors: in fact, fluctuations in the metric related to local density variations, mountains, etc. on Earth are essentially static and it is difficult to find important variations at large frequency scales, e.g. at $f \sim 1kHz$, which is the scale of frequencies for GWs searched by ground based detectors.
Therefore, we can find a distinction between background and gravitational waves based on the condition ($f_B \ll f$).

Thus, we can assume to be in a situation where we can separate the metric into a background plus fluctuations. In this case, our goal is to understand how $h_{\mu\nu}$ affects the background: to do so, we need to expand Einstein equations around $\bar{g}_{\mu\nu}$ and split the contributions from low and high frequency modes.
From this expansion we get that the energy-momentum tensor's explicit expression can be obtained from studying the linear part in $h_{\mu\nu}$.
The derivation lies on integrating out the fast-varying degrees of freedom: in this way, we are left with an effective dynamics for the slowly varying degrees of freedom.
The full derivation can be found in [18] and [27, 28].
The important result is that the effect of GWs on the background is basically identical to that of a source with energy-momentum tensor $t_{\mu\nu}$, where

$$t_{\mu\nu} = \frac{\langle \partial_\mu h_{\alpha\beta} \partial_\nu h^{\alpha\beta} \rangle}{32\pi}. \tag{24}$$

Notice that this holds in the TT gauge.

In particular, the gauge invariant energy density is given by:

$$t^{00} = \frac{1}{32\pi}\langle \dot{h}_{ij}\dot{h}^{ij}\rangle. \tag{25}$$

This quantity will be useful later in our calculations.

2.2.3 The quadrupole formula

For the sake of completeness, we now solve equation 10 without imposing the energy-momentum tensor to be null.
This solution can be achieved by considering the method of Green functions.
Consider $G(x-x')$ being a solution of

$$\Box_x G(x-x') = \delta^4(x-x'), \tag{26}$$

we have that

$$\bar{h}_{\mu\nu}(x) = -16\pi \int d^4x' G(x-x')T_{\mu\nu}(x'). \tag{27}$$

Recall that we are working in the Lorenz Gauge. The solution depends on the boundary conditions that we impose.
The appropriate solution is a retarded Green's function given by:

$$G(x-x') = -\frac{1}{4\pi|\mathbf{x}-\mathbf{x}'|}\delta(t_{ret}-t') \tag{28}$$

where

$$t_{\text{ret}} = t - |\mathbf{x}-\mathbf{x}'|, \tag{29}$$

is the retarded time.
Notice that we are still considering $G = c = 1$.
This tells us that the solution of equation 10 is given by:

$$\bar{h}_{\mu\nu}(t,\mathbf{x}) = 4\int d^3x' \,\frac{1}{|\mathbf{x}-\mathbf{x}'|}\,T_{\mu\nu}(t-|\mathbf{x}-\mathbf{x}'|,\mathbf{x}')\,. \tag{30}$$

Outside the source we can impose the TT gauge.
To do so, we use the tensor $\Lambda_{ij,kl}$ defined as:

$$\Lambda_{ij,kl}(\hat{\mathbf{n}}) = P_{ik}(\hat{\mathbf{n}})\,P_{jl}(\hat{\mathbf{n}}) - \frac{1}{2}P_{ij}(\hat{\mathbf{n}})\,P_{kl}(\hat{\mathbf{n}}), \tag{31}$$

where $\hat{\mathbf{n}}$ is the direction of propagation of $h_{\mu\nu}$ and

$$P_{ij}(\hat{\mathbf{n}}) = \delta_{ij} - n_i n_j. \tag{32}$$

In this way, $h_{ij}^{TT} = \Lambda_{ij,kl} h_{kl} = \Lambda_{ij,kl} \bar{h}_{kl}$.
Therefore, outside the source, we get that:

$$h_{ij}^{\mathrm{TT}}(t, \mathbf{x}) = 4\Lambda_{ij,kl}(\hat{\mathbf{n}}) \int d^3x' \frac{1}{|\mathbf{x} - \mathbf{x}'|} T_{kl}\left(t - |\mathbf{x} - \mathbf{x}'|, \mathbf{x}'\right). \tag{33}$$

where we use $\hat{\mathbf{x}} = \hat{\mathbf{n}}$ and we also denote $|\mathbf{x}| = r$.
Let us also denote d as the typical radius of the source: then, for $d \ll r$, we can write:

$$|\mathbf{x} - \mathbf{x}'| = r - \mathbf{x}' \cdot \hat{\mathbf{n}} + \mathcal{O}\left(\frac{d^2}{r}\right). \tag{34}$$

Finally, we also assume to be very far from the source.
Under these assumptions and using the stress-energy conservation , we find that the leading contribution depends on the second time derivative of the mass quadrupole, given by:

$$Q^{ij} \equiv \int d^3x \rho(t, \mathbf{x})(x^i x^j - \frac{1}{3} r^2 \delta^{ij}). \tag{35}$$

We then have that:

$$h_{ij}^{\mathrm{TT}}(t, \mathbf{x}) = \frac{1}{r} 2\Lambda_{ij,kl}(\hat{\mathbf{n}}) \ddot{Q}^{kl}(t - r) \equiv \frac{1}{r} 2\ddot{Q}_{ij}^{TT}(t - r). \tag{36}$$

See [18] for the full computation.
We see from this equation that the leading term of the multipole expansion is the mass *quadrupole*: for GWs, there is neither monopole nor dipole radiation.

2.3 Stochastic Gravitational Wave Backgrounds

In 1965 Penzias and Wilson discovered that the Universe is permeated by the Cosmic Microwave Background (CMB) electromagnetic radiation ([29, 30], also [31]). This radiation is a relic of the early Universe and is constituted of microwave photons that decoupled from the primordial plasma about 3×10^5 years after the Big Bang. These photons have been propagating since then essentially freely. This discovery, providing direct evidence for the Big Bang, was one of the most significant in the history of cosmology.

There are good reasons to expect that the Universe is permeated also by a stochastic background of GWs generated in the early Universe.
Furthermore, a stochastic background of GWs can also emerge from the incoherent superposition of a large number of astrophysical sources too weak to be detected separately.
In general, as we have seen, we define a stochastic background of gravitational radiation as any random gravitational-wave signal produced by a large number of weak, independent and unresolved sources.
It can be either composed of individual deterministic signals that overlap in time (or in frequency) producing a "confusion" noise or it can be associated with unmodeled stochastic processes.

We recall that we particularly care about detecting a stochastic background of gravitational radiation because it can provide extremely interesting information about cosmological events in the very early Universe, which would be inaccessible by any other kind of signal.

2.3.1 Characterizing a SGWB

We refer to a *stochastic* gravitational wave background since we are dealing with a *random* signal: this means that it can only be described statistically in terms of expectation values.

As we have seen, the metric perturbation can be written as a superposition of waves of all frequencies coming from all directions (see equation 20).
In particular, using the TT gauge :

$$h_{ab}(t, \mathbf{x}) = \sum_{P=+,\times} \int_{-\infty}^{\infty} df \int d^2\hat{\mathbf{n}}\, \tilde{h}_P(f, \hat{\mathbf{n}})\, e^P_{ab}(\hat{\mathbf{n}})\, e^{-2\pi i f\,(t - \hat{\mathbf{n}}\cdot\mathbf{x})}. \tag{37}$$

For a SGWB, we can consider $\tilde{h}_P(f, \hat{\mathbf{n}})$ as *complex random fields*, whose prob-

ability distributions define the statistical properties of the background.

Therefore, the statistical properties of a SGWB are described by quantities such as:

$$\langle h_{ab}(t,\vec{x})\rangle\,, \quad \langle h_{ab}(t,\vec{x})h_{cd}(t',\vec{x}')\rangle\,, \quad \langle h_{ab}(t,\vec{x})h_{cd}(t',\vec{x}')h_{ef}(t'',\vec{x}'')\rangle\,, \quad \cdots \tag{38}$$

or similar expressions in terms of the Fourier coefficients $\tilde{h}_P(f,\hat{\mathbf{n}})$.
Notice that $\langle\rangle$ represents an *ensemble average*, which means that we perform this operation over many copies of the system. However, in this case the system is our Universe and we do not have many copies of it: therefore, we must use the ergodic assumption and replace this ensemble average with a time one.
We will return to this averaging process in more detail later.
We can assume that the background has zero mean :

$$\langle h_{ab}(t,\vec{x})\rangle = 0 \quad \Leftrightarrow \quad \langle \tilde{h}_P(f,\hat{\mathbf{n}})\rangle = 0. \tag{39}$$

Moreover, we expect that the form of the expectation values will depend on the kind of background source. The simplest type of SGWB will be (1) *stationary*, (2) *unpolarized* , (3) *isotropic* and (4) *Gaussian*.

These assumptions might not hold in general, so it is important to thoroughly examine each one of them:

1. the background is stationary. This means that all quantities only depend on the difference between times. So, for example, $\langle h_{ab}(t,\vec{x})h_{cd}(t',\vec{x}')\rangle$ can depend only on $t-t'$ and not separately on t and t'.
   This is a reasonable assumption since the age of the universe is roughly 9 orders of magnitude larger than the longest observation times, ~ 10 yr.
   This tells us that it is unlikely that a SGWB has statistical properties changing over the time scale of observation;

2. we suppose that the background is unpolarized, since it is natural both in a cosmological context and an astrophysical one. This means that quantities such as $\langle \tilde{h}^*_P(f,\hat{\mathbf{n}})\tilde{h}_{P'}(f',\hat{\mathbf{n}}')\rangle$ must be proportional to $\delta_{PP'}$ and that the proportionality coefficient must be independent of the polarization P;

3. the stochastic background is isotropic. This is reasonable to expect since it is well known that the early Universe was highly isotropic. It is then safe to assume that, at least in a first approximation, also a background of GWs will have the same feature;

4. the final assumption is that the SGWB is Gaussian.
   In this case, we know that the second-order moments completely specify the

statistical properties of the signal. If we are considering a sufficiently large number of independent sources, this assumption is justified by the central limit theorem.
In section 4 we will drop this assumption to focus on how we can probe non-Gaussianities of the SGWB.

At this point, following [18, 32] , we can write the following relation for this kind of background :

$$\langle \tilde{h}^*_P(f,\hat{\mathbf{n}})\tilde{h}_{P'}(f',\hat{\mathbf{n}}')\rangle = \delta(f-f')\,\frac{\delta^2(\hat{\mathbf{n}},\hat{\mathbf{n}}')}{4\pi}\,\delta_{PP'}\,\frac{1}{2}S_h(f), \tag{40}$$

where $S_h(f)$ is the one-sided power spectral density (PSD) of the *Fourier modes* of the SGWB (see [18]).

We now compute the energy density of the SGWB per logarithmic frequency interval, in order to characterize how the gravitational-wave energy is distributed across frequencies.
We therefore define

$$\Omega_{\mathrm{SGWB}}(f) \equiv \frac{1}{\rho_c}\frac{d\rho}{d\ln f}, \tag{41}$$

where ρ is the energy density in GWs and $\rho_c = 3H_0^2/8\pi$ is the critical density, with H_0 is the present-day Hubble expansion rate.
At this point we use equation 25 and we get that the energy density is given by:

$$\begin{aligned}\langle \dot{h}_{ij}\dot{h}^{ij}\rangle = &\sum_P\sum_{P'}\int_{-\infty}^{\infty}df\int_{-\infty}^{\infty}df'\int d^2\hat{\mathbf{n}}\int d^2\hat{\mathbf{n}}'\,\langle \tilde{h}^*_P(f,\hat{\mathbf{n}})\tilde{h}_{P'}(f',\hat{\mathbf{n}}')\rangle\\ &\times e_{ij,P}(\hat{\mathbf{n}})e^{ij}_{P'}(\hat{\mathbf{n}}')\times 4\pi^2 ff'\\ &\times \exp\left[-2\pi i(f-f')t + 2\pi i(\hat{\mathbf{n}}-\hat{\mathbf{n}}')\cdot\mathbf{x}\right].\end{aligned} \tag{42}$$

We want to solve this for a gaussian, stationary, unpolarized and isotropic background, therefore we use equation 40.

Knowing that $\int d^2\hat{\mathbf{n}} = 4\pi$ and $\sum_A e_{ij,A}e^{ij}_A = 4$, we convert the frequency integration bounds in equation 42 to $[0,\infty]$ and we obtain

$$\langle \dot{h}_{ij}\dot{h}^{ij}\rangle = 16\pi^2\int_0^{\infty}df\ f^2 S_h(f). \tag{43}$$

Hence

$$\Omega_{\mathrm{SGWB}}(f) \equiv \frac{1}{\rho_c}\frac{d\rho}{d\ln f} = \frac{4\pi^2}{3H_0^2}f^3 S_h(f). \tag{44}$$

2.3.2 Characteristic Strain $h_c(f)$

It is often useful to work with the **characteristic strain amplitude** $h_c(f)$ defined as:

$$h_c(f) \equiv \sqrt{f S_h(f)}\,. \tag{45}$$

It is related to $\Omega_{\rm SGWB}(f)$ via:

$$\Omega_{\rm SGWB}(f) = \frac{4\pi^2}{3H_0^2} f^2 h_c^2(f)\,. \tag{46}$$

Theoretical models of GWBs often predict characteristic strains given by power-law expressions:

$$h_c(f) = A_{\alpha,ref} \left(\frac{f}{f_{\rm ref}}\right)^{\alpha}\,, \tag{47}$$

where α is the spectral index, $f_{\rm ref}$ is typically set to 1/yr and $A_{\alpha,ref}$ is the characteristic strain at the reference frequency.
We then expect $\Omega_{\rm SGWB}(f) \sim f^{2\alpha+2}$ with α given by the kind of sources that we are studying.

2.4 The Gravitational Wave Spectrum

Similarly to electromagnetic radiation, gravitational waves exhibit a characteristic frequency spectrum determined by their sources.
The majority of the GW spectrum being studied by current and future detectors lies below the kHz range.
We can identify three main observational windows:

- nanoHertz frequencies probed with Pulsar Timing Arrays;
- milliHertz frequencies targeted by space-based laser interferometers;
- up to kHz frequencies being analysed by ground-based interferometers.

Figure 2 shows the characteristic strain spectrum of GWs over frequencies, with the sensitivity of current and future detectors and the regions of possible astrophysical targets.

In this project we will especially focus on Pulsar Timing Arrays and on ground-based interferometers.

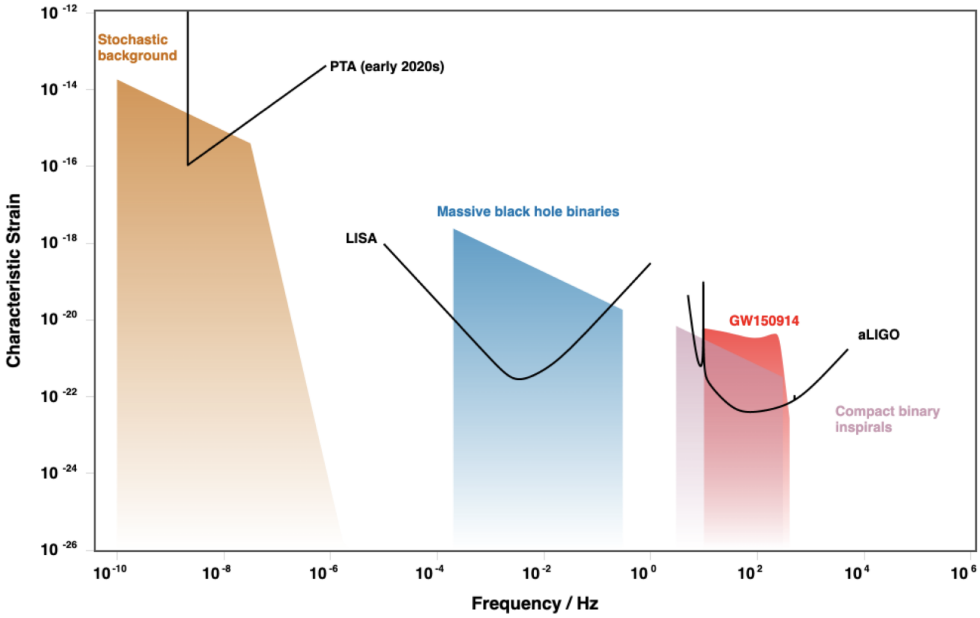

Figure 2: Overview of detectors and sources covering the GW spectrum. Figure taken from [17].

2.5 The response of detectors

$\Omega_{\mathrm{SGWB}}(f)$, $h_c(f)$ and $S_h(f)$ are fundamental quantities for describing a stochastic gravitational background but do not take into account the presence of the detectors.
In this section, we want to make contact with what actually happens in a generic detector when it interacts with a stochastic background of GWs.
We closely follow [32].

2.5.1 Single detector

We start by considering the case of a single detector. Since we measure the response of our detector under the influence of the perturbation rather than the metric perturbation itself, we can write the total output of the detector $S(t)$ as:

$$S(t) = s(t) + n(t) \tag{48}$$

where $n(t)$ is the noise and $s(t)$ is the contribution related to the gravitational wave.
In particular, we can find the relation between the signal $s(t)$ and the metric

perturbation $h_{ab}(t)$ as:

$$s(t) = D^{ab} h_{ab}(t) \tag{49}$$

where D^{ab} is the *detector tensor*.

Considering 37 , we get that

$$s(t) = \sum_{P=+,\times} \int_{-\infty}^{\infty} df \int d^2\hat{\mathbf{n}}\, \tilde{h}_P(f, \hat{\mathbf{n}})\, D^{ab} e^P_{ab}(\hat{\mathbf{n}})\, e^{-2\pi i f t}, \tag{50}$$

where we have set $\vec{x} = 0$ since we're dealing with only one detector.

It is therefore convenient to define the *detector pattern functions* $F^P(\hat{\mathbf{n}}) \equiv D^{ab} e^P_{ab}(\hat{\mathbf{n}})$ so that

$$s(t) = \sum_{P=+,\times} \int_{-\infty}^{\infty} df \int d^2\hat{\mathbf{n}}\, \tilde{h}_P(f, \hat{\mathbf{n}})\, F^P(\hat{\mathbf{n}})\, e^{-2\pi i f t} \tag{51}$$

and the Fourier transform $\tilde{s}(f)$ given by:

$$\tilde{s}(f) = \sum_{P=+,\times} \int d^2\hat{\mathbf{n}}\, \tilde{h}_P(f, \hat{\mathbf{n}})\, F^P(\hat{\mathbf{n}})\,. \tag{52}$$

Notice that the pattern functions F^P depend on the direction $\hat{\mathbf{n}}$ of arrival of the wave.

They actually also depend on an angle ψ, which describes a rotation in the plane orthogonal to $\hat{\mathbf{n}}$, i.e. the plane defined by $\hat{\boldsymbol{\theta}}$ and $\hat{\boldsymbol{\phi}}$ (eq. 16).
Once we have made a definite choice for $\hat{\boldsymbol{\theta}}$ and $\hat{\boldsymbol{\phi}}$, we have chosen the axes with respect to which the + and × polarizations are determined.
While for an astrophysical source there can be a natural choice of axes, for an unpolarized SGWB there is no privileged choice of basis and we expect the angle ψ to cancel from the final result.
We will check this in the specific case of PTAs and interferometers.

We've seen that for a stochastic gravitational wave background we can assume $\langle h_{ab}(t)\rangle = 0$, therefore we have that $\langle s(t)\rangle = 0$.
With only one detector, the most interesting quantity is $\langle s^2(t)\rangle$, given by:

$$\langle s^2(t)\rangle = F \int_{-\infty}^{\infty} df \frac{1}{2} S_h(f) = F \int_0^{\infty} df\, S_h(f) \tag{53}$$

where

$$F = \int \frac{d^2\hat{\mathbf{n}}}{4\pi} \sum_{P=+,\times} F^P(\hat{\mathbf{n}}) F^P(\hat{\mathbf{n}})\,. \tag{54}$$

This quantity has a clear physical meaning: it is obtained by integrating over all waves coming from all directions $\hat{\mathbf{n}}$ and it gives the loss of sensitivity related to the fact that the detector actually has an optimal direction.
To explicitly compute the pattern function we need the expression of the detector tensor D_{ab}, which obviously depends on what kind of detector we're dealing with. We will later obtain these quantities for both PTAs and ground-based interferometers.

2.5.2 The strain sensitivity $\tilde{h}_f$

The ensemble average of the Fourier components of the noise satisfies:

$$\langle \tilde{n}^*(f)\tilde{n}(f')\rangle = \delta(f-f')\frac{1}{2}S_n(f)\,. \tag{55}$$

This equation defines the functions $S_n(f)$, with $S_n(f) = S_n(-f)$ and dimensions inverse of frequency.
The factor $1/2$ is again due to convention, so that the total noise power is obtained integrating $S_n(f)$ over the physical range of the frequency ($0 \leq f < \infty$ rather than $-\infty < f < \infty$):

$$\langle n^2(t)\rangle = \int_0^\infty df\, S_n(f)\,. \tag{56}$$

The function $S_n(f)$ is known as the square spectral noise density[3].
The noise level of the detector is measured by *strain sensitivity* $\tilde{h}_f$

$$\tilde{h}_f = \sqrt{S_n(f)} \tag{57}$$

where now $f > 0$.
Comparing equations 56 and 53, we find that in a single detector a stochastic background will present itself as an excess noise.
This will be observable at a frequency f if

$$S_h(f) \;>\; \frac{1}{F}S_n(f)\,, \tag{58}$$

where F is given by 54.

2.5.3 Two-detectors correlation: overlap reduction functions

SGWBs are quite complicated to detect since their signal is expected to be far too low with respect to the noise level in any existing detector.

[3]This holds following [32], however there is not much agreement in the literature around this definition.

We therefore need a strategy to detect this kind of evidence: a possible way, as we have previously mentioned, consists in performing a correlation between two or more detectors.
We write the output for the i-th detector as:

$$S_i(t) = s_i(t) + n_i(t) \tag{59}$$

where we expect $s_i(t) \ll n_i(t)$.
Using equation 37 we can write:

$$s_i(t) = \sum_{P=+,\times} \int_{-\infty}^{\infty} df \int d^2\hat{\mathbf{n}}\, \tilde{h}_P(f,\hat{\mathbf{n}})\, F_i^P(\hat{\mathbf{n}})\, e^{-2\pi i f(t-\hat{\mathbf{n}}\cdot\mathbf{x}_i)}, \tag{60}$$

where $F_i^P(\hat{\mathbf{n}})$ is the detector pattern function for the i-th detector.
As we have done in the case of a single detector, we compute the Fourier transform of $s_i(t)$:

$$\tilde{s_i}(f) = \sum_{P=+,\times} \int d^2\hat{\mathbf{n}}\, \tilde{h}_P(f,\hat{\mathbf{n}})\, F_i^P(\hat{\mathbf{n}})\, e^{2\pi i f \hat{\mathbf{n}}\cdot\mathbf{x}_i}. \tag{61}$$

At this point we can correlate two outputs ($i = A, B$):

$$S_{AB} = \int_{-T/2}^{T/2} dt \int_{-T/2}^{T/2} dt'\, S_A(t) S_B(t') Q(t-t')\,, \tag{62}$$

where T is the total integration time and Q is a real filter function. Its role is to weight the correlation between the two detector outputs at different times.
In the following section, we will determine how to choose Q to maximize the signal-to-noise ratio (SNR).
Notice that, since we are assuming that both the statistical properties of the SGWB and the noise intrinsic to the detectors are stationary, the filter function $Q(t,t')$ can depend only on the time difference $\Delta t = t - t'$.
$Q(t-t')$ falls rapidly to zero when $|t-t'|$ becomes large compared to the light travel time between the two detectors.
This tells us that we can rewrite equation 62 taking the limit of large T:

$$S_{AB} = \int_{-\infty}^{+\infty} df\, \tilde{S}_A^*(f) \tilde{S}_B(f) \tilde{Q}(f)\,. \tag{63}$$

At this point, we can write the ensemble average of the contribution from the GW background as:

$$\begin{aligned}\langle s_{AB}\rangle \equiv \langle s_A s_B\rangle &= \int_{-\infty}^{+\infty} df\, \langle \tilde{s}_A^*(f)\, \tilde{s}_B(f)\rangle\, \tilde{Q}(f) \\ &= \int_{-\infty}^{+\infty} df \int d^2\hat{\mathbf{n}} \int d^2\hat{\mathbf{n}}'\, e^{2\pi i f(\hat{\mathbf{n}}\cdot\, \mathbf{x}_A - \hat{\mathbf{n}}'\cdot\mathbf{x}_B)} \\ &\quad \times \sum_{P,P'=+,\times} F_A^P(\hat{\mathbf{n}}) F_B^{P'}(\hat{\mathbf{n}}')\, \left\langle \tilde{h}_P^*(f,\hat{\mathbf{n}}) \tilde{h}_{P'}(f,\hat{\mathbf{n}}')\right\rangle \tilde{Q}(f) \\ &= T\int_{-\infty}^{+\infty} df\, \frac{1}{2} S_h(f)\, \Gamma_{AB}(f)\, \tilde{Q}(f)\,.\end{aligned} \tag{64}$$

We have used 40, $\delta(0) = \int_{-T/2}^{T/2} dt = T$ and in the last line we have introduced

$$\Gamma_{AB}(f) \equiv \int \frac{d^2\hat{\mathbf{n}}}{4\pi} \sum_{P=+,\times} F_A^P(\hat{\mathbf{n}}) F_B^P(\hat{\mathbf{n}}) \exp\{2\pi i f \hat{\mathbf{n}}\cdot\Delta\mathbf{x}\}\,, \tag{65}$$

where $\Delta\mathbf{x}$ is the separation between the two detectors.
Let us take a closer look at this expression: we notice that (i) the sum over polarizations P is appropriate for an unpolarized stochastic background; (ii) the integral over $\hat{\mathbf{n}}$ is an isotropic average over all the possible directions of the incoming radiation; (iii) the phase factor is related to the phase shift associated to the time delay between the detectors for the radiation.
We now define

$$F_{AB} \equiv \int \frac{d^2\hat{\mathbf{n}}}{4\pi} \sum_{P=+,\times} F_A^P(\hat{\mathbf{n}}) F_B^P(\hat{\mathbf{n}})|_{\text{aligned}} \tag{66}$$

where this quantity is obtained by taking the two detectors perfectly aligned instead of considering their actual orientation. Notice that if we consider two detectors of the same type F_{AB} is the same as the constant F defined in eq.(54).

Finally, we can define the *overlap reduction function (ORF)* $\gamma_{AB}(f)$ given by:

$$\gamma_{AB}(f) = \frac{\Gamma_{AB}(f)}{F_{AB}}. \tag{67}$$

We will use this normalization in the case of two interferometers (see 3.2.1): F_{AB} takes into account how the angular pattern reduces sensitivity (effect already present in only one interferometer), while $\gamma_{AB}(f)$ separately considers the effect of the separation $\Delta\mathbf{x}$ between the two interferometers and of their relative orientation.

We therefore highlight that there will be a reduction in sensitivity due to: (i) the separation time delay between the two detectors and (ii) the non-parallel alignment of the detector arms.
This tells us that the overlap between the gravitational strains in the two detectors is only partial.
With this definition, $\gamma_{AB}(f) = 1$ if the two detectors perfectly overlap.

2.5.4 Variance of the ORF (Gaussian SGWB)

The ORF can be interpreted as arising from the *mean value* in an ensemble average of GW measurements. Hence its properties can be characterized by a *variance* which should be taken into account when confronting theory with experiment.
There are several possible contributions to the variance of the ORF, depending on the experiment under consideration.

We can write the most general expression of the variance as:

$$\sigma^2_{AB} = \langle s_{AB} s_{AB} \rangle - \langle s_{AB} \rangle^2 = \langle s_A s_B s_A s_B \rangle - \langle s_A s_B \rangle^2. \tag{68}$$

At this point we need to differentiate the kind of SGWB that we are trying to study.
For now, let us focus on a Gaussian SGWB : we can then rewrite the four-point function $\langle s_{AB} s_{AB} \rangle$ using the Wick theorem.
In particular, we use that:

$$\langle s_A s_B s_A s_B \rangle = \langle s_A s_B \rangle \langle s_A s_B \rangle + \langle s_A s_A \rangle \langle s_B s_B \rangle + \langle s_B s_A \rangle \langle s_A s_B \rangle \,. \tag{69}$$

Notice that this equation holds only if we are dealing with a Gaussian SGWB, otherwise we should take into account also the presence of a *connected* part. We will see this in section 4.

Finally, we get that :

$$\sigma^2_{AB} = \langle s_A s_B s_A s_B \rangle - \langle s_A s_B \rangle^2 = \langle s_A s_B \rangle \langle s_A s_B \rangle + \langle s_A s_A \rangle \langle s_B s_B \rangle = \langle s_{AB} \rangle^2 + \langle s_{AA} \rangle \langle s_{BB} \rangle. \tag{70}$$

This relation holds for a general ORF: indeed, we are not specifying what kind of detectors we are taking into account.
This variance is known as *total variance* and we will cover it in detail in the case of PTAs.

2.5.5 Optimal Filtering

As we have said, the correlated output of two detectors is given by:

$$S_{AB} = \int_{-\infty}^{+\infty} df\, \tilde{S}_A^*(f)\tilde{S}_B(f)\tilde{Q}(f)\,. \tag{71}$$

We now find the optimal choice of the filter function $\tilde{Q}(f)$, following [32, 10].

First of all, we notice that in the unphysical region $f < 0$ we have that $S_h(f) = S_h(-f)$: this tells us that $\tilde{Q}(f) = \tilde{Q}(-f)$ and that $\tilde{Q}(f)$ is real (so that $\tilde{Q}(f) = \tilde{Q}^*(-f)$ and $Q(t)$ is real).
We consider the variation of S_{AB} from its average value,

$$N \equiv S_{AB} - \langle S_{AB}\rangle\,. \tag{72}$$

By definition $\langle N\rangle = 0$, while

$$\begin{aligned}\langle N^2\rangle =& \langle S_{AB}^2\rangle - \langle S_{AB}\rangle^2 = \int_{-\infty}^{\infty} df df'\, \tilde{Q}(f)\tilde{Q}^*(f')\times \\ &\times \left[\langle \tilde{S}_A^*(f)\tilde{S}_B(f)\tilde{S}_A(f')\tilde{S}_B^*(f')\rangle - \langle \tilde{S}_A^*(f)\tilde{S}_B(f)\rangle\langle \tilde{S}_B^*(f')\tilde{S}_A(f')\rangle\right]\,.\end{aligned} \tag{73}$$

We are interested in the case $n_i \gg h_i$: this means that $S_i \simeq n_i$.
Moreover, if the noise in a single detector has a Gaussian distribution and the noise in the two detectors is uncorrelated, equation 73 becomes:

$$\langle N^2\rangle \simeq \int_{-\infty}^{\infty} df df'\, \tilde{Q}(f)\tilde{Q}^*(f')\langle \tilde{S}_A^*(f)\tilde{S}_A(f')\rangle\langle \tilde{S}_B^*(f')\tilde{S}_B(f)\rangle. \tag{74}$$

At this point, we recall the relation given by 55. We then can write:

$$\langle \tilde{S}_i^*(f)\tilde{S}_i(f')\rangle \simeq \langle \tilde{n}_i^*(f)\tilde{n}_i(f')\rangle = \delta(f-f')\frac{1}{2}S_n^{(i)}(f)\,. \tag{75}$$

Using $\delta(0) = T$, we therefore get

$$\langle N^2\rangle = \frac{T}{4}\int_{-\infty}^{\infty} df\, |\tilde{Q}(f)|^2 S_n^2(f)\,, \tag{76}$$

where we have defined

$$S_n(f) = \left[S_n^{(A)}(f)S_n^{(B)}(f)\right]^{1/2}\,. \tag{77}$$

From here, we can define the *signal-to-noise-ratio SNR*,

$$\mathrm{SNR} = \left[\frac{\langle s_{AB}\rangle}{\langle N^2\rangle^{1/2}}\right]^{1/2} . \tag{78}$$

Notice that in this definition we have taken the square root since s_{AB} is quadratic in the signal: in this way the SNR is linear in the signal.

We now want to look for the function $\tilde{Q}(f)$ that maximizes the SNR.
For two arbitrary complex functions $M(f), L(f)$, we define the (positive definite) scalar product:

$$(M, L) = \int_{-\infty}^{\infty} df\, M^*(f) L(f) S_n^2(f)\,. \tag{79}$$

Then

$$\langle N^2\rangle = \frac{T}{4}(\tilde{Q}, \tilde{Q}) \tag{80}$$

and, from 64,

$$\langle s_{AB}\rangle = \frac{T}{2}(\tilde{Q}, \frac{S_h \Gamma_{AB}}{S_n^2}). \tag{81}$$

Then we have to maximize

$$(\mathrm{SNR})^4 = \frac{\langle s_{AB}\rangle^2}{\langle N^2\rangle} = T(\tilde{Q}, \frac{\Gamma_{AB} S_h}{S_n^2})^2 \frac{1}{(\tilde{Q}, \tilde{Q})}. \tag{82}$$

The solution of this variational problem is standard.
In fact, this problem is equivalent to having a fixed three-dimensional vector $\vec{A}$ and wanting to find the vector $\vec{Q}$ that maximizes the ratio $(\vec{Q}\cdot\vec{A})^2/(\vec{Q}\cdot\vec{Q})$.
We know that the answer is choosing $\vec{Q}$ pointing in the same direction as $\vec{A}$.
Therefore we get that:

$$\tilde{Q}(f) = c\frac{\Gamma_{AB}(f) S_h(f)}{S_n^2(f)} \tag{83}$$

with c an arbitrary normalization constant.

One of the curious features of the optimal filter function $\tilde{Q}(f)$ is that it depends on the power spectral density (PSD) $S_h(f)$, which we recall is strictly related to the spectrum of the SGWB Ω_{SGWB} via 44.
This tells us that when we perform the data analysis, we should consider a set of possible filters.

Finally, we can now write down the value of the SNR obtained with the optimal filter:

$$(\mathrm{SNR})^4 = T(\frac{\Gamma S_h}{S_n^2}, \frac{\Gamma S_h}{S_n^2})\,, \tag{84}$$

or

$$\mathrm{SNR} = \left[2T \int_0^\infty df\, \Gamma_{AB}^2(f) \frac{S_h^2(f)}{S_n^2(f)}\right]^{1/4}\,. \tag{85}$$

3 Pulsar Timing Arrays and Interferometers

In this chapter, we cover in detail PTAs and interferometers.
We first introduce pulsars and then focus on PTAs: we recover the Hellings-Downs curve and investigate the statistical meaning of its variance.
We then pass on to interferometers: in particular, we explicitly compute the two-point correlator for the response of two interferometers to a common SGWB.

3.1 Pulsar Timing Arrays

3.1.1 Pulsars

A pulsar (pulsating star, on the model of quasar) is a highly magnetized rotating neutron star [4] that emits beams of electromagnetic radiation out of its magnetic poles.
Since their discovery in 1967 by Susan Jocelyn Bell, Antony Hewish and collaborators [33], pulsars have helped us understand many open questions in physics.
Pulsars are rapidly spinning, with periods as small as 1 ms. This is related to how these objects are created: since angular momentum is conserved during the collapse of the star to the neutron star, we have that ωr^2 is constant while r decreases from the typical radius of the original star core down to a radius of around 10 km.
Similarly, assuming that also the magnetic flux is conserved during the collapse, neutron stars have huge magnetic fields (around 10^{12} gauss and higher). This magnetic field is usually not aligned with the rotation axis, so it has the structure of a rotating dipole (see figure 3).

If ρ is the distance from the rotation axis, there is a critical distance ρ_c such that the magnetic field lines that reach distances larger than this ρ_c ($\rho > \rho_c$) can get to infinity, while the others are closed. Inside the cylinder of radius ρ_c there is a "magnetosphere" composed of ionized plasma mostly corotating with the neutron star.
High-energy particles in the magnetosphere emit radiation that can be observed (most easily in the radio waves) and preferentially beamed along the magnetic poles. Basically, each beam draws a circle in the sky.

[4] Neutron stars are collapsed cores of massive stars that have undergone supernovae, leaving only small $\sim 10 - 15$ km objects that are supported against gravitational collapse by neutron degeneracy pressure.

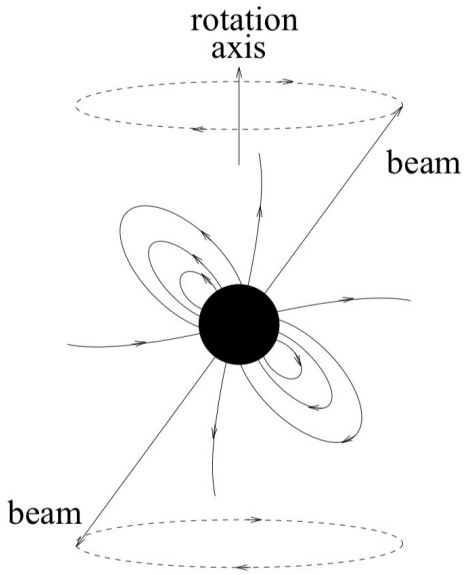

Figure 3: Pulsar magnetosphere and the outgoing beams of radiation. Figure taken from [18].

This means that an observer that happens to be along one point of this circle receives a short radio pulse when the beam of radiation sweeps along her line of sight: this is known as "lighthouse model". The pulse period is then a measure of the pulsar's rotation period. Given the high value of the moment of inertia of neutron stars, we expect the pulse period to be extremely stable.
To be precise, if we observe single pulses from a given pulsar we find that each pulse from one rotation to the next varies randomly, reflecting fluctuations in the radiation mechanism due to the complex dynamics of the magnetosphere. However, the pulse shape *averaged* over rotations is remarkably stable: this can be considered as a fingerprint of the pulsar. This stability allows for precision timing. As a result, we have an exceptional precision regarding pulsars' data since these objects are astonishing time keepers.

Therefore, this extremely precise fingerprint of the pulsar allows us to easily recognise deviations from it when we are observing times of arrival ($TOAs$).
These phase offsets must be produced by physics happening between us and the pulsars: this means that by analysing these variations in time we can obtain information about these physical phenomena. In particular, we are most interested in how *gravitational waves* modify the pulse profile.
Notice that the TOAs of the pulses in a Earth-based laboratory are also modulated

by many other time-dependent factors that should be taken into account. For example, we must consider the motion of the Earth around the Sun (and of the Sun around the solar system barycenter) and the presence of the gravitational field of the solar system.
For a deeper investigation on precision pulsar timing see [17].

3.1.2 Pulsar Timing Arrays and Experiments

We now discuss how pulsar timing arrays (PTAs) can be used to search for SGWBs.
A gravitational wave passing between a pulsar and the Earth induces a shift in the observed times of arrival of the pulses. However, for only a single pulsar, this kind of alteration will be hidden by many other effects and sources of noise. All these additional masking effects can be mitigated by correlating the signals from multiple pulsars.
A SGWB induces correlations among the timing residuals of different pulsars, leaving a distinct trace.
For example, if we look for the signature of a SGWB correlating the timing residuals, we obtain the Hellings-Downs curve (see section 3.1.4).
In contrast to ground based and space based GW observatories, the Earth–pulsar distance effectively plays the role of an interferometric arm. This allows us to explore the nanohertz GW band (as we have seen in figure 2). These frequencies probe both astrophysical sources, such as supermassive binary black holes, and cosmological sources, such as early-Universe phase transitions or cosmic strings.

Current PTAs are, as we have seen, the North American Nanohertz Observatory for Gravitational Waves (NANOGrav) [34], the Parkes Pulsar Timing Array (PPTA) [35] and the European Pulsar Timing Array (EPTA) [36] , which together form the International Pulsar Timing Array (IPTA) [37]. There are also other experiments, such as the Chinese Pulsar Timing Array (CPTA) [5].
These collaborations have been collectively observing about a hundred millisecond pulsars for years now in hopes of providing evidence of the SGWB.
Recent data releases have provided compelling evidence for a common-spectrum stochastic process across millisecond pulsars, consistent with the presence of a SGWB.

3.1.3 GW effect on the timing of a single pulsar

We first want to study what happens when a GW passes between the Earth and a pulsar and in particular how it affects the observed periodicity of the pulses on Earth. We closely follow [38].

We put the Earth at the origin of the coordinate system and we denote by $\hat{\mathbf{n}}_a$ the unit vector from the earth toward the pulsar. Since we are for now considering only one pulsar we can align $\hat{\mathbf{n}}_a$ with the unit vector $\hat{\mathbf{x}}$. We also fix the pulsar to be at a distance d_a , with a given rotational frequency ν_a, so $T_a = 1/\nu_a$ is its rotational period.

To understand how the observed periodicity of the pulsar changes as a GW passes between the Earth and the star we need to study how the photon geodesics are modified.
To do so, we work in the TT gauge, in which the metric can be written as

$$ds^2 = -dt^2 + \left[\delta_{ij} + h_{ij}^{\mathrm{TT}}(t, \mathbf{x})\right] dx^i dx^j. \tag{86}$$

At this point we consider photons emitted at t_{em}, when the beam points toward the Earth. We recall that we've fixed the pulsar along the $\hat{\mathbf{x}}$ axis and that photons travel along null geodesics ($ds^2 = 0$) , therefore these conditions give us:

$$dx^2 = \frac{dt^2}{1 + h_{xx}^{\mathrm{TT}}[t, \mathbf{x}(t)]}, \tag{87}$$

where $\mathbf{x(t)}$ is the photon trajectory.

We also need to take into account that we are describing photons traveling from the pulsar, at $\mathbf{x} = d_a\hat{\mathbf{x}}$, toward the observer at $\mathbf{x} = 0$, therefore in the $-\hat{\mathbf{x}}$ direction. We then have:

$$dx = -\frac{dt}{\left\{1 + h_{xx}^{\mathrm{TT}}[t, \mathbf{x}(t)]\right\}^{1/2}} = -\left\{1 - \tfrac{1}{2} h_{xx}^{\mathrm{TT}}[t, \mathbf{x}(t)]\right\} dt \tag{88}$$

where the second equality holds at first order in h.

Thus, the photons will arrive at the observer on Earth at a time t_{obs} given by:

$$d_a = t_{\mathrm{obs}} - t_{\mathrm{em}} - \frac{1}{2}\int_{t_{\mathrm{em}}}^{t_{\mathrm{obs}}} dt'\, h_{xx}^{\mathrm{TT}}[t', \mathbf{x}(t')]. \tag{89}$$

Since we expect h_{xx}^{TT} to be a small quantity, we can replace t_{obs} in the integral by its zeroth-order value $t_{obs} = t_{em} + d_a$ and for the photons' trajectory we can

take the unperturbed path $\hat{\mathbf{x}}$=$(t_{obs} - t)\hat{\mathbf{n}}_a$.

We also should generalize this expression to the case where the pulsar is not necessarily along the $\hat{\mathbf{x}}$ axis: to achieve this, we must replace $h^{\rm TT}_{xx}$ with $n^i_a n^j_a h^{TT}_{ij}$. Consequently, we obtain to first order in h:

$$t_{\rm obs} = t_{\rm em} + d_a + \frac{n^i_a n^j_a}{2}\int_{t_{\rm em}}^{t_{\rm em}+d_a} dt'\, h^{\rm TT}_{ij}[t', (t_{em} + d_a - t')\hat{\mathbf{n}}_a]. \tag{90}$$

Notice that the dependence of t_{obs} on the GW is fully given by the factor $h^{\rm TT}_{ij}$ in the integrand since in the TT gauge the coordinates $x = 0$ and $x = d_a$ are *defined* by, respectively, the position of the Earth and of the pulsar, even when the GW is passing.

Consider now photons emitted after one rotational period at $t'_{em} = t_{em} + T_a$, which is when the beam of the pulsar is again pointed toward the Earth.

We expect that they will be observed at a time t'_{obs} given by:

$$\begin{aligned} t'_{\rm obs} &= t_{\rm em} + T_a + d_a + \frac{n^i_a n^j_a}{2}\int_{t_{\rm em}+T_a}^{t_{\rm em}+T_a+d_a} dt'\, h^{\rm TT}_{ij}[t', (t_{\rm em} + T_a + d_a - t')\hat{\mathbf{n}}_a] \\ &= t_{\rm em} + T_a + d_a + \frac{n^i_a n^j_a}{2}\int_{t_{\rm em}}^{t_{\rm em}+d_a} dt'\, h^{\rm TT}_{ij}[t' + T_a, (t_{\rm em} + d_a - t')\hat{\mathbf{n}}_a] \end{aligned} \tag{91}$$

where notice that we have defined $t' = t'' + T_a$ and then we have renamed t'' as t'.

Then, subtracting 91 from 90:

$$t'_{\rm obs} - t_{\rm obs} = T_a + \Delta T_a \tag{92}$$

where

$$\Delta T_a = \frac{n^i_a n^j_a}{2}\int_{t_{\rm em}}^{t_{\rm em}+d_a} dt' \left\{h^{\rm TT}_{ij}[t' + T_a, \mathbf{x}_0(t')] - h^{\rm TT}_{ij}[t', \mathbf{x}_0(t')]\right\} \tag{93}$$

and

$$\mathbf{x}_0(t') = (t_{\rm em} + d_a - t')\hat{n}_a. \tag{94}$$

From 92 we can explicitly see how the time separation between two consecutive pulses observed by Earth is not only the rotational period T_a but also has an extra term ΔT_a induced by the GW.

We now recall that for pulsars we have $T_a \sim ms$, while the GWs that can be detected have periods $T_{gw} = 2\pi/\omega_{gw}$ of the order of the observation time, of order 10 years. This means that we expect $\omega_{gw} T_a$ to be extremely small: we can therefore Taylor-expand $h_{ij}^{\rm TT}[t' + T_a, \mathbf{x}_0(t')]$ to first order in T_a, finally obtaining:

$$\frac{\Delta T_a}{T_a} = \frac{1}{2} n_a^i n_a^j \int_{t_{\rm em}}^{t_{\rm em}+d_a} dt' \left[\frac{\partial}{\partial t'} h_{ij}^{\rm TT}(t', \mathbf{x}) \right]_{\mathbf{x}=\mathbf{x}_0(t')} . \tag{95}$$

We observe that the partial derivative is acting only on the first argument and not on the time dependence in $\mathbf{x}(t')$.

In order to find a more explicit expression of $\Delta T_a/T_a$, we consider a monochromatic GW propagating along the $\hat{\mathbf{n}}$ direction :

$$h_{ij}^{\rm TT}(t, \mathbf{x}) = A_{ij}(\hat{\mathbf{n}}) \cos[\omega_{\rm gw}(t - \hat{\mathbf{n}} \cdot \mathbf{x})] \, . \tag{96}$$

Substituting this into equation 95, considering $\hat{n}^i A_{ij}(\hat{\mathbf{n}}) = 0$ and that at first order $t_{obs} = t_{em} + d_a$, we get:

$$\begin{aligned} \frac{\Delta T_a}{T_a} &= \frac{1}{2} n_a^i n_a^j \int_{t_{\rm em}}^{t_{\rm em}+d_a} dt' \left[A_{ij}(\hat{\mathbf{n}}) \frac{\partial}{\partial t'} \cos[\omega_{\rm gw}(t' - \hat{\mathbf{n}} \cdot \mathbf{x})] \right]_{\mathbf{x}=\mathbf{x}_0(t')} = \\ &= \frac{n_a^i n_a^j A_{ij}}{2(1 + \hat{\mathbf{n}} \cdot \hat{\mathbf{n}}_a)} \big[\cos(\omega_{\rm gw} t_{\rm obs}) - \cos(\omega_{\rm gw} t_{em} - \omega_{\rm gw} \tau_a \, \hat{\mathbf{n}} \cdot \hat{\mathbf{n}}_a) \big], \end{aligned} \tag{97}$$

where $\tau_a = d_a$ is the standard light travel time between the pulsar and the Earth.
Finally, we define the quantity :

$$z_a(t) = \frac{\nu_0 - \nu(t)}{\nu_0} = \frac{\Delta T_a}{T_a}. \tag{98}$$

Thus $z_a(t) = -(\Delta\nu_a/\nu_a)(t) = \Delta T_a/T_a$. Therefore, we can write:

$$z_a(t) = \frac{n_a^i n_a^j}{2(1 + \hat{\mathbf{n}} \cdot \hat{\mathbf{n}}_a)} \left[h_{ij}^{\rm TT}(t, \mathbf{x} = 0) - h_{ij}^{\rm TT}(t - \tau_a, \mathbf{x}_a) \right] , \tag{99}$$

where now t_{obs} is simply t and the pulsar's position is $\mathbf{x}_a = d_a \hat{\mathbf{n}}_a$ while $\mathbf{x} = 0$ is the observer's position.

We can also define the timing residuals R_a of the a-th pulsar as:

$$R_a(t) = \int_0^t dt' \, z_a(t'). \tag{100}$$

3.1.4 Response to a stochastic GW background

We now want to apply what we've found to the case of a stochastic background of gravitational waves. As we've seen, for this kind of signal we consider the form (see equation 37)

$$h_{ij}(t,\mathbf{x}) = \sum_{P=+,\times} \int_{-\infty}^{\infty} df \int d^2\hat{\mathbf{n}}\, \tilde{h_P}(f,\hat{\mathbf{n}})\, e^P_{ij}(\hat{\mathbf{n}})\, e^{-2\pi i f\,(t-\hat{\mathbf{n}}\cdot\mathbf{x})}. \tag{101}$$

We recall that the polarization tensors $\hat{e}^+(\hat{\mathbf{n}})$ and $\hat{e}^\times(\hat{\mathbf{n}})$ are given in 18, while $\tilde{h}_P(f,\hat{\mathbf{n}})$ are complex random fields that define the statistical properties of the stochastic background. We work in the TT gauge.
We insert this expression in equation 99 and we get :

$$z_a(t) = \sum_{P=+,\times} \int_{-\infty}^{\infty} df \int d^2\hat{\mathbf{n}}\, \tilde{h_P}(f,\hat{\mathbf{n}})\, F^P_a(\hat{\mathbf{n}})\, e^{-2\pi i f t}\left[1 - e^{2\pi i f \tau_a(1+\hat{\mathbf{n}}\cdot\hat{\mathbf{n}}_a)}\right], \tag{102}$$

where

$$F^P_a(\hat{\mathbf{n}}) = \frac{n^i_a n^j_a e^P_{ij}(\hat{\mathbf{n}})}{2\,(1+\hat{\mathbf{n}}\cdot\hat{\mathbf{n}}_a)}. \tag{103}$$

Notice that the above quantity is the equivalent, for the a-th pulsar, of the pattern function of the i-th detector (see 60).

Since we are studying the interaction with a SGWB, we are interested in the quantity $\langle z_a(t) z_b(t)\rangle$, where the brackets denote the ensemble average over the stochastic variables $\tilde{h}_P(f,\hat{\mathbf{n}})$.
Assuming that the GW background is stationary, isotropic, unpolarized and gaussian, the ensemble average can be computed using equation 40 that we rewrite here:

$$\langle \tilde{h}^*_P(f,\hat{\mathbf{n}}) \tilde{h}_{P'}(f',\hat{\mathbf{n}}')\rangle = \delta(f-f')\,\frac{\delta^2(\hat{\mathbf{n}},\hat{\mathbf{n}}')}{4\pi}\,\delta_{PP'}\,\frac{1}{2}S_h(f). \tag{104}$$

This gives us :

$$\langle z_a(t) z_b(t)\rangle = \frac{1}{2}\int_{-\infty}^{\infty} df\, S_h(f) \int \frac{d^2\hat{\mathbf{n}}}{4\pi}\,\mathcal{K}_{ab}(f;\hat{\mathbf{n}}) \sum_{P=+,\times} F^P_a(\hat{\mathbf{n}}) F^P_b(\hat{\mathbf{n}}), \tag{105}$$

with

$$\mathcal{K}_{ab}(f;\hat{\mathbf{n}}) = \left[1 - e^{-2\pi i f \tau_a(1+\hat{\mathbf{n}}\cdot\hat{\mathbf{n}}_a)}\right]\left[1 - e^{+2\pi i f \tau_b(1+\hat{\mathbf{n}}\cdot\hat{\mathbf{n}}_b)}\right]. \tag{106}$$

There is something quite interesting about this equation: by comparing it to equation 65 we can see that the integral over $d^2\hat{\mathbf{n}}$ is the equivalent of the overlap reduction function in the case of two GW interferometers.

We also notice that in $\mathcal{K}_{ab}(f;\hat{\mathbf{n}})$ the two terms in each square brackets originate from the terms $h_{ij}^{\mathrm{TT}}(t,\mathbf{x}=0)$ and $h_{ij}^{\mathrm{TT}}(t-\tau_a,\mathbf{x}_a)$ in equation 99.

Thus, the four terms obtained by expanding 106 correspond to terms derived by computing separately:

$$\begin{aligned}&\langle h_{ij}(t,\mathbf{x}=0)\,h_{kl}(t,\mathbf{x}=0)\rangle, \quad \langle h_{ij}(t,\mathbf{x}=0)\,h_{kl}(t-\tau_b,\mathbf{x}_b)\rangle,\\ &\langle h_{ij}(t-\tau_a,\mathbf{x}_a)\,h_{kl}(t,\mathbf{x}=0)\rangle, \quad \langle h_{ij}(t-\tau_a,\mathbf{x}_a)\,h_{kl}(t-\tau_b,\mathbf{x}_b)\rangle.\end{aligned} \tag{107}$$

Let us now focus on these contributions: we observe that terms at different spacetime points are negligible. This can be explained by the fact that PTAs are sensitive to GWs with a period $T = O(10)$ yr. This is very small compared with the times τ_a and τ_b taken by the electromagnetic signals to travel from the pulsars to the observer. This means that $h_{ij}(t,\mathbf{x}=0)$ and $h_{kl}(t-\tau_a,\mathbf{x}_a)$ are uncorrelated, the same holds for $h_{ij}(t,\mathbf{x}=0)$ and $h_{kl}(t-\tau_b,\mathbf{x}_b)$. Similarly, also the terms at the space-time location of the two pulsars will be uncorrelated to each other.

From this, one can see that the last three terms of 107 are negligible with respect to $\langle h_{ij}(t,\mathbf{x}=0)\,h_{kl}(t,\mathbf{x}=0)\rangle$.

Thus, we can replace

$$K_{ab}(f;\hat{\mathbf{n}}) \simeq 1. \tag{108}$$

Under this approximation, we can write:

$$\langle z_a(t) z_b(t)\rangle = \frac{1}{2}\int_{-\infty}^{\infty} df\, S_h(f) \int \frac{d^2\hat{\mathbf{n}}}{4\pi} \sum_{P=+,\times} F_a^P(\hat{\mathbf{n}}) F_b^P(\hat{\mathbf{n}}). \tag{109}$$

Finally, it's possible to analytically perform the angular integral and the result is given by:

$$C(\zeta) = \int \frac{d^2\hat{\mathbf{n}}}{4\pi} \sum_{P=+,\times} F_a^P(\hat{\mathbf{n}}) F_b^P(\hat{\mathbf{n}}) = x_{ab}\ln x_{ab} - \tfrac{1}{6}x_{ab} + \tfrac{1}{3}, \tag{110}$$

where

$$x_{ab} = \tfrac{1}{2}\left(1-\cos\zeta\right), \tag{111}$$

and ζ is the angle between the vectors pointing from the Earth towards pulsar a and b respectively. This expression for $C(\zeta)$ is known as Hellings-Downs curve. This function is shown in Figure 3.1.4 and the calculations to obtain it can be found in Appendix 5.

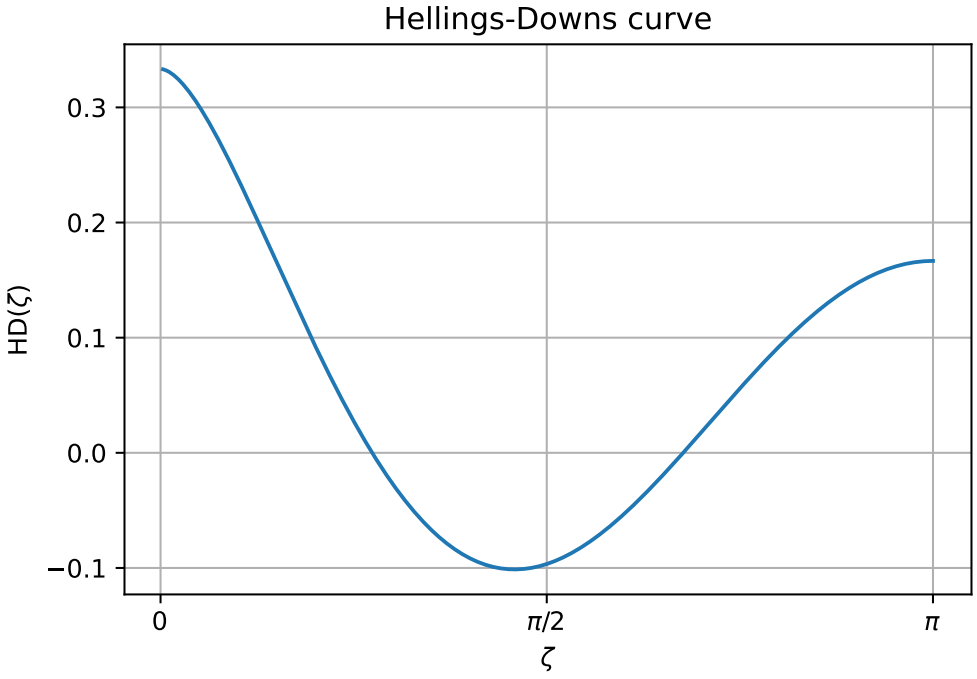

Figure 4: Hellings-Downs curve

We have therefore obtained the curve characterizing the response of two pulsar–Earth baselines to an isotropic stochastic gravitational-wave background.

We notice that using $S_h(f) = S_h(-f)$, we finally obtain:

$$\langle z_a(t) z_b(t) \rangle = C(\zeta) \int_0^\infty df\, S_h(f). \tag{112}$$

It is also interesting to write the result in terms of the correlation between the timing residuals $R_a(t)$ (defined in equation 100):

$$r_{ab}(t) \equiv \langle R_a(t) R_b(t) \rangle. \tag{113}$$

To do so, we insert equation 102 in equation 100 and get:

$$\begin{aligned} R_a(t) &= \int_0^t dt' \sum_{P=+,\times} \int_{-\infty}^{\infty} df \int d^2\hat{\mathbf{n}}\, \tilde{h}_P(f, \hat{\mathbf{n}})\, F_a^P(\hat{\mathbf{n}})\, e^{-2\pi i f t'} \\ &= \sum_{P=+,\times} \int_{-\infty}^{\infty} df \int d^2\hat{\mathbf{n}}\, \tilde{h}_P(f, \hat{\mathbf{n}})\, F_a^P(\hat{\mathbf{n}})\, \frac{1}{(-2\pi i f)} \left(e^{-2\pi i f t} - 1 \right). \end{aligned} \tag{114}$$

By computing again the correlation we get:

$$\begin{aligned} r_{ab}(t) &= \langle R_a(t) R_b(t) \rangle \\ &= \langle \sum_{P=+,\times} \int_{-\infty}^{\infty} df \int d^2\hat{\mathbf{n}}\, \tilde{h}_P(f,\hat{\mathbf{n}})^*\, F_a^P(\hat{\mathbf{n}})\, \frac{1}{(+2\pi i f)} \left(e^{+2\pi i f t} - 1\right) \\ &\sum_{P'=+,\times} \int_{-\infty}^{\infty} df' \int d^2\hat{\mathbf{n}}'\, \tilde{h}_{P'}(f',\hat{\mathbf{n}}')^*\, F_b^{P'}(\hat{\mathbf{n}}')\, \frac{1}{(-2\pi i f')} \left(e^{-2\pi i f' t} - 1\right) \rangle \\ &= C(\zeta) \int_0^{\infty} df \frac{S_h(f)}{(2\pi f)^2} 2[1 - \cos(2\pi f t)] \end{aligned} \tag{115}$$

We finally notice that this correlator depends explicitly on time.

3.1.5 Hellings-Downs features and statistical meaning

Let us now consider in more detail the Hellings-Downs curve: in particular, we want to first focus on some of its properties and then on its statistical meaning.

We start by discussing the normalization factor: the curve given by 110 is normalized to 1/3 at zero angular separation, while in other papers it is usually normalized to 1/2. Moreover, the case $\zeta = 0$ corresponds to two *distinct* pulsars separated by 0°, which is different from the case of a single pulsar ($a = b$).
In fact, the first case has a correlation coefficient equal to 1/3 or 1/2 (depending on the chosen normalization), while the second case has correlation equal to unity. As explained in [39], the choice of normalization amounts to an overall scaling and physical observables are independent of this convention.
Historically, the factors 1/3 and 1/2 appeared in the literature for different reasons. The value 1/2 arises when the HD curve is interpreted as a correlation coefficient for the redshift response of two pulsars induced by the same GW source.
In this interpretation, one requires that the expected correlation for two identical pulsars is twice that for two distinct pulsars separated by 0°. Since two identical pulsars must have unit correlation, this fixes the normalization to 1/2.
To be consistent with all these information, we consider the Hellings-Downs curve given by:

$$C(\zeta) \;=\; \frac{3}{2}\,\frac{1-\cos\zeta}{2}\,\ln\!\left(\frac{1-\cos\zeta}{2}\right) - \frac{1}{4}\,\frac{1-\cos\zeta}{2} + \frac{1}{2}\,(1+\delta_{ab})\,. \tag{116}$$

Notice that we've now switched to the 1/2 normalization.

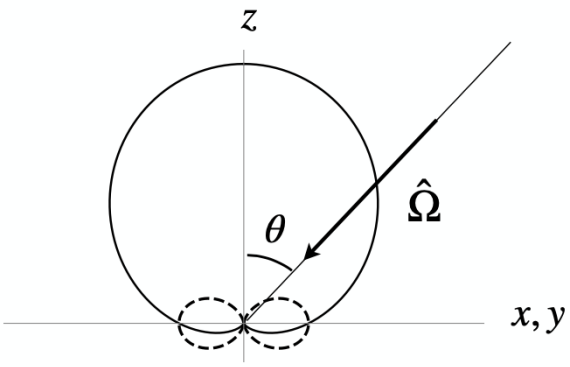

Figure 5: Integrands of the Hellings-Downs correlation curve for two pulsars separated by 0° ($\hat{\mathbf{n}}_a = \hat{\mathbf{n}}_b = \hat{\mathbf{z}}$, solid curve) and by 180° ($\hat{\mathbf{n}}_a = -\hat{\mathbf{n}}_b = \hat{\mathbf{z}}$, dashed curve). Figure taken by [40].

We also want to highlight the fact that the profile $C(\zeta)$ does not depend on the GW frequency. This is related to the approximation that we've considered in equation 108: we have in fact neglected the terms containing the frequency dependence.

Another interesting characteristic of the HD curve is that it is asymmetric: in fact, it has different values at 0° and 180°.
This is related to the different denominators $1 + \hat{\mathbf{n}} \cdot \hat{\mathbf{n}}_a$ and $1 + \hat{\mathbf{n}} \cdot \hat{\mathbf{n}}_b$ which appear in $F^P_{a/b}(\hat{\mathbf{n}})$.
To understand the difference between these two situations, we can study the two cases $\hat{\mathbf{n}}_a = \hat{\mathbf{n}}_b = \hat{\mathbf{z}}$ and $\hat{\mathbf{n}}_a = -\hat{\mathbf{n}}_b = \hat{\mathbf{z}}$: this distinction is clearly shown in figure 5, where we can see the integrand $F^+_a(\hat{\mathbf{n}})F^+_b(\hat{\mathbf{n}}) + F^\times_a(\hat{\mathbf{n}})F^\times_b(\hat{\mathbf{n}})$ of the Hellings and Downs correlation for these two different cases.

Notice that in this case $\hat{\mathbf{n}} = \hat{\Omega}$.
Moreover, we can see that if the GWB consisted of waves that only came from directions perpendicular to the Earth-pulsar baselines (in this case the xy-plane), then the values of the HD curve would be the same at 0° and 180°. However, since an isotropic GWB has equal contributions from GWs coming from all directions on the sky, the HD curve results different values for these two cases.
Finally, we notice that the value of the HD curve for two pulsars separated by 180° is exactly half that for the angular separation of 0° (considering two different pulsars) and that the most negative value of the HD curve is not obtained for

90°. This is again a consequence of the fact that $F^P(\hat{\mathbf{n}})$ are not symmetric under $\hat{\mathbf{n}}_{a/b} \to -\hat{\mathbf{n}}_{a/b}$.

We now want to address the statistical meaning of the HD curve: in the previous calculation, we have used equation 40 to write the ensemble average. This process is known as *source averaging approach* [40] and is based on keeping the pulsars fixed and averaging over GW source directions $\hat{\mathbf{n}}$, assuming that the sources are *unpolarized* and *isotropic* in the sky.
This is the operation employed by Hellings and Downs [41] :in doing this, they implicitly assumed that distinct sources were uncorrelated, since they neglected cross-terms arising from the interference between different GW sources. This is valid if we compute an average over many possible realizations of the gravitational-wave source population (i.e. over many statistical realizations of the Universe). In any given realization, however, these cross-terms do not vanish, but instead contribute to statistical fluctuations around the Hellings–Downs curve.

The second form of averaging is called *pulsar averaging*. Originally employed by Cornish and Sesana [42], for a fixed set of GW sources we average the correlation over all pulsar pairs separated by the same angle, assuming that one has access to a large number of pulsar pairs uniformly distributed on the sky.
Pulsar averaging corresponds to observational practice. In fact, PTA collaborations observe many pulsars distributed across the sky, so they can average together the correlations from all pulsar pairs lying in an angular separation bin centered on an angle. As more pulsars are added to a PTA, this pulsar averaging will get closer to ideal pulsar averaging, where, in principle, we have access to an infinite number of pulsar pairs uniformly distributed over the sky.

In contrast, source averaging is not observationally possible, since we have access to only one Universe and its associated (fixed) collection of GW sources. As shown in [39], pulsar averaging yields the same mean correlation as the original Hellings and Downs source-averaging prescription for a single GW source, while for multiple GW sources the result of pulsar averaging is more complicated.

Finally, we present the PTA data reported by the NANOGrav collaboration [2] to show the behaviour that we actually expect from observations. This is shown in figure 6.

We therefore highlight that PTA observations provide an estimate of the correlation obtained by averaging the measured cross-correlations over all pulsar pairs that share approximately the same angular separation. This empirical procedure

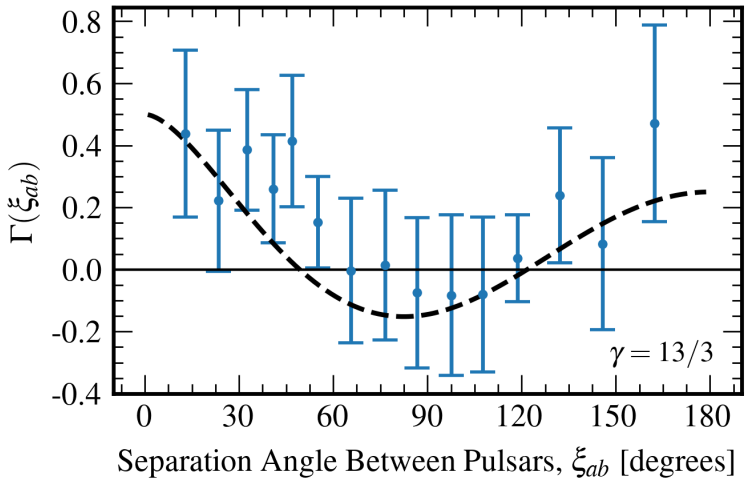

Figure 6: The spatial correlations observed in the pulsar timing residuals for the NANOGrav 15-year dataset [2] are shown in blue while the HD curve/prediction is shown in black. The blue points and error bars are weighted averages of approximately 150 pulsar-pair correlations in each angular separation bin, which take into account covariances between the correlations induced by the GWB itself.

represents a *finite-sample* version of the ideal pulsar averaging discussed above. However, the average is performed using only the actual set of observed pulsars, which are limited in number and unevenly distributed across the sky. As a result, the measured correlation is not the ensemble-averaged Hellings–Downs function, but a single statistical realization constructed from this particular pulsar sample and from the specific gravitational-wave background present in our Universe. Consequently, PTA observations should be interpreted as statistical estimators of the Hellings–Downs correlation, whose variance sets a fundamental limit on how closely measured correlations can approach the ensemble-averaged prediction.

We now wish to address more in detail the Hellings-Downs variance.

3.1.6 HD's variance

As we have said, there are many collaborations studying collectively around a hundred pulsars. Even if the data are coherent with predictions for many possible GW sources, the noise in the present PTA data sets is still too large to allow us to infer whether the spatial correlations are due to SGWB.
This may be due, among other factors, to the limitations in the optimal statistic analysis, but recently the question of whether variances in the Hellings-Downs

correlation also play a role has been put forward.
We expect that these variances also bring information about the nature of the sources. This means that it can be interesting to pay attention also to these quantities. Therefore, we now want to address the case of the Hellings-Downs curve's variance.

We can find many possible variances for the HDs curve: this is related to what kind of effects we are taking into account.
The first variance that we want to address is the *total variance*: this is defined as the variance of a single pulsar pair, whose pulsar timing residuals are correlated by the SGWB.

The explicit form of this variance can be obtained by computing the terms of 70 using 64. By doing so, we get that the variance between two pulsars (A, B) is given by an integral that depends on :

$$\Sigma^2_{\text{disc}}(f, f') = \Gamma_{AB}(f)\Gamma_{AB}(f') + \Gamma_{AA}(f)\Gamma_{AA}(f'). \tag{117}$$

where we recall that $\Gamma_{AB}(f)$ is the overlap reduction function for two pulsars. This is coherent with [43].
These are the only contributions to the so called *total variance* when we are considering a Gaussian SGWB.

This variance quantifies all the possible effects that give us statistical fluctuations around the HDs: mainly, it includes the so-called *cosmic variance* and the *pulsar variance*.
This is the type of variance that we will extend to the non-Gaussian SGWB case in the next section.
At this point, we want to focus on the mentioned contributions to the total variance.
We start with the *cosmic variance*. See for example [43], [39].

To better understand this term, we may ask whether, in the future, with more sensitive telescopes, a larger number of pulsars, and longer observing times, PTA experiments will recover the Hellings–Downs curve exactly.

If we could average over an infinite set of statistical realizations of the gravitational-wave source population (i.e. over an ensemble of possible universes sharing the same statistical properties), we would recover the Hellings–Downs curve exactly, since it is defined as this ensemble average. However, in any given realization, such as our own Universe, we would find something different from the curve.

The difference between what we would observe in a specific realization and the ensemble-averaged over many universes is the so called *cosmic variance*.

This effect arises because, in our Universe, we know that there are many GW sources radiating at frequencies that are close enough that they cannot be resolved individually by PTA experiments. The gravitational-wave background is therefore produced by the incoherent superposition of a large number of independent emitters with random phases. As a consequence, the resulting signal is a stochastic field and any single realization exhibits statistical fluctuations with respect to its ensemble average. In the following, we outline how the explicit expression of the cosmic variance can be derived, closely following [43].
In order to do so, let us consider two pulsars A and B. We need to introduce
the correlation operator, given by :

$$\mathbf{\Gamma}_{AB} = \boldsymbol{\beta}_A^\dagger \boldsymbol{\beta}_B \,, \tag{118}$$

where the quantity $\boldsymbol{\beta}_A$ admits the multipolar expansion given by

$$\boldsymbol{\beta}_A = \sum_{lm} \boldsymbol{b}_{lm} Y_{lm} \left(\hat{\mathbf{n}}_A\right) \tag{119}$$

with $\hat{\mathbf{n}}_A$ is the unit vector pointing from earth toward the pulsar A. The quantities $\mathbf{\Gamma}_{AB}$ and $\boldsymbol{\beta}_A$ represent the SGWB induced spatial correlation.
The ORF can then be obtained by considering the *ensemble* average, denoted by $\langle \cdots \rangle$, of the correlation operator.
We can substitute (119) into (118) and take the ensemble average to obtain

$$\langle \boldsymbol{\beta}_A^\dagger \boldsymbol{\beta}_B \rangle = \sum_{l_1 m_1} \sum_{l_2 m_2} \langle \boldsymbol{b}_{l_1 m_1}^\dagger \boldsymbol{b}_{l_2 m_2} \rangle Y_{l_1 m_1}^* \left(\hat{\mathbf{n}}_A\right) Y_{l_2 m_2} \left(\hat{\mathbf{n}}_B\right) \,. \tag{120}$$

Then, assuming spatial isotropy, we write down

$$\langle \boldsymbol{b}_{l_1 m_1}^\dagger \boldsymbol{b}_{l_2 m_2} \rangle = C_{l_1} \delta_{l_1 l_2} \delta_{m_1 m_2} \,, \tag{121}$$

where the C_l's are the power spectrum multipoles of the SGWB (see [44]).
The ensemble average of the correlation operator reduces to

$$\langle \boldsymbol{\beta}_A^\dagger \boldsymbol{\beta}_B \rangle = \sum_{lm} C_l Y_{lm}^* \left(\hat{\mathbf{n}}_A\right) Y_{lm} \left(\hat{\mathbf{n}}_B\right) \,. \tag{122}$$

At this point, we want to use the completeness identity of the spherical harmonics:

$$P_l \left(\hat{\mathbf{n}}_A \cdot \hat{\mathbf{n}}_B\right) = \frac{4\pi}{2l+1} \sum_m Y_{lm}^* \left(\hat{\mathbf{n}}_A\right) Y_{lm} \left(\hat{\mathbf{n}}_B\right) \,, \tag{123}$$

where $P_l(x)$'s are the Legendre polynomials. Using this relation, we can write

$$\langle \boldsymbol{\beta}_A^\dagger \boldsymbol{\beta}_B \rangle = \sum_l \frac{2l+1}{4\pi} C_l P_l \left(\hat{\mathbf{n}}_A \cdot \hat{\mathbf{n}}_B \right) , \tag{124}$$

which is the expression of the ORF given the angular power spectrum multipoles C_l (see [44]).
This allows us to identify the ORF with the correlation operator:

$$\Gamma_{AB} \left(\zeta \right) = \langle \boldsymbol{\beta}_A^\dagger \boldsymbol{\beta}_B \rangle , \tag{125}$$

where ζ is the angle between the two pulsars observed from Earth.

We are now ready to compute the cosmic variance. In order to isolate this quantity, we perform a full sky averaging with a fixed angle over a pulsar pair. This averaging represents the limit of an infinitely dense PTA uniformly sampling the sky. In symbols, we write this as

$$\{ \cdots \}_{\mathrm{S}} = \text{full sky averaging} = \int d\Omega d\Omega' \cdots d\Omega'' \left(\cdots \right) . \tag{126}$$

The two point spherical harmonics can then be identified as [45]:

$$\{ Y^*_{l'm'} \left(\hat{\mathbf{n}}' \right) Y_{lm} \left(\hat{\mathbf{n}} \right) \}_{\mathrm{S}} = P_l \left(\cos \zeta \right) \frac{\delta_{ll'} \delta_{mm'}}{4\pi} , \tag{127}$$

where ζ corresponds to the fixed separation angle on the sky.

To consider full sky averaging, we compute:

$$\begin{aligned} \{ \boldsymbol{\beta}_A^\dagger \boldsymbol{\beta}_B \}_{\mathrm{S}} &= \sum_{l_1 m_1} \sum_{l_2 m_2} \boldsymbol{b}^\dagger_{l_1 m_1} \boldsymbol{b}_{l_2 m_2} \{ Y^*_{l_1 m_1} \left(\hat{\mathbf{n}}_A \right) Y_{l_2 m_2} \left(\hat{\mathbf{n}}_B \right) \}_{\mathrm{S}} \\ &= \sum_{l_1 m_1} \sum_{l_2 m_2} \boldsymbol{b}^\dagger_{l_1 m_1} \boldsymbol{b}_{l_2 m_2} \left(P_{l_1} \left(\cos \zeta \right) \frac{\delta_{l_1 l_2} \delta_{m_1 m_2}}{4\pi} \right) \\ \{ \boldsymbol{\beta}_A^\dagger \boldsymbol{\beta}_B \}_{\mathrm{S}} &= \sum_{lm} \frac{\boldsymbol{b}^\dagger_{lm} \boldsymbol{b}_{lm}}{4\pi} P_l \left(\cos \zeta \right) . \end{aligned} \tag{128}$$

To simplify this further, we define the operator

$$\boldsymbol{C}_l = \sum_m \frac{\boldsymbol{b}^\dagger_{lm} \boldsymbol{b}_{lm}}{2l+1} , \tag{129}$$

which is related to the power spectrum multipoles (121).
In fact, we notice that by performing an ensemble averaging over this operator,

$$\begin{aligned}\langle \boldsymbol{C}_l \rangle &= \sum_m \frac{\langle \boldsymbol{b}^\dagger_{lm} \boldsymbol{b}_{lm} \rangle}{2l+1} \\ &= \sum_m \frac{C_l}{2l+1} \\ \langle \boldsymbol{C}_l \rangle &= (2l+1)\frac{C_l}{2l+1}\,,\end{aligned} \tag{130}$$

which leads to

$$\langle \boldsymbol{C}_l \rangle = C_l\,. \tag{131}$$

We then obtain the full sky averaging of the correlation operator as

$$\{\boldsymbol{\beta}^\dagger_A \boldsymbol{\beta}_B\}_{\rm S} = \sum_l \frac{2l+1}{4\pi} \boldsymbol{C}_l P_l\left(\cos\zeta\right)\,. \tag{132}$$

Clearly, this is related to the ORF via an ensemble average,

$$\langle \{\boldsymbol{\beta}^\dagger_a \boldsymbol{\beta}_b\}_{\rm S} \rangle = \Gamma_{AB}\left(\zeta\right)\,. \tag{133}$$

The cosmic variance can be obtained from the full sky averaged second moment of the correlation. In symbols, to obtain the cosmic variance, we calculate

$$\mathrm{CV} = \langle \{\boldsymbol{\beta}^\dagger_A \boldsymbol{\beta}_B\}^2_{\rm S} \rangle - \langle \{\boldsymbol{\beta}^\dagger_A \boldsymbol{\beta}_B\}_{\rm S} \rangle^2\,. \tag{134}$$

The second term is simply the square of (132). Thus, we focus on the first term. We write

$$\{\boldsymbol{\beta}^\dagger_A \boldsymbol{\beta}_B\}^2_{\rm S} = \sum_{ll'} \frac{(2l+1)(2l'+1)}{(4\pi)^2} \boldsymbol{C}_l \boldsymbol{C}_{l'} P_l\left(\cos\zeta\right) P_{l'}\left(\cos\zeta\right) \tag{135}$$

and we consider the ensemble average,

$$\langle \{\boldsymbol{\beta}^\dagger_A \boldsymbol{\beta}_B\}^2_{\rm S} \rangle = \sum_{ll'} \frac{(2l+1)(2l'+1)}{(4\pi)^2} \langle \boldsymbol{C}_l \boldsymbol{C}_{l'} \rangle P_l\left(\cos\zeta\right) P_{l'}\left(\cos\zeta\right)\,. \tag{136}$$

We then simplify $\langle \boldsymbol{C}_l \boldsymbol{C}_{l'} \rangle$ by using the definition (129),

$$\begin{aligned}\langle \boldsymbol{C}_l \boldsymbol{C}_{l'} \rangle =& \left\langle \sum_m \frac{\boldsymbol{b}^\dagger_{lm} \boldsymbol{b}_{lm}}{2l+1} \sum_{m'} \frac{\boldsymbol{b}^\dagger_{l'm'} \boldsymbol{b}_{l'm'}}{2l'+1} \right\rangle \\ =& \sum_{mm'} \frac{1}{(2l+1)(2l'+1)} \langle \boldsymbol{b}^\dagger_{lm} \boldsymbol{b}_{lm} \boldsymbol{b}^\dagger_{l'm'} \boldsymbol{b}_{l'm'} \rangle\,.\end{aligned} \tag{137}$$

Performing explicitly the average for Gaussian fields (see [43]), we eventually obtain

$$\langle\{\boldsymbol{\beta}_A^\dagger\boldsymbol{\beta}_B\}_{\mathrm{S}}^2\rangle = \left(\sum_l \frac{2l+1}{4\pi} C_l P_l\left(\cos\zeta\right)\right)^2 + \sum_l \frac{2l+1}{8\pi^2} C_l^2 P_l\left(\cos\zeta\right)^2 \,. \tag{138}$$

We clearly see that the first squared sum term above is $\langle\{\boldsymbol{\beta}_a^\dagger\boldsymbol{\beta}_b\}_{\mathrm{S}}\rangle^2 = \Gamma_{ab}(\zeta)^2$, which is the square of the ORF.
Putting all the above information together back into (134), we finally get to the cosmic variance given by

$$\mathrm{CV} = \sum_l \frac{2l+1}{8\pi^2} C_l^2 P_l\left(\cos\zeta\right)^2 \,. \tag{139}$$

This is the residual uncertainty that remains even in the limit of an arbitrarily large number of pulsar pairs.

Finally, we consider that the power spectrum multipoles of the HD correlation can be shown to be [44]:

$$C_l^{\mathrm{HD}} = \frac{8\pi^{3/2}}{(l-1)l(l+1)(l+2)} \,. \tag{140}$$

We now present the HDs curve and its variances together with the 12.5 year NANOGrav data set [34]. This is shown in Figure 7. In particular, the considered uncertainty emerges from the total and cosmic variances.
Notice that we also have an horizontal dotted line that represents a monopolar spatial correlation.

The total variance σ^2_{TV} (Figure 7 red '\' hatched region) is what we would expect for the uncertainty for a single pulsar pair whose timing residuals are correlated by the SGWB.
We can see that the present NANOGrav data set is consistent with the total variance as an upper bound to its spatial correlation data points. There are 990 pulsar pairs (over 45 pulsars) in the NANOGrav 12.5 year data set.

The cosmic variance σ^2_{CV} (Figure 7, red '/' hatched region) is the residual variance that survives in the limit of a large number of cross-correlated pulsar pairs. This is generally nonvanishing, but we can notice that it reaches a minimum at certain angular separations, where the mean of the HD correlation hits the zero mark. In Figure 7, these spatial minima of the cosmic variance appear at $\zeta \sim 55°$ and $\zeta \sim 125°$.

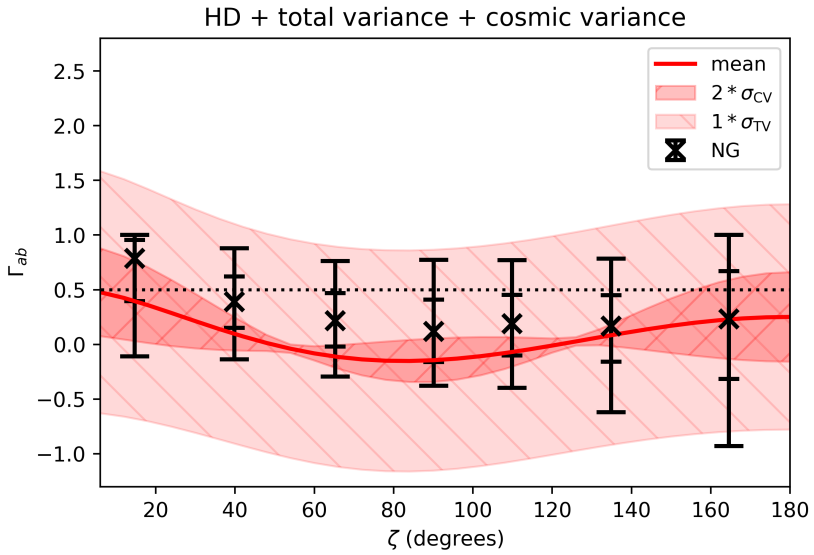

Figure 7: Hellings-Downs curve and uncertainty from the total (117) and cosmic (139) variances. The $2 * \sigma$ error bars and extreme values are obtained from the NANOGrav 12.5 year data [34]. We include only the first thirty multipoles for the power spectrum calculation. Figure taken from [43].

We now want to focus on the *pulsar variance*, which is the second contribution to the total variance that we have mentioned. The pulsar variance is related to *how* we observe pulsars. When we consider PTAs, we are observing along given directions ($\hat{\mathbf{n}}_a$: pulsars' positions) rather than the whole sky. This means that instead of actually computing an integral over $\hat{\mathbf{n}}$, we are considering a sum over the $\hat{\mathbf{n}}_a$. This introduces an error due to the fact that we are sampling a continuous function over the sky with a set of discrete observations.

Finally, we want to highlight the difference between these two contributions by imagining to be experimentally able to perform the *full sky averaging* over pulsar pairs of the same angular separation, as we have mathematically done previously. In this ideal situation, we would then have a continuous sampling for a continuous quantity and we would succeed in cutting off the pulsar variance.
However, we would still have the cosmic one, which cannot be cancelled even if we are considering a perfect averaging of the whole sky.

In summary, the goal of this chapter is to emphasize that the Hellings–Downs curve should be interpreted not as a deterministic prediction to be exactly reproduced by observations, but as the ensemble-averaged correlation of a stochastic gravitational-wave background.
Real pulsar timing array measurements probe a single, discretely sampled realization of this random field, so that both the cosmic and the pulsar variance affect how closely the measured correlations can approach the theoretical expectation.

3.2 Interferometers

We now present the modern efforts to detect gravitational radiation on Earth: these focus on the use of laser interferometry.
The idea behind interferometric detection of GWs is in principle simple and elegant.
All of the GW laser interferometers in the past, as well as those planned for the next decade, are essentially based on Michelson interferometers.
Obviously, a GW interferometer is actually an extremely complex instrument, with many degrees of freedom that must be kept under control.
Their development has required the building up of large collaborations as well as more than 30 years of preparation.
The global network of ground-based interferometric detectors includes the two LIGO observatories in the United States [46], Virgo Collaboration in Italy [47] and KAGRA in Japan [48], which together form the current second generation of detectors .
There also exists GEO600 [49] and additional projects such as LIGO-India will extend this network within the same generation [50].

Planned third-generation detectors include the Einstein Telescope in Europe [51] and the Cosmic Explorer in the United States [52], which aim to achieve an order-of-magnitude improvement in sensitivity.
Finally, space-based interferometers such as LISA are also under development [53]:while based on the same interferometric principle, they target different source populations and rely on very different technologies.

We now illustrate the basic concepts behind a Michelson interferometer: this object was used in the classical Michelson-Morley experiment in 1887 that demonstrated the non-existence of ether. This is a remarkably accurate instrument for measuring changes in the travel time of light in its arms. The conceptual scheme is shown in figure 8.

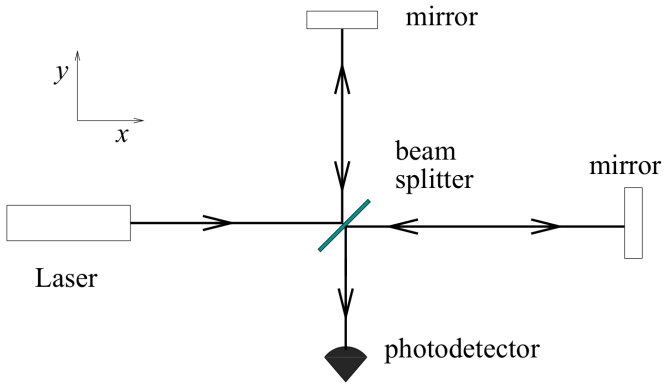

Figure 8: Simple Michelson-Morley interferometer. Figure taken from [18].

It consists of a monochromatic light source (which today is a laser) whose light is sent on a beam splitter that separates the light, with equal probability amplitudes, into a beam going along one arm and a beam travelling in a second orthogonal arm. At the end of each arm we have reflecting mirrors.
After going back and forth, the two beams recombine at the beam-splitter and part of the resulting ray goes to a photodetector, that measures its intensity. The interesting thing is that the power measured by the photodetector depends on the difference between the lengths of the arms (see [18] for more details). This means that any variation in the length of an arm results in a corresponding variation of the power of the photodetector.

We now discuss how to apply this idea to GW detection. In the TT gauge description, the physical effect of the GW manifests itself in affecting the propagation of light between the mirrors.
Assuming for the moment that the GW has only the plus polarization, we consider it coming from the z direction. In the $z = 0$ plane of the interferometer we therefore have:

$$h_+(t) = h_0 \cos(\omega_{gw} t). \tag{141}$$

Recalling equation 22, we get the new metric:

$$ds^2 = -dt^2 + dz^2 + \big(1 + h_+(t)\big)\, dx^2 + \big(1 - h_+(t)\big)\, dy^2. \tag{142}$$

We know that photons travel along null geodesics (i.e. $ds^2 = 0$): let us then

consider, for example, the light travelling along the x arm. To first order in h_0:

$$dx = \pm dt\big[1 - \frac{1}{2}h_+(t)\big], \tag{143}$$

where the plus sign holds for the travel from the beam-splitter to the mirror and the minus sign for the return trip.
From this we can clearly see that there is a variation in the propagation of light caused by the gravitational wave passing through the interferometer. In fact, if we consider a photon leaving the beam splitter at a time t_0, reaching the mirror at the fixed coordinate $x = L_x$ and coming back to the beam-splitter at a time t_2, we get that :

$$t_2 - t_0 = 2L_x + L_x h(t_0 + L_x)\frac{\sin(\omega_{gw}L_x)}{\omega_{gw}L_x}. \tag{144}$$

Along the y arm the analysis is similar.

These effects induce a differential phase shift in the electromagnetic field recombining at the photodetector. This phase offset moves the interferometer away from perfect destructive interference, resulting in a modulation of the total power measured at the photodetector due to the GW signal.

Finally, the interesting thing is that to measure GWs with frequencies of a few hundreds Hz, the optimal choice would be an arm-lenght L of several hundreds kms. However, for Earth-based interferometers this is in practice impossible. Moreover, we know that earth-based detectors have arms of lenghts around $L = 4$ km or less, so how are they actually probing GWs with these kind of frequencies?
The solution lies on the idea of "folding" the optical path of light, making it bounce back and forth many times in each arm, before recombining the two beams. To do so, LIGO and VIRGO transform each arm into a Fabry-Perot cavity. For more details, see [54], [18].

3.2.1 Response of a single interferometer

In this section we will present how a single interferometer behaves when interacting with a SGWB. To do so, we need to explicitly compute the detector pattern functions $F^P(\hat{\mathbf{n}}) \equiv D^{ab}e^P_{ab}(\hat{\mathbf{n}})$ (see section 2.5.1): therefore we need the explicit expressions for the detector tensor D^{ab} and the polarization tensors e^P_{ab} . For an

interferometer with arms along $\hat{u}$ and $\hat{v}$ directions,

$$D^{ab} = \frac{1}{2}(\hat{u}^a\hat{u}^b - \hat{v}^a\hat{v}^b). \tag{145}$$

Notice that this tensor is traceless, i.e. $D^{aa} = 0$, as well as the fact that the tensor is independent from the GW direction $\hat{\mathbf{n}}$ and momentum.
To consider the explicit expression of the polarization tensors we need to recall equations 17, 16 and 18. We now want to slightly modify the vectors 16 by rotating them of an angle ψ: this is done to consider the most general choice for the axes with respect to which the + and × polarizations are defined.

We therefore define

$$\begin{aligned} \hat{\boldsymbol{\theta}}' &= \hat{\boldsymbol{\theta}}\cos\psi - \hat{\boldsymbol{\phi}}\sin\psi, \\ \hat{\boldsymbol{\phi}}' &= \hat{\boldsymbol{\theta}}\sin\psi + \hat{\boldsymbol{\phi}}\cos\psi \end{aligned} \tag{146}$$

Using these new expressions, we get that in the case of interferometers with perpendicular arms:

$$F_+(\theta,\phi,\psi) = \frac{1}{2}(1+\cos^2\theta)\cos 2\phi\cos 2\psi - \cos\theta\sin 2\phi\sin 2\psi \tag{147}$$

and

$$F_\times(\theta,\phi,\psi) = \frac{1}{2}(1+\cos^2\theta)\cos 2\phi\sin 2\psi + \cos\theta\sin 2\phi\cos 2\psi. \tag{148}$$

The factor F is then given by

$$F \equiv \int \frac{d\hat{\Omega}}{4\pi} \sum_{P=+,\times} F^P(\hat{\Omega},\psi)F^P(\hat{\Omega},\psi) = \frac{2}{5} \tag{149}$$

We remind that this factor enters the most interesting quantity for a single detector, which is $\langle s^2(t)\rangle$ (eq. 53) : we therefore see how this physical quantity is indeed independent of the angle ψ.

3.2.2 Overlap reduction function

As we've said in 2.5, SGWBs' signals are expected to be much smaller than the detector's noise level, being therefore difficult to detect with only one detector. We thus examine the strategy of correlating the outputs of many detectors that interact with a SGWB to see what kind of behaviour we need to look for. In this section we will focus on obtaining the overlap reduction function for two interferometers.

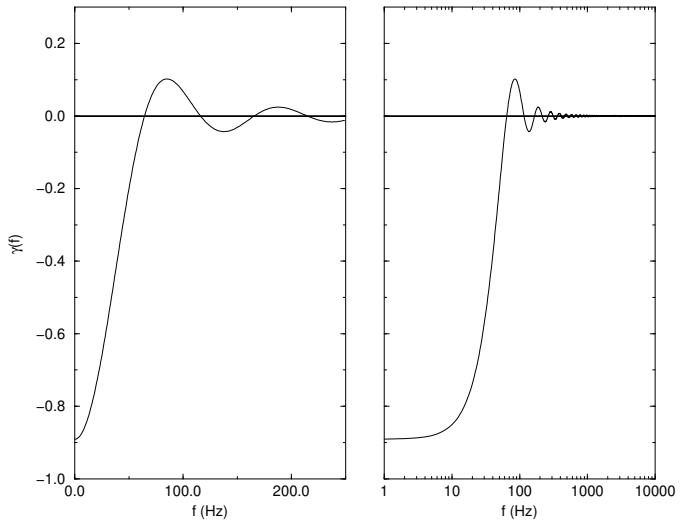

Figure 9: Overlap reduction function $\gamma(f)$ for Hanford,WA and Livingston,LA LIGO pair. The graph on the left has a linear horizontal axis while the one on the right has a logarithmic scale ($\log_{10}$). Figure taken from [32].

The expression for the overlap reduction function for two interferometers (A, B) is given by (consider equations 65, 67 and 149):

$$\gamma(f) \equiv \frac{5}{8\pi} \int d^2\hat{\mathbf{n}} \sum_P F_A^P(\hat{\Omega}) F_B^P(\hat{\Omega}) \exp\left\{ 2\pi i f \hat{\mathbf{n}} \cdot \frac{\Delta\mathbf{x}}{c} \right\}, \quad (150)$$

where, we remind, $\hat{\mathbf{n}}$ is a unit vector specifying a direction on the two-sphere, $\Delta\mathbf{x} := \mathbf{x}_A - \mathbf{x}_B$ is the separation vector between the central stations of the two interferometer sites. Moreover,

$$F_i^P(\hat{\mathbf{n}}) \equiv D_i^{ab} e_{ab}^P(\hat{\mathbf{n}}) = \frac{1}{2}(\hat{u}_i^a \hat{u}_i^b - \hat{v}_i^a \hat{v}_i^b) e_{ab}^P(\hat{\mathbf{n}}) \quad (151)$$

is the response of the ith detector ($i = A, B$) to the $P = +, \times$ polarization.

The overlap reduction function $\gamma(f)$ is equal to 1 for coincident and coaligned interferometers while it is smaller than the unity if the detectors are shifted apart or disaligned.

The overlap reduction function between the Hanford,WA and Livingston,LA LIGO pair is shown in figure 9.

From this figure we can notice interesting features of the overlap reduction function:

- For the LIGO detector pair $\gamma(f)$ is negative as $f \to 0$: this is due to the rotation of 90° between the arms of the two detectors;
- The absolute value of $\gamma(0)$ is not equal to 1 since the planes of the detectors are different, therefore they are not exactly parallel ;
- The first zero of $\gamma(f)$ is at $64Hz$. This depends on how the gravitational plane wave interacts with a pair of detectors: we have a in-coincidence excitation when the positive (negative) part of the wave is passing through both the detectors at the same time; we instead have an anti-coincidence excitation when the positive (negative) part of the wave is affecting one detector while the negative (positive) part is passing by the other detector (shown in figure 10). Provided that the wavelength of the considered gravitational wave is larger than twice the distance between the two detectors, the two interferometers will be in-coincidence more than in anti-coincidence. In the LIGO detector pair case this means that the two detectors will be driven in-coincidence (on average) if the SGWB has a frequency of less $f = c/(2\ |\Delta\vec{x}|) = 50$ Hz. The actual frequency of the zero is slightly larger since $\gamma(f)$ can be rewritten as three Bessel functions that do not vanish exactly at 50 Hz.

We want to obtain the explicit expression for two interferometers by computing the integral in equation 150. In this part we will follow [32] 's calculations, while in 4 we will see how to get the same result in a simpler way.

We start off by defining the following quantities:

$$\Delta\mathbf{x} := d\ \hat{s} \quad \text{and} \quad \alpha := \frac{2\pi f d}{c}\ , \tag{152}$$

where $\hat{s}$ is the unit vector that connects the distance between the two detectors. At this point, recalling equation 151, we can write equation 150 as:

$$\gamma(f) = D_A^{ab} D_B^{cd}\ \Gamma_{abcd}(\alpha, \hat{s})\ , \tag{153}$$

where

$$\Gamma_{abcd}(\alpha, \hat{s}) := \frac{5}{8\pi} \sum_P \int d^2\hat{\mathbf{n}}\ e^{i\alpha\hat{\mathbf{n}}\cdot\hat{s}}\ e^P_{ab}(\hat{\mathbf{n}}) e^P_{cd}(\hat{\mathbf{n}})\ . \tag{154}$$

This is exactly the same expression of [10].
We notice that this kind of tensor is symmetric under interchanges $a \leftrightarrow b$, $c \leftrightarrow d$, $ab \leftrightarrow cd$. It is also tracefree with respect to the ab and cd index pairs.

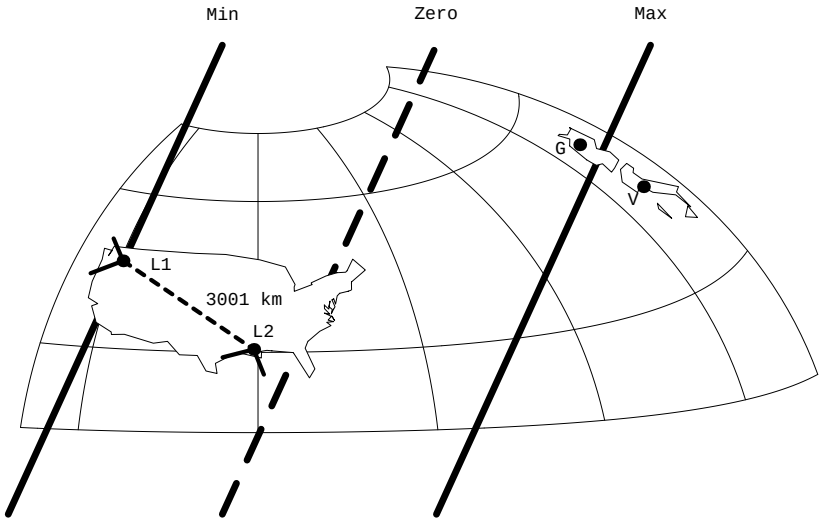

Figure 10: Earth's surface including the LIGO detectors in Hanford,WA (L1) and Livingston,LA (L2), the VIRGO detector in Pisa, Italy (V) and the GEO-600 in Hanover, Germany (G). We can also see the perpendicular arms of the LIGO detectors. A plane wave is passing through Earth and it is shown via its successive minimum, zero and maximum. In the moment shown, we then have a in-coincidence excitation for the detectors since they are both affected by the negative part of the wave. Figure taken from [32].

To evaluate $\Gamma_{abcd}(\alpha,\hat{s})$, we consider the most general form of a tensor constructed using δ_{ab} and s_a that has the symmetry properties mentioned above:

$$\begin{aligned}\Gamma_{abcd}(\alpha,\hat{s}) &= A(\alpha)\ \delta_{ab}\delta_{cd} + B(\alpha)\ (\delta_{ac}\delta_{bd}+\delta_{bc}\delta_{ad}) + C(\alpha)\ (\delta_{ab}s_c s_d + \delta_{cd}s_a s_b) + \\ &\quad D(\alpha)\ (\delta_{ac}s_b s_d + \delta_{ad}s_b s_c + \delta_{bc}s_a s_d + \delta_{bd}s_a s_c) + E(\alpha)\ s_a s_b s_c s_d. \quad (155)\end{aligned}$$

We now want to find the explicit expressions of the coefficients: to do so, we contract (155) with $\delta^{ab}\delta^{cd}$, $(\delta^{ac}\delta^{bd}+\delta^{bc}\delta^{ad})$, $\cdots$, $s^a s^b s^c s^d$ to find a linear system of equations for the functions $A, B, \cdots, E$:

$$\begin{bmatrix} 9 & 6 & 6 & 4 & 1 \\ 6 & 24 & 4 & 16 & 2 \\ 6 & 4 & 8 & 8 & 2 \\ 4 & 16 & 8 & 24 & 4 \\ 1 & 2 & 2 & 4 & 1 \end{bmatrix} \begin{bmatrix} A \\ B \\ C \\ D \\ E \end{bmatrix} (\alpha) = \begin{bmatrix} p \\ q \\ r \\ s \\ t \end{bmatrix} (\alpha)\ , \quad (156)$$

where

$$\begin{aligned} p(\alpha) &:= \Gamma_{abcd}(\alpha,\hat{s})\ \delta^{ab}\delta^{cd}\ , \\ q(\alpha) &:= \Gamma_{abcd}(\alpha,\hat{s})\ (\delta^{ac}\delta^{bd}+\delta^{bc}\delta^{ad})\ , \\ r(\alpha) &:= \Gamma_{abcd}(\alpha,\hat{s})\ (\delta^{ab}s^c s^d + \delta^{cd}s^a s^b)\ , \\ s(\alpha) &:= \Gamma_{abcd}(\alpha,\hat{s})\ (\delta^{ac}s^b s^d + \delta^{ad}s^b s^c + \delta^{bc}s^a s^d + \delta^{bd}s^a s^c)\ , \\ t(\alpha) &:= \Gamma_{abcd}(\alpha,\hat{s})\ s^a s^b s^c s^d\ . \end{aligned} \quad (157)$$

From Eq. (154), we see that the functions $p, q, \cdots, t$
are scalar integrals that involve contractions of the polarization tensors $e^P_{ab}(\hat{\mathbf{n}})$.
To compute these integrals, we choose (without loss of generality) a coordinate system where the unit vector $\hat{s}$ coincides with unit vector $\hat{z}$. Then

$$\hat{\mathbf{n}}\cdot\hat{s} = \cos\theta\ , \quad \hat{\boldsymbol{\theta}}\cdot\hat{s} = -\sin\theta, \quad \hat{\boldsymbol{\phi}}\cdot\hat{s} = 0, \quad (158)$$

and

$$\begin{aligned} p(\alpha) &= 0\ , \\ q(\alpha) &= = 20\ j_0(\alpha)\ , \\ r(\alpha) &= 0\ , \\ s(\alpha) &= = \frac{40}{\alpha}\ j_1(\alpha)\ , \\ t(\alpha) &= \frac{20}{\alpha^2}\ j_2(\alpha)\ , \end{aligned} \quad (159)$$

where $j_0(\alpha)$, $j_1(\alpha)$, and $j_2(\alpha)$ are the standard spherical Bessel functions:

$$\begin{aligned} j_0(\alpha) &= \frac{\sin\alpha}{\alpha}, \\ j_1(\alpha) &= \frac{\sin\alpha}{\alpha^2} - \frac{\cos\alpha}{\alpha}\ , \\ j_2(\alpha) &= 3\ \frac{\sin\alpha}{\alpha^3} - 3\ \frac{\cos\alpha}{\alpha^2} - \frac{\sin\alpha}{\alpha}\ . \end{aligned} \tag{160}$$

We notice that $p(\alpha) = 0$ and $r(\alpha) = 0$ are immediate consequences of the tracefree property of $\Gamma_{abcd}(\alpha, \hat{s})$.

We now want to invert the above linear system of equations (156) to get the coefficients' expressions:

The results are:

$$\begin{bmatrix} A \\ B \\ C \\ D \\ E \end{bmatrix}(\alpha) = \frac{1}{2\alpha^2} \begin{bmatrix} -5\alpha^2 & 10\alpha & 5 \\ 5\alpha^2 & -10\alpha & 5 \\ 5\alpha^2 & -10\alpha & -25 \\ -5\alpha^2 & 20\alpha & -25 \\ 5\alpha^2 & -50\alpha & 175 \end{bmatrix} \begin{bmatrix} j_0 \\ j_1 \\ j_2 \end{bmatrix}(\alpha)\ . \tag{161}$$

Finally, to obtain the overlap reduction function $\gamma(f)$, we substitute (155) into (153). Since D_i^{ab} $(i = A, B)$ is tracefree, it follows that

$$\gamma(f) = 2B(\alpha)\ D_A^{ab} D_{B,ab} + 4D(\alpha)\ D_A^{ab} D_{B,ac} s_b s_c + E(\alpha)\ D_A^{ab} D_B^{cd} s_a s_b s_c s_d\ . \tag{162}$$

Substituting the expressions for the functions B, D, E given by (161) into (162) yields

$$\gamma(f) = \rho_1(\alpha)\ D_A^{ab} D_{B,ab} + \rho_2(\alpha)\ D_A^{ab} D_{B,ac} s_b s_c + \rho_3(\alpha)\ D_A^{ab} D_B^{cd} s_a s_b s_c s_d\ , \tag{163}$$

where

$$\begin{bmatrix} \rho_1 \\ \rho_2 \\ \rho_3 \end{bmatrix}(\alpha) = \frac{1}{2\alpha^2} \begin{bmatrix} 10\alpha^2 & -20\alpha & 10 \\ -20\alpha^2 & 80\alpha & -100 \\ 5\alpha^2 & -50\alpha & 175 \end{bmatrix} \begin{bmatrix} j_0 \\ j_1 \\ j_2 \end{bmatrix}(\alpha)\ . \tag{164}$$

This is the desired result.

4 Probing Non-Gaussianity in the SGWB with PTAs and Interferometers

4.1 Definitions and motivations

In this section, we present our analysis of non-Gaussian GW correlators. In particular, we will focus on a set-up where the SGWB originated during the early Universe. Under this assumption, many early-Universe scenarios predict non-vanishing connected higher-order GW correlators, leading to observational consequences for GW experiments.
Since three-point correlators of an isotropic SGWB cannot be directly detected with interferometers and pulsar timing arrays (see [55]), we focus on four-point correlators and study how GW experiments can probe the quantity known as *trispectrum*.

We therefore investigate the implications of SGWB non-Gaussianities for GW experiments. The SGWB will be characterized by specific geometrical configurations predicted by the theoretical models under consideration.
There are two possible strategies to test GW non-Gaussianities:

- We may examine how a GW trispectrum with given features *modulates* the statistical properties of the two-point function, inducing distinctive and potentially observable deviations from the Gaussian expectation;

- Alternatively, we can study the *direct detectability* of higher-order correlators, such as the GW four-point function, by analysing the response of GW experiments to this observable and exploring corresponding detection prospects.

We consider examples of both approaches: in fact, we will first cover how the presence of a GW trispectrum affects the statistical properties of the two-point function by investigating pulsar timing arrays. In particular, we will see how non-Gaussianity induces an alteration in the usual variance of Hellings-Downs.
We will then study how to detect four-point correlators using interferometers: this means that we will consider correlating measurements of a non-Gaussian SGWB across *four* distinct detectors.

4.2 New conventions

First of all we have to introduce a new set of conventions. Up to now we have considered expressions related to the features of the SGWB based on the decomposition given in equation 37, which is the usual form found in the literature.
This means that, for example, we have written relations as functions of the frequency (see equation 40). However, for this section we will use slightly different notations to be consistent with the considered theoretical models.
Therefore, we rewrite some relations that we have already seen. We start by writing the tensor corresponding to a GW performing a Fourier decomposition in the spatial coordinates only:

$$h_{ij}(\tau, \mathbf{x}) = \sum_{\lambda=\pm 2} \int \frac{d^3\mathbf{k}}{(2\pi)^3}\, e^{i\mathbf{k}\cdot\mathbf{x}}\, e_{ij}^{(\lambda)}(\hat{\mathbf{k}})\, h_{\mathbf{k}}^{(\lambda)}(\tau), \tag{165}$$

where $e_{ij}^{(\lambda)}(\hat{\mathbf{k}})$ are the spin-2, transverse traceless (TT) polarization tensors in the circular basis $(R, L) = \pm 2$.
The spin-2 polarization tensors in circular basis $(R, L) = (+2, -2)$ are related to those in the $(+, \times)$ basis by the formula

$$e_{ij}^{(\pm 2)}(\hat{\mathbf{k}}) \;=\; \frac{e_{ij}^{(+)}(\hat{\mathbf{k}}) \pm i\, e_{ij}^{(\times)}(\hat{\mathbf{k}})}{\sqrt{2}}\,. \tag{166}$$

We assume that the polarization tensors $e_{ij}^{(+,\times)}$ are real, hence $\left(e_{ij}^{(\pm 2)}\right)^* = e_{ij}^{(\mp 2)}$.

In this section, we will use both these new polarization tensors and the $(+, \times)$ ones. We will always specify which ones we are considering.
The following combination of spin-2 polarization tensors define the transverse-traceless projector, an important quantity in our analysis:

$$\begin{aligned}
\Lambda_{ij\ell m} &= \sum_{\lambda=\pm 2} e_{ij}^{(\lambda)} e_{\ell m}^{(\lambda)*} \\
&= e_{ij}^{(L)} e_{\ell m}^{(L)*} + e_{ij}^{(R)} e_{\ell m}^{(R)*} = e_{ij}^{(+)} e_{\ell m}^{(+)} + e_{ij}^{(\times)} e_{\ell m}^{(\times)} \\
&= \Big(\pi_{i\ell}\pi_{jm} + \pi_{j\ell}\pi_{im} - \pi_{ij}\pi_{\ell m}\Big),
\end{aligned} \tag{167}$$

where

$$\pi_{ij} = \delta_{ij} - \hat{k}_i \hat{k}_j. \tag{168}$$

In order to ensure that $h_{ij}(\tau, \mathbf{x})$ is real, we assume $h_{\mathbf{k}}^{(\lambda)*}(\tau) = h_{-\mathbf{k}}^{(-\lambda)}(\tau)$.

At this point, we also want to rewrite equation 40 in our new conventions:

$$\langle h_{\mathbf{k}}^{(\lambda_1)}(\tau)\, h_{\mathbf{q}}^{(\lambda_2)*}(\tau)\rangle = (2\pi)^3\delta^{(3)}(\mathbf{k}-\mathbf{q})\,\delta_{\lambda_1,\lambda_2}\,\langle h_{\mathbf{k}}^{(\lambda_1)}(\tau)\, h_{\mathbf{k}}^{(\lambda_1)*}(\tau)\rangle_\Delta. \tag{169}$$

Here, the δ-function for the polarizations is related to the conservation of helicity for the spin-2 massless modes[5].

Using this Fourier decomposition, we define the tensor spectrum as:

$$\mathcal{P}_h(k) \;=\; \frac{k^3}{2\pi^2}\sum_{\lambda=\pm 2}\langle h_{\mathbf{k}}^{(\lambda)}(\tau)\, h_{\mathbf{k}}^{(\lambda)*}(\tau)\rangle_\Delta. \tag{170}$$

At this point, we also rewrite equation 64: with our new notation we get that

$$\begin{aligned}\langle s_{AB}\rangle &= \sum_{\lambda=\pm 2}\int k^2 dk\,\frac{d^2\hat{\mathbf{n}}}{(2\pi)^3}\,F_A^{(\lambda)}(\hat{\mathbf{n}})F_B^{(-\lambda)}(\hat{\mathbf{n}})\,e^{ik\,\hat{\mathbf{n}}\cdot(\mathbf{x}_A-\mathbf{x}_B)}\,\langle h_{\mathbf{k}}^{(\lambda)}h_{\mathbf{k}}^{(\lambda)^*}\rangle_\Delta \\ &= \int d\ln k\,\Gamma_{AB}(k)\,\mathcal{P}_h(k)\end{aligned}$$

where

$$\Gamma_{AB}(k) \;=\; \frac{1}{4\pi}\int d^2\hat{\mathbf{n}}\;\left(\sum_{\lambda=\pm 2}F_1^{(\lambda)}(\hat{\mathbf{n}})F_2^{(-\lambda)}(\hat{\mathbf{n}})\right)\,e^{ik\,\hat{\mathbf{n}}\cdot\,(\mathbf{x}_A-\mathbf{x}_B)} \tag{171}$$

is the *overlap reduction function* (ORF) that we have already seen in equation 65 [6].

We recall that this quantity controls how two-point correlations depend on the detector properties and configurations.

The ORF is the bridge between theoretical predictions of GW properties and experimental quantities. Its features allow us to investigate whether the measured signal is due to a GW background.

[5] This is an important point on which we return again when discussing non-Gaussian correlators.

[6] The overall factor controlling the ORF normalization in Eq. (171) can change depending on conventions for each type of GW experiment. We will be explicit on the normalization definitions in what comes next.

4.3 Theoretical models and their consequences

Now that we have defined the convention adopted in this work and its relation to the standard one used in the literature, we discuss how non-Gaussianities can be probed in a stochastic gravitational-wave background.
In order to address this question, we need to specify the class of backgrounds under consideration. We focus on primordial, cosmological SGWBs, since early-Universe mechanisms naturally allow for non-vanishing higher-order (non-Gaussian) gravitational-wave correlators.

We refer to models in which gravitational waves are produced during the era of radiation domination and are induced by fluctuations of primordial fields.
In particular, primordial perturbations, of scalar, vector, or tensor nature, can act as effective sources for gravitational waves at second order. The resulting signal is commonly referred to as induced gravitational waves (see [15] for a review).
In this thesis, we take into account theoretical frameworks in which gravitational waves are induced by primordial magnetic fields, whose energy-momentum tensor acts as a source for gravitational waves.
These vector fields may correspond to primordial magnetic fields associated with Standard Model electromagnetism and magnetogenesis mechanisms [13], or to the magnetic components of dark vector models proposed in the context of dark matter (see e.g. [56]).
Since in our setup the SGWB is sourced non-linearly by primordial vector fluctuations, the resulting signal is expected to exhibit non-vanishing connected higher-order correlators.
This feature motivates the analysis of higher-order statistics and their potential observational consequences for gravitational-wave experiments.

We will not focus on these theoretical frameworks. In particular, the specific model taken into account can be found in [57].
However, we will consider the consequences that these models have on our calculations in order to simplify intermediate steps and reach the final results.

Since, as we have said, we want to focus on probing non-Gaussianities in SGWB, we need to examine higher-order correlators. In particular, we want to study four-point correlation functions and we are particularly interested in the trispectrum, which is the generalization of the GW power spectrum for four-point correlators.
This means that we are interested in the combination given by:

$$\sum_{\lambda_i} \langle h^{(\lambda_1)}_{\mathbf{k_1}}(\tau) h^{(\lambda_2)*}_{\mathbf{k_2}}(\tau) h^{(\lambda_3)}_{\mathbf{k_3}}(\tau) h^{(\lambda_4)*}_{\mathbf{k_4}}(\tau) \rangle_{\Delta} \tag{172}$$

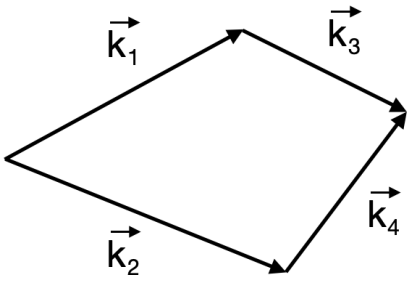

Figure 11: Graphical representation of a closed quadrilateral associated with the GW trispectrum.

where $\lambda_i = \pm 2$. In fact, keep in mind that we are trying to find an extension of equation 170 for four-point correlators.
In writing the previous equation we impose the momentum-conserving relation

$$\mathbf{k}_1 + \mathbf{k}_3 = \mathbf{k}_2 + \mathbf{k}_4 \tag{173}$$

associated with the translational invariance of the background. This is marked by the Δ in expression 172. Therefore, the momenta $\mathbf{k}_i$ form a closed quadrilateral: this is shown in figure 11.

To achieve this generalization of the GW power spectrum for four-point functions, we first need to introduce in detail the constraints given by the aforementioned theoretical models.

Based on how the SGWB originates in the early Universe, in this theoretical framework the GW spectrum can be factorized in a time integral (τ) and a momentum one [57, 58]. This assumption can also be applied to the case of the trispectrum: in particular, the integral in time gives us the needed information to perform our calculations.
In fact, the integral in time in the limit of large observation time τ ($\tau \to \infty$) has *non-zero* contributions given only from configurations that respect:

$$\sum_{j=1}^{4} \alpha_j k_j = 0, \qquad \alpha_j = \pm 1. \tag{174}$$

Thus, configurations obeying the vectorial closure condition 173 contribute at late times only if they also respect 174.
For both conditions to be satisfied, the momenta $\mathbf{k_i}$ must correspond to a *flattened*

or *folded* configurations, in which the four sides are superimposed.
This configuration can be also found in [59].
In other words, in our set-up the surviving contributions correspond to configurations in which the four momenta are collinear and aligned along a common direction $\hat{\mathbf{n}}$. Each momentum can then be parametrized as

$$\mathbf{k}_i = s_i\, k_i\, \hat{\mathbf{n}}. \qquad s_i = \pm 1, \qquad k_i > 0. \tag{175}$$

Therefore, to also satisfy the quadrilateral condition (173) (together with 174) we impose that (use equation 175) :

$$s_1 k_1 + s_3 k_3 = s_2 k_2 + s_4 k_4\,. \tag{176}$$

In this work, we will consider the configuration where

$$k_1 + k_3 = k_2 + k_4\,. \tag{177}$$

We then refer to this condition as *stationarity* of the trispectrum and stress that it is an unavoidable consequence of the structure of the time integrals for the considered frameworks.
Therefore, our notion of *stationary GW non-Gaussianity* singles out a specific class of non-Gaussian signatures that are related to GWs originating from the *same direction.*

This feature of our set-up is helpful because it allows us to introduce another simplification, which is the conservation of the total helicity in the correlator (172). This follows from requiring the trispectrum to be a scalar under rotations.
Specifically, considering a rotation by an angle θ around the $\hat{\mathbf{n}}$ axis (we have seen that all tensor modes are collinear), the correlator transforms as

$$\sum_{\lambda_i} \langle h^{(\lambda_1)}_{\mathbf{k_1}}(\tau) h^{(\lambda_2)\,*}_{\mathbf{k_2}}(\tau) h^{(\lambda_3)}_{\mathbf{k_3}}(\tau) h^{(\lambda_4)\,*}_{\mathbf{k_4}}(\tau)\rangle_\Delta \quad \longrightarrow \tag{178}$$

$$\sum_{\lambda_i} e^{i\theta(\lambda_1-\lambda_2+\lambda_3-\lambda_4)} \langle h^{(\lambda_1)}_{\mathbf{k_1}}(\tau) h^{(\lambda_2)\,*}_{\mathbf{k_2}}(\tau) h^{(\lambda_3)}_{\mathbf{k_3}}(\tau) h^{(\lambda_4)\,*}_{\mathbf{k_4}}(\tau)\rangle_\Delta. \tag{179}$$

In order for this to be invariant, we require it to be invariant piecewise (i.e. each term of the sum must be invariant, because each term represents a particular physical configuration of the trispectrum that must therefore be invariant under rotation). Hence, we impose the following law of conservation for the helicity

$$\lambda_1 - \lambda_2 + \lambda_3 - \lambda_4 = 0 \tag{180}$$

where $\lambda_i = \pm 2 = (R, L)$.

From this condition, we see that λ_i can assume the values $(LLLL)$, $(LLRR)$, $(LRRL)$, up to exchange of L with R.
In this work, for definiteness, we assume that only the configurations that satisfy $\lambda_1 = \lambda_2$ and $\lambda_3 = \lambda_4$ are turned on. This is satisfied by the couples in (λ, λ) $(LLLL)$ and $(LLRR)$ (up to exchange of R and L). We therefore can define the trispectrum as

$$\mathcal{T}_h(k_i) = 4\pi \frac{k_1^3 k_2^3 k_3^3}{(2\pi)^9} \sum_{\lambda_{1,2}=\pm 2} \langle h^{(\lambda_1)}_{\mathbf{k_1}}(\tau) h^{(\lambda_1)*}_{\mathbf{k_2}}(\tau) h^{(\lambda_2)}_{\mathbf{k_3}}(\tau) h^{(\lambda_2)*}_{\mathbf{k_4}}(\tau) \rangle_\Delta. \tag{181}$$

This structure respects the condition given by equation 180. Notice that we get a structure of the trispectrum that can be seen as the square of the power spectrum (recall 170).
The chosen normalization is to obtain a factor $1/4\pi$ in the connected part of the four-point correlator (see equation 185).

In summary, we now investigate implications for GW experiments of non-Gaussianities in the SGWB from the early universe, with the following characteristics:

- we have a flattened shape for the trispectrum, whose momenta are aligned along a common direction $\hat{\mathbf{n}}$ and such that:

$$k_1 + k_3 = k_2 + k_4. \tag{182}$$

- we only consider configurations given by $(LLLL)$, $(LLRR)$, $(RRRR)$ and $(RRLL)$.

These assumptions will help us streamline our calculations and obtain the final results, allowing us to actually reach observational implications of these results and analyse their phenomenological consequences for gravitational-wave experiments.

4.4 PTAs

We start by considering how the effect of non-Gaussianities in the SGWB can be researched for using pulsar timing arrays.
In section 3.1.6 we have studied in detail the variance of the HD curve in the case of a Gaussian SGWB. We want to see how this variance changes if we consider a *non*-Gaussian background.

Consequently, we want to study the variance of the overlap reduction function (see equation 171).
In particular, we are interested in the form of the *connected* part, since we have already studied the disconnected one.
We therefore recall that the ORF can be interpreted as arising from the *mean value* in an ensemble average of GW measurements. Hence its properties can be characterized by a *variance*, which should be taken into account when confronting the theory with experiments.
We estimate the contribution of the connected term of a four-point function to what we defined *total variance*.
Let us consider again the general definition for the variance of an ORF:

$$\sigma^2_{AB} = \langle s_A s_B s_A s_B \rangle - \langle s_A s_B \rangle^2. \tag{183}$$

Besides its disconnected parts, let us assume a non-vanishing connected contribution related to the trispectrum, characterized by a flattened shape as discussed in the previous section.

This implies that all momenta are forced to align along a common direction $\hat{\mathbf{n}}$. The connected part of the signal four-point function can then be expressed as

$$\langle s_A s_B s_A s_B \rangle_{\rm conn} = \int d\ln k_1\, d\ln k_2\, d\ln k_3\, \mathcal{T}_h(k_i)_{conn}\, \Sigma^2_{\rm conn} \tag{184}$$

where

$$\Sigma^2_{\rm conn} = \frac{1}{4\pi} \int d^2\hat{\mathbf{n}} \left(\sum_{\lambda_{1,2}=\pm 2} F_A^{(\lambda_1)}(\hat{\mathbf{n}}) F_B^{(-\lambda_1)}(\hat{\mathbf{n}}) F_A^{(\lambda_2)}(\hat{\mathbf{n}}) F_B^{(-\lambda_2)}(\hat{\mathbf{n}}) \right) e^{i(k_1+k_3)\,\hat{\mathbf{n}}\cdot(\mathbf{x}_A - \mathbf{x}_B)}. \tag{185}$$

We have used the alignment condition where all of the four momenta are along a common direction $\hat{\mathbf{n}}$ and the relation between k_i given by 182.
Moreover, we highlight that we have defined $\mathcal{T}_h(k_1, k_2, k_3)_{conn}$ as the connected contribution to the trispectrum. Finally, notice that in the (R, L) basis one has

$e_{ij}^{(\lambda)\,*} = e_{ij}^{-\lambda}$: this gives us the structure of the sum on $\lambda_{1,2}$ for the detector pattern functions. This sum over polarization indices satisfy the helicity conservation given by equation (180).

We therefore have that:

$$\sigma^2_{AB} = \langle s_A s_B s_A s_B \rangle - \langle s_A s_B \rangle^2$$
$$= \int d\ln k_1 d\ln k_2 \; \mathcal{P}_h(k_1)\mathcal{P}_h(k_2) \left[\Sigma^2_{\rm disc}(k_1,k_2) + \int d\ln k_3 \frac{\mathcal{T}_h(k_1,k_2,k_3)_{conn}}{\mathcal{P}_h(k_1)\mathcal{P}_h(k_2)} \, \Sigma^2_{\rm conn}(k_1,k_2) \right]$$

with

$$\Sigma^2_{\rm disc}(k_1,k_2) = \Gamma_{AB}(k_1)\Gamma_{AB}(k_2) + \Gamma_{AA}(k_1)\Gamma_{AA}(k_2). \tag{186}$$

The first term within the parenthesis depends on the disconnected contributions to the four-point function, while the last term depends on its connected part. Hence, we can clearly see that the connected part of the GW trispectrum in a flattened configuration contributes to the total variance of the two-point function. Consequently, it potentially affects GW measurements.

We compute for the first time the connected part contribution, which corresponds to the last term of equation 186.
In particular, we are referring to the quantity in equation 185, including an overall factor of 3/4 to match the aforementioned Hellings-Downs normalization convention (also see [60]) .
Notice that we use the same approximation employed to obtain the Hellings-Downs curve, where we neglect the pulsar terms (see equation 108).
We recall that this holds for the case of *non*-coincident pulsars. We find:

$$\Sigma^2_{\rm conn} = \frac{3}{16\pi} \int d^2\hat{\mathbf{n}} \left[\left(\sum_{\lambda_{1,2}=\pm 2} F_A^{(\lambda_1)}(\hat{\mathbf{n}}) F_B^{(-\lambda_1)}(\hat{\mathbf{n}}) F_A^{(\lambda_2)}(\hat{\mathbf{n}}) F_B^{(-\lambda_2)}(\hat{\mathbf{n}}) \right) \right] \tag{187}$$
$$= \frac{3}{16\pi} \int d^2\hat{\mathbf{n}} \left[\left(F_A^{(+)}(\hat{\mathbf{n}}) F_B^{(+)}(\hat{\mathbf{n}}) F_A^{(+)}(\hat{\mathbf{n}}) F_B^{(+)}(\hat{\mathbf{n}}) \right) \right] \tag{188}$$
$$= \frac{1}{40} \left[6 + (134 - 139y)y + 30y(2+3y)\ln y \right] \tag{189}$$

where we call $y = (1-\cos\zeta)/2$ and we denote $\left(F_A^{(L)} F_B^{(R)} \right) = F_A^{ij} F_B^{pq} \, e_{ij}^{(L)} e_{pq}^{(R)}$.

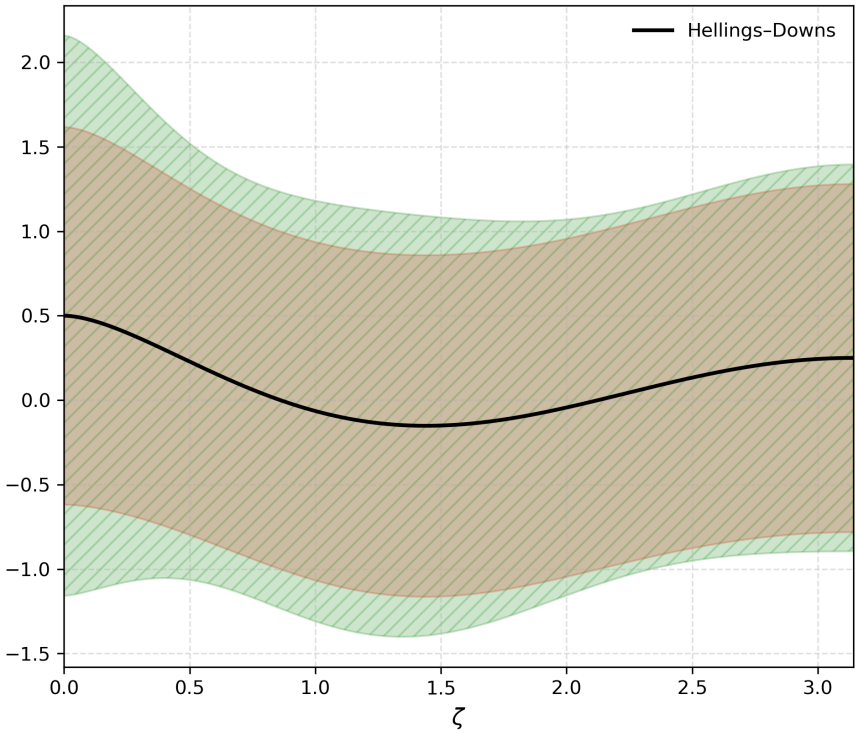

Figure 12: Representation of the Hellings-Down function (black line); its total variance associated with disconnected contributions to the four-point function (brown band); finally, the total variance accounting for non-vanishing contributions of the connected GW trispectrum (green band). See main text for details.

This calculation can be done by first considering the relation between the two basis of polarizations given by 167. In this way, we are able to obtain this expression in terms of the $(+, \times)$ basis of polarizations.
This is extremely useful: in fact, in this basis we have vanishing factors that help us simplify the process.
In fact, consider the same configuration of pulsars used to compute the Hellings-Downs curve (see appendix 5). This setting of pulsars gives us $F_A^{(\times)}(\hat{\mathbf{n}}) = 0$, cancelling out many terms. The only surviving contribution is given by the product of the four $F_{A/B}^{(+)}$.
At this point, once we have obtained the new integral, the procedure to find the result is quite similar to the one used for the HD curve (see Appendix 5).

We plot in figure 12 the Hellings-Downs ORF $\Gamma_{AB}(\zeta)$ as a function of the angle between pulsars.

We include the effect of the variances as coloured bands. The brown band represents the disconnected contribution to the variance, delimited by the region

$$\Gamma_{AB} \pm \Sigma_{\text{disc}}. \tag{190}$$

(Compare with figure 7).
The green band shows the total variance including the connected contribution, corresponding to the region

$$\Gamma_{AB} \pm \sqrt{\Sigma^2_{\text{disc}} + 10\,\Sigma^2_{\text{conn}}}. \tag{191}$$

For illustration purposes, we fix the integral over $\ln k_3$ to the constant value 10. in this way, we isolate the angular dependence of the connected contribution.

We learn that the presence of GW non-Gaussianity can increase the total variance of the Hellings-Downs ORF, hence allowing for scattering of experimental data around the mean Hellings-Downs for single pulsar-pair measurements.
It would be interesting in the future to further study the observational implications on PTA data of the amplification effects on the size of the variance induced by the connected part of the non-Gaussian GW trispectrum.

4.5 Interferometers

We now move on to study how non-Gaussianities in the SGWB can be probed via interferometers. This section will be divided into two parts:

- first, we show that the result for the two-point function obtained following [32] in section 3.2.2 can also be derived via another calculation.
  We want to show this because the original results of this section are obtained via an extension to the four-point function of this kind of calculation.
- In the second part, we present the results for the four-point function for interferometers.

4.5.1 Two-point correlation function

We want to look at a new possible way to obtain the correlation function for two interferometers, as an alternative to the calculations given in section 3.2.2.
To do so, we start by taking into account equation 154.
We can rewrite this integral using:

$$\begin{aligned}\Lambda_{abcd} &= \sum_A e^A_{ab}(\hat{\mathbf{n}})e^A_{cd}(\hat{\mathbf{n}}) = e^{(+)}_{ab}(\hat{\mathbf{n}})e^{(+)}_{cd}(\hat{\mathbf{n}}) + e^{(\times)}_{ab}(\hat{\mathbf{n}})e^{(\times)}_{cd}(\hat{\mathbf{n}}) \\ &= \Big(\pi_{ac}(\hat{\mathbf{n}})\pi_{bd}(\hat{\mathbf{n}}) + \pi_{bc}(\hat{\mathbf{n}})\pi_{ad}(\hat{\mathbf{n}}) - \pi_{ab}(\hat{\mathbf{n}})\pi_{cd}(\hat{\mathbf{n}})\Big), \end{aligned} \tag{192}$$

where

$$\pi_{ab} = \delta_{ab} - \hat{n}_a\hat{n}_b. \tag{193}$$

This means that we can write 154 as:

$$\Gamma_{abcd}(\alpha, \hat{s}) = \frac{5}{8\pi}\int d^2\hat{\mathbf{n}}e^{i\alpha\hat{\mathbf{n}}\cdot\hat{s}}\Lambda_{abcd}. \tag{194}$$

At this point, we explicitly compute Λ_{abcd}, obtaining:

$$\begin{aligned}\Lambda_{abcd} =& \delta_{ad}\delta_{bc} + \delta_{ac}\delta_{bd} - \delta_{ab}\delta_{cd} \\ &+\delta_{cd}\hat{n}_a\hat{n}_b + \delta_{ab}\hat{n}_c\hat{n}_d - \delta_{bd}\hat{n}_a\hat{n}_c - \delta_{ac}\hat{n}_b\hat{n}_d - \delta_{bc}\hat{n}_a\hat{n}_d - \delta_{ad}\hat{n}_b\hat{n}_c \\ &+\hat{n}_a\hat{n}_b\hat{n}_c\hat{n}_d. \end{aligned} \tag{195}$$

From here we can see that we have three kind of integrals that we need to compute: Γ^0_{abcd} with no dependence from $\hat{n}$, Γ^2_{abcd} that contains two powers of $\hat{n}$ (such as $\hat{n}_a\ \hat{n}_b$) and Γ^4_{abcd} that contains $\hat{n}_a\hat{n}_b\hat{n}_c\hat{n}_d$. In particular:

- $$\Gamma^0_{abcd} = \frac{5}{8\pi}\int d^2\hat{\mathbf{n}} e^{i\alpha\hat{\mathbf{n}}\cdot\hat{s}}(\delta_{ad}\delta_{bc}+\delta_{ac}\delta_{bd}-\delta_{ab}\delta_{cd}) = \frac{5}{2}\frac{\sin\alpha}{\alpha}(\delta_{ad}\delta_{bc}+\delta_{ac}\delta_{bd}-\delta_{ab}\delta_{cd}) = \frac{5}{2}j_0(\alpha)(\delta_{ad}\delta_{bc}+\delta_{ac}\delta_{bd}-\delta_{ab}\delta_{cd}) \tag{196}$$

- $$\Gamma^2_{abcd} = \frac{5}{8\pi}\int d^2\hat{\mathbf{n}} e^{i\alpha\hat{\mathbf{n}}\cdot\hat{s}}(\delta_{cd}\hat{n}_a\hat{n}_b+\delta_{ab}\hat{n}_c\hat{n}_d-\delta_{bd}\hat{n}_a\hat{n}_c -\delta_{ac}\hat{n}_b\hat{n}_d-\delta_{bc}\hat{n}_a\hat{n}_d-\delta_{ad}\hat{n}_b\hat{n}_c\hat{n}_a); \tag{197}$$

- $$\Gamma^4_{abcd} = \frac{5}{8\pi}\int d^2\hat{\mathbf{n}} e^{i\alpha\hat{\mathbf{n}}\cdot\hat{s}}\hat{n}_a\hat{n}_b\hat{n}_c\hat{n}_d. \tag{198}$$

The first integral is straightforward, while the other two are a little bit more difficult. However, we can use the same method that we have seen in the previous section 3.2.2 when we have obtained equation 163.
We focus on Γ^2_{abcd}: for the moment, we neglect the δ terms and we only consider the contributions entering the integral. This means that, for example, for the term

$$\frac{5}{8\pi}\int d^2\hat{\mathbf{n}} e^{i\alpha\hat{\mathbf{n}}\cdot\hat{s}}(\delta_{cd}\hat{n}_a\hat{n}_b) \tag{199}$$

we only focus on

$$\Delta^{(2)}_{ab} = \frac{5}{8\pi}\int d^2\hat{\mathbf{n}} e^{i\alpha\hat{\mathbf{n}}\cdot\hat{s}}\hat{n}_a\hat{n}_b. \tag{200}$$

To solve this integral, we consider the most general form of a tensor constructed with δ_{ab} and s_a. This is exactly what we did to obtain 155.
We then write:

$$\Delta^{(2)}_{ab} = G(\alpha)\delta_{ab} + H(\alpha)s_a s_b \tag{201}$$

and we get the coefficients $G(\alpha)$ and $H(\alpha)$ in the same way employed to find the coefficients of 155.
This means that the term 199 that we have considered as an example can be written as:

$$\frac{5}{8\pi}\int d^2\hat{\mathbf{n}} e^{i\alpha\hat{\mathbf{n}}\cdot\hat{s}}(\delta_{cd}\hat{n}_a\hat{n}_b) = G(\alpha)\delta_{ab}\delta_{cd} + H(\alpha)s_a s_b\delta_{cd}. \tag{202}$$

In particular, we find that:

$$G(\alpha) = \frac{5}{2}\frac{j_1(\alpha)}{\alpha} \tag{203}$$

$$H(\alpha) = -\frac{5}{2}j_2(\alpha). \tag{204}$$

We expect that all the terms that contribute to Γ^2_{abcd} have the same structure but with permutated indices.

We consider the same steps also for Γ^4_{abcd}: in this case we only have a contribution, therefore we can directly write the most general solution for this integral using tensors constructed with δ_{ab} and s_a. We then have:

$$\begin{aligned}\Gamma^4_{abcd} &= L(\alpha)(\delta_{bc}\delta_{ad} + \delta_{ac}\delta_{bd} + \delta_{ab}\delta_{cd}) \\ &+ M(\alpha)(\delta_{cd}s_a s_b + \delta_{ab}s_c s_d + \delta_{bd}s_a s_c + \delta_{ac}s_b s_d + \delta_{bc}s_a s_d + \delta_{ad}s_b s_c) \\ &+ N(\alpha)(s_a s_b s_c s_d).\end{aligned} \tag{205}$$

With the usual procedure we can obtain the coefficients. We get that:

$$L(\alpha) = \frac{5}{2\alpha^2} j_2(\alpha) \tag{206}$$

$$M(\alpha) = \frac{5}{2\alpha^2}(\alpha j_1(\alpha) - 5 j_2(\alpha)) \tag{207}$$

$$N(\alpha) = \frac{5}{2}\left(35\,\frac{j_2(\alpha)}{\alpha^2} - 10\,\frac{j_1(\alpha)}{\alpha} + j_0(\alpha)\right). \tag{208}$$

At this point, we have all the needed pieces to build the final integral. To finally check whether this method gives us the same result of equation 163, we need to recall that

$$\gamma(f) = D^{ab}_A D^{cd}_B \Gamma_{abcd}(\alpha, \hat{s}) \tag{209}$$

and that the tensors D^{ab}_i are traceless ($D^{aa}_i = 0$).
This tells us that some of the terms in equation 195 will give us a null contribution.

Putting everything together, we finally find the same result found in section 3.2.2, which coincides with the result of [32].

4.5.2 Four-point correlation function

We now present the results for the correlation of four different interferometers.
For this class of detectors, we have analysed the direct detectability of higher-order correlators, such as the GW four-point function, by studying the response of GW experiments to this observable.
The key observable for directly probing the four-point correlator will then be the ORF four-point function.

Improvements in the sensitivity of ground-based detector networks, both within modern detectors and future facilities such as the Einstein Telescope [51], open new opportunities to detect primordial SGWBs in the frequency range of tens of Hertz, should such signals exist.
Cosmological sources capable of producing backgrounds in this band, including second-order induced SGWBs, are reviewed in [32]. It is therefore essential to investigate their detectability prospects in scenarios where the signal is non-Gaussian, as in the framework considered here.

In our analysis of implications of GW non-Gaussianities, an advantage of ground-based detectors is that the relevant integrals that enter calculations can be evaluated analytically.
Here we consider correlating measurements of a non-Gaussian SGWB across *four* distinct detectors. Explicit examples to have in mind can be LIGO Hanford, LIGO Livingston [46], Virgo [47] and KAGRA [48] (see figure 10).
In the presence of a connected component to the gravitational-wave trispectrum, such four-detector correlation is non-vanishing and deviates from the standard-Gaussian case.

We will now see explicitly how a trispectrum can be measured directly by taking the *four-point function* of the GW signal.
Assuming that the trispectrum shape acquires only a flattened configuration, within the hypothesis discussed above, we need to compute the associated *four-point ORF* through the formula

$$\Gamma_{ABCD} = \frac{1}{4\pi}\int d^2\hat{\mathbf{n}} \left(\sum_{\lambda_{1,2}=\pm 2} F_A^{(\lambda_1)} F_B^{(-\lambda_1)} F_C^{(\lambda_2)} F_D^{(-\lambda_2)}\right) \times e^{ik_1\,\hat{\mathbf{n}}\cdot(\mathbf{x}_A-\mathbf{x}_D)}\, e^{-ik_2\,\hat{\mathbf{n}}\cdot(\mathbf{x}_B-\mathbf{x}_D)}\, e^{ik_3\hat{\mathbf{n}}\cdot(\mathbf{x}_C-\mathbf{x}_D)} \tag{210}$$

where the $F's$ are the detector pattern functions (equation 151 for interferometers) and depend on the common GW direction $\hat{\mathbf{n}}$, while the $\hat{\mathbf{x}}$'s are the detector positions. This is simply an extension of 185 for the case of four distinct detectors.

The polarization indices are the ones that we have selected in the previous section given the form of the trispectrum in equation 172. We have also used the condition on the alignment of momenta along $\hat{\mathbf{n}}$, satisfying the condition (182).
Notice that in this case we are not taking into account a normalization factor equivalent to the one for the case of two interferometers (see factor F given by equation 149).
This angular integral leads to the four-point ORF: we will present for the first time its analytical computation for the case of ground based interferometers.

We know that for ground based interferometers the detector tensor is given by 145 and we also recall that it is traceless.

In this set-up, we can write equation 210 as follows

$$\begin{aligned}\Gamma_{ABCD}(k_1,k_2,k_3) \;=\; & \frac{D_A^{ab}D_B^{cd}D_C^{ef}D_D^{gh}}{4\pi}\int d^2\hat{\mathbf{n}}\left(\sum_{\lambda_{1,2}=\pm 2} e_{ab}^{(\lambda_1)}e_{cd}^{(-\lambda_1)}e_{ef}^{(\lambda_2)}e_{gh}^{(-\lambda_2)}\right)\\ & \times e^{ik_1\,\hat{\mathbf{n}}\cdot(\mathbf{x}_A-\mathbf{x}_D)}e^{-ik_2\,\hat{\mathbf{n}}\cdot(\mathbf{x}_B-\mathbf{x}_D)}\,e^{ik_3\hat{\mathbf{n}}\cdot(\mathbf{x}_C-\mathbf{x}_D)}.\end{aligned} \tag{211}$$

Therefore, using the identity (167):

$$\begin{aligned}\Gamma_{ABCD}(k_1,k_2,k_3) \;=& \frac{D_A^{ab}D_B^{cd}D_C^{ef}D_D^{gh}}{4\pi}\int d^2\hat{\mathbf{n}}\,\Lambda_{abcd}(\hat{\mathbf{n}})\Lambda_{efgh}(\hat{\mathbf{n}})\\ & \times e^{ik_1\,\hat{\mathbf{n}}\cdot(\mathbf{x}_A-\mathbf{x}_D)}e^{-ik_2\,\hat{\mathbf{n}}\cdot(\mathbf{x}_B-\mathbf{x}_D)}\,e^{ik_3\hat{\mathbf{n}}\cdot(\mathbf{x}_C-\mathbf{x}_D)}.\end{aligned} \tag{212}$$

To proceed, inspired by [32], we introduce the combinations

$$\alpha \;=\; k_1\,|\mathbf{x}_A-\mathbf{x}_D| - k_2\,|\mathbf{x}_B-\mathbf{x}_D| + k_3\,|\mathbf{x}_C-\mathbf{x}_D| \tag{213}$$

$$\hat{s} \;=\; \frac{k_1\,(\mathbf{x}_A-\mathbf{x}_D) - k_2\,(\mathbf{x}_B-\mathbf{x}_D) + k_3\,(\mathbf{x}_C-\mathbf{x}_D)}{k_1\,|\mathbf{x}_A-\mathbf{x}_D| - k_2\,|\mathbf{x}_B-\mathbf{x}_D| + k_3\,|\mathbf{x}_C-\mathbf{x}_D|} \tag{214}$$

which correspond to a weighted size α of GW momenta, and an average direction $\hat{s}$.

Under these new definitions, we can write the integral in equation 212 as

$$\Gamma_{ABCD}(\alpha,s) \;=\; \frac{D_A^{ab}D_B^{cd}D_C^{ef}D_D^{gh}}{4\pi}\int d^2\hat{\mathbf{n}}\,\Lambda_{abcd}(\hat{\mathbf{n}})\Lambda_{efgh}(\hat{\mathbf{n}})e^{i\alpha\hat{\mathbf{n}}\cdot\hat{s}} \tag{215}$$

.

This is the integral that we need to compute.
We now recall equation 195, which gives us the total expression for this tensor.

To simplify the product between these two kind of tensors, we define the following combinations controlling correlations among two detectors:

$$\begin{aligned} F^{(0)}_{AB} =& D^{ab}_A D^{cd}_B \left(\delta_{ad}\delta_{bc} + \delta_{ac}\delta_{bd} - \delta_{ab}\delta_{cd}\right) \\ F^{(2)}_{AB} =& D^{ab}_A D^{cd}_B \left(\delta_{cd}\hat{n}_a\hat{n}_b + \delta_{ab}\hat{n}_c\hat{n}_d - \delta_{bd}\hat{n}_a\hat{n}_c - \delta_{ac}\hat{n}_b\hat{n}_d - \delta_{bc}\hat{n}_a\hat{n}_d - \delta_{ad}\hat{n}_b\hat{n}_c\right) \\ F^{(4)}_{AB} =& D^{ab}_A D^{cd}_B \hat{n}_a\hat{n}_b\hat{n}_c\hat{n}_d, \end{aligned} \tag{216}$$

where the index (p) indicates the power of unit vector $\hat{\mathbf{n}}$ involved.
The integral we need to deal with formally becomes:

$$\Gamma_{ABCD} = \frac{1}{4\pi}\int d^2\hat{\mathbf{n}} \left(F^{(0)}_{AB} + F^{(2)}_{AB} + F^{(4)}_{AB}\right)\left(F^{(0)}_{CD} + F^{(2)}_{CD} + F^{(4)}_{CD}\right) e^{i\alpha\,\hat{s}\cdot\hat{\mathbf{n}}}. \tag{217}$$

It is convenient to multiply the two parenthesis in equation 217 and define the following combinations:

$$\begin{aligned} G^{(0)}_{ABCD} &= F^{(0)}_{AB}F^{(0)}_{CD} && (218)\\ G^{(2)}_{ABCD} &= F^{(2)}_{AB}F^{(0)}_{CD} + F^{(0)}_{AB}F^{(2)}_{CD} && (219)\\ G^{(4)}_{ABCD} &= F^{(4)}_{AB}F^{(0)}_{CD} + F^{(2)}_{AB}F^{(2)}_{CD} + F^{(0)}_{AB}F^{(4)}_{CD} && (220)\\ G^{(6)}_{ABCD} &= F^{(4)}_{AB}F^{(2)}_{CD} + F^{(2)}_{AB}F^{(4)}_{CD} && (221)\\ G^{(8)}_{ABCD} &= F^{(4)}_{AB}F^{(4)}_{CD} && (222) \end{aligned}$$

which depend on all four detectors and assemble the powers of unit vector $\hat{\mathbf{n}}$.

We can now use the identity:

$$e^{i\alpha\hat{\mathbf{n}}\cdot\hat{s}} = \sum_{\ell=0}^{\infty} i^\ell \left(2\ell+1\right) j_\ell(\alpha)\, P_\ell(\hat{\mathbf{n}}\cdot\hat{s}) \tag{223}$$

with j_ℓ the spherical Bessel function and P_ℓ the Legendre polynomial of order ℓ. Plugging this into equation 215 and expanding, we find that the four point ORF can be expressed as

$$\Gamma_{ABCD} = \sum_{n=0}^{4} I^{(2n)}, \tag{224}$$

where each $I^{(2n)}$ reads

$$I^{(2n)} = \sum_{\ell=0}^{n} (-)^\ell \frac{(4\ell+1)}{4\pi}\, j_{(2\ell)}(\alpha) \int d^2\hat{\mathbf{n}}\, P_{(2\ell)}(\hat{\mathbf{n}}\cdot\hat{s})\, G^{(2n)}(\hat{\mathbf{n}}). \tag{225}$$

Hence we reduce the problem to compute integrals of Legendre polynomials, weighted by polynomials in $\hat{\mathbf{n}}$, which is a straightforward operation that can be carried on analytically.

For example, let us work out explicitly the computation for $I^{(0)}$ and $I^{(2)}$. Starting from $I^{(0)}$:

$$\begin{aligned} I^{(0)} &= \frac{j_0(\alpha)}{4\pi}\int d^2\hat{\mathbf{n}}\, P_{(0)}(\hat{\mathbf{n}}\cdot\hat{s})\, G^{(0)}(\hat{\mathbf{n}}) && (226)\\ &= 4\frac{j_0(\alpha)}{4\pi}\left(D_A^{ab}D_B^{ab}\right)\left(D_C^{cd}d_D^{cd}\right)\int d^2\hat{\mathbf{n}}\, P_{(0)}(\hat{\mathbf{n}}\cdot\hat{s}) && (227)\\ &= 4j_0(\alpha)\,\mathrm{tr}(D_{AB})\mathrm{tr}(D_{CD}) && (228)\end{aligned}$$

where we use the abbreviation $\mathrm{tr}(D_{AB}) = \left(D_A^{ab}D_B^{ab}\right)$.

For $I^{(2)}$, using the abbreviation $sD_{AB}s = s_a s_c D_A^{ab} D_B^{bc}$, we get that:

$$\begin{aligned} I^{(2)} =& -8\left[\frac{j_1(\alpha)}{\alpha}\,\mathrm{tr}(D_{AB})\,\mathrm{tr}(D_{CD}) - j_2(\alpha) sD_{AB}s\,\mathrm{tr}(D_{CD})\right]\\ & -8\left[\frac{j_1(\alpha)}{\alpha}\,\mathrm{tr}(D_{AB})\,\mathrm{tr}(D_{CD}) - j_2(\alpha) sD_{CD}s\,\mathrm{tr}(D_{AB})\right]\\ =& -16\frac{j_1(\alpha)}{\alpha}\,\mathrm{tr}(D_{AB})\,\mathrm{tr}(D_{CD})\\ & +8(j_2(\alpha) sD_{AB}s\,\mathrm{tr}(D_{CD}) + j_2(\alpha) sD_{CD}s\,\mathrm{tr}(D_{AB})).\end{aligned} \quad (229)$$

This calculation can be found in the Appendix 5.

The other contributions $I^{(4)}$, $I^{(6)}$, $I^{(8)}$ can be computed analogously.

5 Conclusions

In this thesis, we have investigated the observational signatures of primordial non-Gaussian stochastic gravitational-wave backgrounds in the correlators of Pulsar Timing Arrays and ground-based interferometers.

After reviewing the theoretical framework for gravitational waves and stochastic gravitational-wave backgrounds, we illustrated in detail the two point correlation functions for both classes of detectors.
Specifically, for PTAs we derived the Hellings-Downs curve and showed its main characteristics. We then focused on studying its variance and understanding its statistical meaning.
For ground-based interferometers, we instead computed the two-point correlation function between detector pairs.

Building on this foundation, we presented our original results.
We started by briefly introducing the theoretical scenario considered for generating a non-Gaussian background, paying close attention to the physical characteristics relevant for our analysis.
In particular, these physical ingredients provided assumptions underlying the performed calculations throughout this work.
At this point, we demonstrated that the non-gaussianity of the signal (mathematically represented by the connected part of the trispectrum) gives a non-null contribution to the variance of the Hellings–Downs curve, highlighting how higher-order statistics modify the expected fluctuations around the standard Gaussian prediction.
We point out that along these calculations, we had to select a representative subset of configurations out of all the possible ones. This choice was motivated by computational tractability and by the fact that the chosen configurations capture the physical contributions relevant for our purpose.
In the context of ground-based interferometers, we showed an alternative computation for the two-point correlation function and extended the analysis to the four-point correlator for four distinct detectors, providing a computation of this quantity in the presence of a non-Gaussian background.
We notice that we have not explicitly computed all the contributions to the four-point correlation function since the other terms can be obtained in a very similar way.

Our results demonstrate that non-Gaussian features of primordial SGWBs leave measurable signatures in detector correlators.

Moreover, we have shown that the cross-correlation framework can be extended beyond the Gaussian paradigm to probe early-Universe physics.

Our analysis can be extended in several ways.
A natural next step would be to completely evaluate the connected contribution to the variance of the Hellings-Downs curve by taking into account all the possible configurations.
Furthermore, on the interferometer side, a full numerical study of the four-point function and its detectability with next-generation detectors represents a compelling prospect for future work.
Finally, it would also be interesting to extend this analysis to other specific cosmological scenarios, take into account realistic detector noise and, as we have said, assess more in detail the detectability of these signatures with current and forthcoming experiments.

The study of higher-order statistics thus represents a promising direction for extracting new physical information on our Universe from the emerging multi-frequency gravitational-wave landscape.

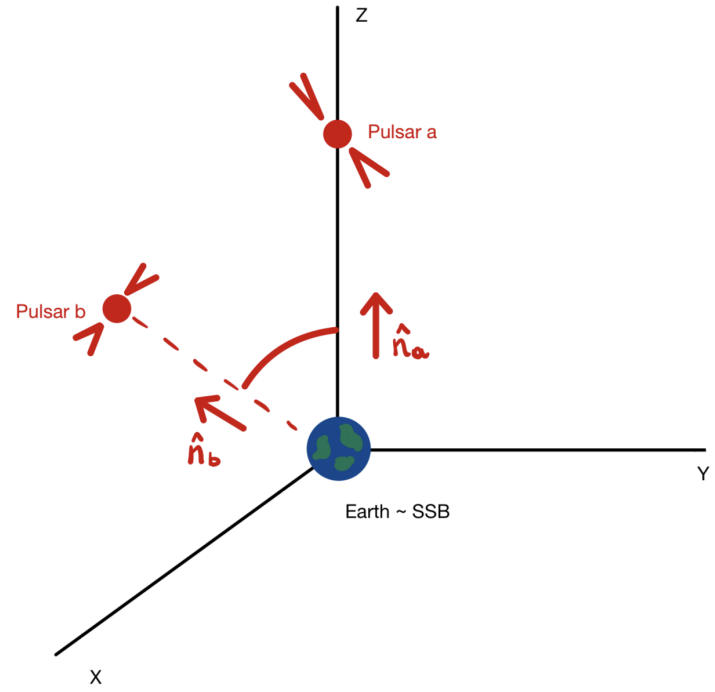

Figure 13: System considered to derive Hellings-Downs curve.

Appendix

Hellings-Downs computation

In this Appendix we want to show the explicit computation to obtain the Hellings-Downs curve. We closely follow [61].
Let us consider the system shown in figure 13, where the two pulsars are located in directions $\hat{\mathbf{n}}_a = \hat{\mathbf{z}}$ and $\hat{\mathbf{n}}_b = \sin\zeta\hat{\mathbf{x}} + \cos\zeta\hat{\mathbf{z}}$.

Considering $\hat{\mathbf{n}}$ given by 17, we have that:

$$\begin{aligned} \hat{\mathbf{n}} \cdot \hat{\mathbf{n}}_a &= \cos\theta\,, \\ \hat{\mathbf{n}} \cdot \hat{\mathbf{n}}_b &= \cos\zeta\cos\theta + \sin\zeta\sin\theta\cos\phi\,. \end{aligned} \tag{230}$$

By considering $F^P_{a/b}(\hat{\mathbf{n}})$ given by (103), we can rewrite equation (110):

$$C(\zeta) = \int \frac{d^2\hat{\mathbf{n}}}{4\pi} \sum_{P=+,\times} \frac{1}{2}\left(\frac{\hat{\mathbf{n}}_a \otimes \hat{\mathbf{n}}_a}{1+\hat{\mathbf{n}}\cdot\hat{\mathbf{n}}_a}\right) : \hat{\mathbf{e}}^P(\hat{\mathbf{n}})\, \frac{1}{2}\left(\frac{\hat{\mathbf{n}}_b \otimes \hat{\mathbf{n}}_b}{1+\hat{\mathbf{n}}\cdot\hat{\mathbf{n}}_b}\right) : \hat{\mathbf{e}}^P(\hat{\mathbf{n}}), \tag{231}$$

where

$$\hat{\mathbf{n}}_I \otimes \hat{\mathbf{n}}_I : \hat{\mathbf{e}}_P(\hat{\mathbf{n}}) \equiv \sum_{i=1}^{3}\sum_{j=1}^{3} n_I^i n_I^j \, e_{ij}^P(\hat{\mathbf{n}}) \,, \quad I = \{a, b\}. \tag{232}$$

Using the definition given by equation (18) for the gravitational-wave polarization tensors, we can obtain the following relations:

$$\begin{aligned}
\hat{\mathbf{n}}_a \otimes \hat{\mathbf{n}}_a : \hat{\mathbf{e}}^+(\hat{\mathbf{n}}) &= \sum_{i=1}^{3}\sum_{j=1}^{3} n_a^i n_a^j \, e_{ij}^+(\hat{\mathbf{n}}) = e_{33}^+(\hat{\mathbf{n}}) = \sin^2\theta \,, \\
\hat{\mathbf{n}}_a \otimes \hat{\mathbf{n}}_a : \hat{\mathbf{e}}^\times(\hat{\mathbf{n}}) &= \sum_{i=1}^{3}\sum_{j=1}^{3} n_a^i n_a^j \, e_{ij}^\times(\hat{\mathbf{n}}) = e_{33}^\times = 0 \,, \\
\hat{\mathbf{n}}_b \otimes \hat{\mathbf{n}}_b : \hat{\mathbf{e}}^+(\hat{\mathbf{n}}) &= \sum_{i=1}^{3}\sum_{j=1}^{3} n_b^i n_b^j \, e_{ij}^+(\hat{\mathbf{n}}) = (\sin\zeta\cos\theta\cos\phi - \cos\zeta\sin\theta)^2 - \sin^2\zeta\sin^2\phi \,, \\
\hat{\mathbf{n}}_b \otimes \hat{\mathbf{n}}_b : \hat{\mathbf{e}}^\times(\hat{\mathbf{n}}) &= \sum_{i=1}^{3}\sum_{j=1}^{3} n_b^i n_b^j \, e_{ij}^\times(\hat{\mathbf{n}}) = -2(\sin\zeta\cos\theta\cos\phi - \cos\zeta\sin\theta)\sin\zeta\sin\phi \,.
\end{aligned} \tag{233}$$

From here, we can now compute equation 231 by evaluating the following quantities:

$$\begin{aligned}
F_a^+(\hat{\mathbf{n}}) &= \frac{1}{2}\frac{\sin^2\theta}{1+\cos\theta} = \frac{1}{2}(1-\cos\theta), \\
F_a^\times(\hat{\mathbf{n}}) &= 0, \\
F_b^+(\hat{\mathbf{n}}) &= \frac{1}{2}\left[\frac{-\sin^2\zeta\sin^2\phi + (\sin\zeta\cos\theta\cos\phi - \cos\zeta\sin\theta)^2}{1+\cos\zeta\cos\theta+\sin\zeta\sin\theta\cos\phi}\right] = \\
&= \frac{1}{2}\left[\frac{1-(\cos\zeta\cos\theta+\sin\zeta\sin\theta\cos\phi)^2 - 2\sin^2\zeta\sin^2\phi}{1+\cos\zeta\cos\theta+\sin\zeta\sin\theta\cos\phi}\right] \\
&= \frac{1}{2}\left[(1-\cos\zeta\cos\theta-\sin\zeta\sin\theta\cos\phi) - \frac{2\sin^2\zeta\sin^2\phi}{1+\cos\zeta\cos\theta+\sin\zeta\sin\theta\cos\phi}\right], \\
F_b^\times(\hat{\mathbf{n}}) &= -\frac{1}{2}\left[\frac{\sin^2\zeta\cos\theta\sin 2\phi - \sin 2\zeta\sin\theta\sin\phi}{1+\cos\zeta\cos\theta+\sin\zeta\sin\theta\cos\phi}\right].
\end{aligned} \tag{234}$$

At this point, the Hellings-Downs function can be simplified to:

$$C(\zeta) = \int \frac{d^2\hat{\mathbf{n}}}{4\pi} F_a^+(\hat{\mathbf{n}}) F_b^+(\hat{\mathbf{n}}) = \frac{1}{8\pi}\int_{-1}^{1} \mathrm{d}x \, (1-x) I(x,\zeta), \tag{235}$$

where $x = \cos\theta$ and

$$\begin{aligned} I(x,\zeta) \equiv & \int_0^{2\pi} \mathrm{d}\phi \, F_b^+(\hat{\mathbf{n}}) = \\ = & \frac{1}{2}\int_0^{2\pi} \mathrm{d}\phi \, \left[(1 - x\cos\zeta - \sqrt{1-x^2}\sin\zeta\cos\phi) - \frac{2\sin^2\zeta\sin^2\phi}{1 + x\cos\zeta + \sqrt{1-x^2}\sin\zeta\cos\phi}\right] \\ \equiv & \frac{1}{2}\left[I_1 - I_2\right]. \end{aligned} \tag{236}$$

I_1 can be computed easily and it gives:

$$I_1 = \pi(1 - x\cos\zeta). \tag{237}$$

I_2 can be instead evaluated using contour integration. By considering $z = e^{i\phi}$, then $\cos\phi = \frac{1}{2}(z + z^{-1})$ and

$$\begin{aligned} I_2(x,\zeta) \equiv & -\sin^2\zeta \int_0^{2\pi} \mathrm{d}\phi \, \frac{\sin^2\phi}{1 + x\cos\zeta + \sqrt{1-x^2}\sin\zeta\cos\phi} \\ = & -\sin^2\zeta \oint_C \mathrm{d}z \, f(z)\,, \end{aligned} \tag{238}$$

where

$$\begin{aligned} f(z) = & \frac{1 - (z - z^{-1})^2/4}{[(1 + x\cos\zeta) + \sqrt{1-x^2}/2\sin\zeta(z + 1/z)]iz} \\ = & \frac{i(z^2-1)^2}{z^2\left[4z(1 + x\cos\zeta) + 2\sqrt{1-x^2}\sin\zeta(z^2+1)\right]} \end{aligned} \tag{239}$$

and C is the unit circle in the complex z-plane.

From here, we focus on the denominator of $f(z)$. This can be factorized using:

$$\begin{aligned} & 4z(1 + x\cos\zeta) + 2\sqrt{1-x^2}\sin\zeta(z^2+1) \\ & \qquad = 2\sqrt{1-x^2}\sin\zeta(z - z_+)(z - z_-)\,, \end{aligned} \tag{240}$$

where

$$z_+ \equiv -\sqrt{\left(\frac{1 \mp \cos\zeta}{1 \pm \cos\zeta}\right)\left(\frac{1 \mp x}{1 \pm x}\right)}, \quad z_- \equiv \frac{1}{z_+}\,. \tag{241}$$

In the above expression, the top signs correspond to the region $-\cos\zeta \le x \le 1$ and the bottom signs to the region $-1 \le x \le -\cos\zeta$.

For both of these regions, z_+ is inside the unit circle C (i.e., $|z_+| \le 1$), while z_- doesn't.

This means that z_+ contributes to the contour integral, while z_- doesn't.
In addition, $z = 0$ lies inside the unit circle and contributes to the contour integral as a pole of order two.

At this point we use the residue theorem,

$$\oint_C f(z)\,\mathrm{d}z = 2\pi i \sum_i \mathrm{Res}(f, z_i) \tag{242}$$

with

$$\begin{aligned}
&\mathrm{Res}(f, z_+) = \lim_{z\to z_+} \{(z - z_+)f(z)\} = \frac{i(z_+ - z_-)}{2\sqrt{1-x^2}\sin\zeta}\,,\\
&\mathrm{Res}(f, 0) = \lim_{z\to 0} \left\{ \frac{d}{dz}\left[z^2 f(z)\right] \right\} =\\
&= \lim_{z\to 0} -\frac{i(z^2-1)^2 2\sqrt{1-x^2}\sin\zeta(2z - z_- - z_+)}{4(1-x^2)\sin^2\zeta(z-z_+)^2(z-z_-)^2} =\\
&= \frac{i(z_+ + z_-)}{2\sqrt{1-x^2}\sin\zeta}.
\end{aligned} \tag{243}$$

Therefore,

$$\oint_C f(z)\,\mathrm{d}z = \frac{2\pi}{(1\pm x)(1\pm\cos\zeta)}\,. \tag{244}$$

Finally, we get that

$$\begin{aligned}
I(x,\zeta) =& I_1 + I_2 = \pi(1 - x\cos\zeta) - 2\pi\frac{\sin^2\zeta}{(1\pm x)(1\pm\cos\zeta)} =\\
=& \pi(1 - x\cos\zeta) - 2\pi\frac{(1\mp\cos\zeta)}{(1\pm x)}\,.
\end{aligned} \tag{245}$$

We now need to evaluate the integral over x to obtain $C(\zeta)$. In order to do so, we need to remember that the integral over x must be split into two regions (the one where $-\cos\zeta \le x \le 1$ and the one where $-1 \le x \le -\cos\zeta$), since the function to be integrated is different based on the considered region.

We finally obtain that:

$$
\begin{aligned}
C(\zeta) =& \frac{1}{8}\Bigg\{ \int_{-1}^{1} \mathrm{d}x\,(1-x)(1-x\cos\zeta) - 2\int_{-1}^{-\cos\zeta} \mathrm{d}x\,(1+\cos\zeta) + \\
& - 2\int_{-\cos\zeta}^{1} \mathrm{d}x\,\frac{(1-x)}{(1+x)}(1-\cos\zeta)\Bigg\} = \\
=& \frac{1}{8}\Bigg\{ 2 + \frac{2}{3}\cos\zeta - 2(1+\cos\zeta)(1-\cos\zeta) + \\
& - 2(1-\cos\zeta)\left[2\ln\left(\frac{2}{1-\cos\zeta}\right) - (1+\cos\zeta)\right]\Bigg\} \\
=& \frac{1}{3} - \frac{1}{6}\left(\frac{1-\cos\zeta}{2}\right) + \left(\frac{1-\cos\zeta}{2}\right)\ln\left(\frac{1-\cos\zeta}{2}\right) .
\end{aligned}
\tag{246}
$$

$I^{(2)}$ computation

We want to compute the integral for I^2 given by equation 238. This means that we want to solve:

$$I^{(2)} = \sum_{\ell=0}^{1} (-)^{\ell} \frac{(4\ell+1)}{4\pi} j_{(2\ell)}(\alpha) \int d^2n \, P_{(2\ell)}(\hat{\mathbf{n}} \cdot \hat{s}) \, G^{(2)}(\hat{\mathbf{n}}). \tag{247}$$

To compute this, we can see from 217 that this integral is related to:

$$\Gamma^{(2)}_{ABCD} = \frac{1}{4\pi} \int d^2\hat{\mathbf{n}} \left(G^{(2)}_{ABCD} \right) e^{i\alpha \, \hat{s}\cdot\hat{\mathbf{n}}}. \tag{248}$$

Therefore, we need to compute :

$$\Gamma^{(2)}_{ABCD} = -8\frac{1}{4\pi} \int d^2\hat{\mathbf{n}} \left(\hat{n} D_{AB} \hat{n} \ \mathrm{tr}(D_{CD}) + \hat{n} D_{CD} \hat{n} \ \mathrm{tr}(D_{AB}) \right) e^{i\alpha \, \hat{s}\cdot\hat{\mathbf{n}}}, \tag{249}$$

where we consider the abbreviation $\mathrm{tr}(D_{AB}) = \left(D^{ab}_A D^{ab}_B \right)$ and $\hat{n} D_{AB} \hat{n} = \hat{n}_a \hat{n}_c D^{ab}_A D^{bc}_B$.

At this point, we know how to compute these kind of integrals. In fact, these are clearly related to the ones that we have computed in section 4.5.1.
In particular, this kind of integral can be derived considering equations 202 and 203. At this point, keeping the previous results in mind, we can write:

$$\begin{aligned} I^{(2)} =& -8 \left[\frac{j_1(\alpha)}{\alpha} \ \mathrm{tr}(D_{AB}) \ \mathrm{tr}(D_{CD}) - j_2(\alpha) s D_{AB} s \ \mathrm{tr}(D_{CD}) \right] \\ & -8 \left[\frac{j_1(\alpha)}{\alpha} \ \mathrm{tr}(D_{AB}) \ \mathrm{tr}(D_{CD}) - j_2(\alpha) s D_{CD} s \ \mathrm{tr}(D_{AB}) \right] \\ =& -16 \frac{j_1(\alpha)}{\alpha} \ \mathrm{tr}(D_{AB}) \ \mathrm{tr}(D_{CD}) \\ & + 8 (j_2(\alpha) s D_{AB} s \ \mathrm{tr}(D_{CD}) + j_2(\alpha) s D_{CD} s \ \mathrm{tr}(D_{AB})), \end{aligned} \tag{250}$$

which is exactly what we have in equation 229.

6 Acknowledgements

I would like to sincerely thank my external supervisor, Prof. Gianmassimo Tasinato, for his constant support and guidance throughout this first experience in research. It has been truly inspiring to work with him and to freely discuss open questions in physics. I will always cherish the time I spent at Swansea University under his supervision, as part of a welcoming and collaborative research group.
I am also deeply grateful to my internal supervisor, Dr. Michele Lucente, for his guidance, encouragement and availability. His support has been fundamental throughout this work and I am sincerely thankful for his help and advice.
I would like to thank Prof. Silvia Pascoli for encouraging me to carry out this thesis at Swansea University.
I am also grateful for the dynamic and stimulating environment of the theoretical physics group at the University of Bologna.
Finally, I am profoundly thankful for the unwavering support I have received from my loved ones, both those I have known for many years and those with whom I have shared this Master's journey.
They have been my pillars throughout these wonderful and exciting years.

References

[1] B. P. Abbott et al. "Observation of Gravitational Waves from a Binary Black Hole Merger". In: *Physical Review Letters* 116.6 (Feb. 2016). ISSN: 1079-7114. DOI: 10.1103/physrevlett.116.061102. URL: http://dx.doi.org/10.1103/PhysRevLett.116.061102.

[2] Gabriella Agazie et al. "The NANOGrav 15 yr Data Set: Evidence for a Gravitational-wave Background". In: *The Astrophysical Journal Letters* 951.1 (June 2023), p. L8. ISSN: 2041-8213. DOI: 10.3847/2041-8213/acdac6. URL: http://dx.doi.org/10.3847/2041-8213/acdac6.

[3] PPTA Collaboration. "The Parkes Pulsar Timing Array Third Data Release". In: *Publications of the Astronomical Society of Australia* 40 (2023), e045. DOI: 10.1017/pasa.2023.30. arXiv: 2306.16215 [astro-ph.HE].

[4] J. Antoniadis et al. "The second data release from the European Pulsar Timing Array: III. Search for gravitational wave signals". In: *Astronomy amp; Astrophysics* 678 (Oct. 2023), A50. ISSN: 1432-0746. DOI: 10.1051/0004-6361/202346844. URL: http://dx.doi.org/10.1051/0004-6361/202346844.

[5] H. Xu and et al. "Searching for the nano-Hertz stochastic gravitational wave background with the Chinese Pulsar Timing Array Data Release I". In: *Research in Astronomy and Astrophysics* 23.7 (2023), p. 075024. DOI: 10.1088/1674-4527/acdfa5. arXiv: 2306.16216 [astro-ph.HE].

[6] Joseph D. Romano and Neil. J. Cornish. "Detection methods for stochastic gravitational-wave backgrounds: a unified treatment". In: *Living Reviews in Relativity* 20.1 (Apr. 2017). ISSN: 1433-8351. DOI: 10.1007/s41114-017-0004-1. URL: http://dx.doi.org/10.1007/s41114-017-0004-1.

[7] Tania Regimbau. "The astrophysical gravitational wave stochastic background". In: *Research in Astronomy and Astrophysics* 11.4 (Mar. 2011), pp. 369–390. ISSN: 1674-4527. DOI: 10.1088/1674-4527/11/4/001. URL: http://dx.doi.org/10.1088/1674-4527/11/4/001.

[8] Chiara Caprini and Daniel G Figueroa. "Cosmological backgrounds of gravitational waves". In: *Classical and Quantum Gravity* 35.16 (July 2018), p. 163001. ISSN: 1361-6382. DOI: 10.1088/1361-6382/aac608. URL: http://dx.doi.org/10.1088/1361-6382/aac608.

[9] Michele Maggiore. "Gravitational wave experiments and early universe cosmology". In: *Physics Reports* 331.6 (July 2000), pp. 283–367. ISSN: 0370-1573. DOI: 10.1016/s0370-1573(99)00102-7. URL: http://dx.doi.org/10.1016/S0370-1573(99)00102-7.

[10] Bruce Allen. *The stochastic gravity-wave background: sources and detection*. 1996. arXiv: gr-qc/9604033 [gr-qc]. URL: https://arxiv.org/abs/gr-qc/9604033.

[11] Peter Adshead and Eugene A. Lim. "Three-point statistics of cosmological stochastic gravitational waves". In: *Physical Review D* 82.2 (July 2010). ISSN: 1550-2368. DOI: 10.1103/physrevd.82.024023. URL: http://dx.doi.org/10.1103/PhysRevD.82.024023.

[12] Ogan Özsoy and Gianmassimo Tasinato. "Inflation and Primordial Black Holes". In: *Universe* 9.5 (Apr. 2023), p. 203. ISSN: 2218-1997. DOI: 10.3390/universe9050203. URL: http://dx.doi.org/10.3390/universe9050203.

[13] Ruth Durrer and Andrii Neronov. "Cosmological magnetic fields: their generation, evolution and observation". In: *The Astronomy and Astrophysics Review* 21.1 (June 2013). ISSN: 1432-0754. DOI: 10.1007/s00159-013-0062-7. URL: http://dx.doi.org/10.1007/s00159-013-0062-7.

[14] Marco Fabbrichesi, Emidio Gabrielli, and Gaia Lanfranchi. *The Physics of the Dark Photon: A Primer*. Springer International Publishing, 2021. ISBN: 9783030625191. DOI: 10.1007/978-3-030-62519-1. URL: http://dx.doi.org/10.1007/978-3-030-62519-1.

[15] Guillem Domenech. "Scalar Induced Gravitational Waves Review". In: *Universe* 7.11 (Oct. 2021), p. 398. ISSN: 2218-1997. DOI: 10.3390/universe7110398. URL: http://dx.doi.org/10.3390/universe7110398.

[16] Jonas El Gammal et al. *Reconstructing Primordial Curvature Perturbations via Scalar-Induced Gravitational Waves with LISA*. 2025. arXiv: 2501.11320 [astro-ph.CO]. URL: https://arxiv.org/abs/2501.11320.

[17] Stephen R. Taylor. *The Nanohertz Gravitational Wave Astronomer*. 2021. arXiv: 2105.13270 [astro-ph.HE]. URL: https://arxiv.org/abs/2105.13270.

[18] Michele Maggiore. *Gravitational Waves. Volume 1: Theory and Experiments*. Oxford University Press, 2007. ISBN: 9780198570745. DOI: 10.1093/acprof:oso/9780198570745.001.0001.

[19] A. Einstein. "Näherungsweise Integration der Feldgleichungen der Gravitation". In: *Sitzungsberichte der Königlich Preußischen Akademie der Wissenschaften (Berlin)* (1916), pp. 688–696.

[20] A. Einstein. "Über Gravitationswellen". In: *Sitzungsberichte der Königlich Preußischen Akademie der Wissenschaften (Berlin)* (1918), pp. 154–167.

[21] R. A. Hulse and J. H. Taylor. "Discovery of a Pulsar in a Binary System". In: *Astrophysical Journal Letters* 195 (1975), pp. L51–L53.

[22] Sean M. Carroll. *Spacetime and Geometry: An Introduction to General Relativity*. Addison Wesley, 2004.

[23] Bernard F. Schutz. *A First Course in General Relativity*. 2nd ed. Cambridge University Press, 2009.

[24] Charles W. Misner, Kip S. Thorne, and John A. Wheeler. *Gravitation*. W. H. Freeman, 1973.

[25] Nigel T. Bishop and Luciano Rezzolla. "Extraction of gravitational waves in numerical relativity". In: *Living Reviews in Relativity* 19.1 (Oct. 2016). ISSN: 1433-8351. DOI: 10.1007/s41114-016-0001-9. URL: http://dx.doi.org/10.1007/s41114-016-0001-9.

[26] B. S. Sathyaprakash and Bernard F. Schutz. "Physics, Astrophysics and Cosmology with Gravitational Waves". In: *Living Reviews in Relativity* 12 (2009), p. 2.

[27] R. A. Isaacson. "Gravitational Radiation in the Limit of High Frequency. I. The Linear Approximation and Geometrical Optics". In: *Physical Review* 166 (1968), p. 1263.

[28] R. A. Isaacson. "Gravitational Radiation in the Limit of High Frequency. II. Nonlinear Terms and the Effective Stress Tensor". In: *Physical Review* 166 (1968), p. 1272.

[29] A. A. Penzias and R. W. Wilson. "A Measurement of Excess Antenna Temperature at 4080 Mc/s". In: *The Astrophysical Journal* 142 (1965), pp. 419–421.

[30] R. H. Dicke, P. J. E. Peebles, P. G. Roll, and D. T. Wilkinson. "Cosmic Black-Body Radiation". In: *The Astrophysical Journal* 142 (1965), pp. 414–419.

[31] Planck Collaboration. "Planck 2018 results. I. Overview and the cosmological legacy of Planck". In: *Astronomy & Astrophysics* (2020).

[32] Bruce Allen and Joseph D. Romano. "Detecting a stochastic background of gravitational radiation: Signal processing strategies and sensitivities". In: *Physical Review D* 59.10 (Mar. 1999). ISSN: 1089-4918. DOI: 10.1103/physrevd.59.102001. URL: http://dx.doi.org/10.1103/PhysRevD.59.102001.

[33] A. Hewish, S. J. Bell, J. D. H. Pilkington, P. F. Scott, and R. A. Collins. "Observation of a Rapidly Pulsating Radio Source". In: *Nature* 217 (1968), pp. 709–713. DOI: 10.1038/217709a0.

[34] Zaven Arzoumanian et al. "The NANOGrav 12.5 yr Data Set: Search for an Isotropic Stochastic Gravitational-wave Background". In: *The Astrophysical Journal Letters* 905.2 (Dec. 2020), p. L34. ISSN: 2041-8213. DOI: 10.3847/2041-8213/abd401. URL: http://dx.doi.org/10.3847/2041-8213/abd401.

[35] R. M. Shannon et al. "Gravitational waves from binary supermassive black holes missing in pulsar observations". In: *Science* 349.6255 (Sept. 2015), pp. 1522–1525. ISSN: 1095-9203. DOI: 10.1126/science.aab1910. URL: http://dx.doi.org/10.1126/science.aab1910.

[36] L. Lentati et al. "European Pulsar Timing Array limits on an isotropic stochastic gravitational-wave background". In: *Monthly Notices of the Royal Astronomical Society* 453.3 (Aug. 2015), pp. 2577–2599. ISSN: 1365-2966. DOI: 10.1093/mnras/stv1538. URL: http://dx.doi.org/10.1093/mnras/stv1538.

[37] G Hobbs et al. "The International Pulsar Timing Array project: using pulsars as a gravitational wave detector". In: *Classical and Quantum Gravity* 27.8 (Apr. 2010), p. 084013. ISSN: 1361-6382. DOI: 10.1088/0264-9381/27/8/084013. URL: http://dx.doi.org/10.1088/0264-9381/27/8/084013.

[38] Michele Maggiore. *Gravitational Waves. Vol. 2: Astrophysics and Cosmology.* Oxford University Press, Mar. 2018. ISBN: 978-0-19-857089-9.

[39] Bruce Allen. "Variance of the Hellings-Downs correlation". In: *Physical Review D* 107.4 (Feb. 2023). ISSN: 2470-0029. DOI: 10.1103/physrevd.107.043018. URL: http://dx.doi.org/10.1103/PhysRevD.107.043018.

[40] J D Romano and B Allen. "Answers to frequently asked questions about the pulsar timing array Hellings and Downs curve". In: *Classical and Quantum Gravity* 41.17 (July 2024), p. 175008. ISSN: 1361-6382. DOI: 10.1088/1361-6382/ad4c4c. URL: http://dx.doi.org/10.1088/1361-6382/ad4c4c.

[41] R. W. Hellings and G. S. Downs. "Upper limits on the isotropic gravitational radiation background from pulsar timing analysis." In: 265 (Feb. 1983), pp. L39–L42. DOI: 10.1086/183954.

[42] Neil J Cornish and A Sesana. "Pulsar timing array analysis for black hole backgrounds". In: *Classical and Quantum Gravity* 30.22 (Nov. 2013), p. 224005. ISSN: 1361-6382. DOI: 10.1088/0264-9381/30/22/224005. URL: http://dx.doi.org/10.1088/0264-9381/30/22/224005.

[43] Reginald Christian Bernardo and Kin-Wang Ng. "Pulsar and cosmic variances of pulsar timing-array correlation measurements of the stochastic gravitational wave background". In: *Journal of Cosmology and Astroparticle Physics* 2022.11 (Nov. 2022), p. 046. ISSN: 1475-7516. DOI: 10.1088/1475-7516/2022/11/046. URL: http://dx.doi.org/10.1088/1475-7516/2022/11/046.

[44] Reginald Christian Bernardo and Kin-Wang Ng. "Stochastic gravitational wave background phenomenology in a pulsar timing array". In: *Physical Review D* 107.4 (Feb. 2023). ISSN: 2470-0029. DOI: 10.1103/physrevd.107.044007. URL: http://dx.doi.org/10.1103/PhysRevD.107.044007.

[45] KIN-WANG NG and GUO-CHIN LIU. "CORRELATION FUNCTIONS OF CMB ANISOTROPY AND POLARIZATION". In: *International Journal of Modern Physics D* 08.01 (Feb. 1999), pp. 61–83. ISSN: 1793-6594. DOI: 10.1142/s0218271899000079. URL: http://dx.doi.org/10.1142/S0218271899000079.

[46] J. et al. (LIGO Scientific Collaboration) Aasi. "Advanced LIGO". In: *Classical and Quantum Gravity* 32.7 (2015), p. 074001. DOI: 10.1088/0264-9381/32/7/074001.

[47] F. et al. (Virgo Collaboration) Acernese. "Advanced Virgo: a second-generation interferometric gravitational wave detector". In: *Classical and Quantum Gravity* 32.2 (2015), p. 024001. DOI: 10.1088/0264-9381/32/2/024001.

[48] Y. et al. Aso. "Interferometer design of the KAGRA gravitational wave detector". In: *Physical Review D* 88.4 (2013), p. 043007. DOI: 10.1103/PhysRevD.88.043007.

[49] H Lück and the GEO600 Team. "The GEO600 project". In: *Classical and Quantum Gravity* 14.6 (June 1997), p. 1471. DOI: 10.1088/0264-9381/14/6/012. URL: https://doi.org/10.1088/0264-9381/14/6/012.

[50] B. et al. Iyer. *LIGO-India: Proposal of the Consortium for Indian Initiative in Gravitational-wave Observations (IndIGO)*. LIGO-India Project Proposal. 2011.

[51] M. et al. Punturo. "The Einstein Telescope: a third-generation gravitational wave observatory". In: *Classical and Quantum Gravity* 27.19 (2010), p. 194002. DOI: 10.1088/0264-9381/27/19/194002.

[52] B. P. et al. Abbott. "Exploring the Sensitivity of Next Generation Gravitational Wave Detectors". In: *Classical and Quantum Gravity* 34.4 (2017), p. 044001. DOI: 10.1088/1361-6382/aa51f4.

[53] P. et al. Amaro-Seoane. "Laser Interferometer Space Antenna". In: *arXiv e-prints* (2017). arXiv: 1702.00786 [astro-ph.IM].

[54] Rana X. Adhikari. "Gravitational radiation detection with laser interferometry". In: *Reviews of Modern Physics* 86.1 (Feb. 2014), pp. 121–151. ISSN: 1539-0756. DOI: 10.1103/revmodphys.86.121. URL: http://dx.doi.org/10.1103/RevModPhys.86.121.

[55] N. M. Jiménez Cruz, Flavio C. Sánchez, and Gianmassimo Tasinato. *New test of modified gravity with gravitational wave experiments*. 2025. arXiv: 2509.08273 [gr-qc]. URL: https://arxiv.org/abs/2509.08273.

[56] Arko Bhaumik, Theodoros Papanikolaou, and Anish Ghoshal. *Vector induced Gravitational Waves sourced by Primordial Magnetic Fields*. 2025. arXiv: 2504.10477 [astro-ph.CO]. URL: https://arxiv.org/abs/2504.10477.

[57] Bill Atkins, Debika Chowdhury, Alisha Marriott-Best, and Gianmassimo Tasinato. *Inflationary magnetogenesis beyond slow-roll and its induced gravitational waves*. 2025. arXiv: 2507.01772 [astro-ph.CO]. URL: https://arxiv.org/abs/2507.01772.

[58] H. V. Ragavendra, Gianmassimo Tasinato, and L. Sriramkumar. *Chiral gravitational waves from multi-phase magnetogenesis*. 2026. arXiv: 2602.16575 [astro-ph.CO]. URL: https://arxiv.org/abs/2602.16575.

[59] Cari Powell and Gianmassimo Tasinato. "Probing a stationary non-Gaussian background of stochastic gravitational waves with pulsar timing arrays". In: *Journal of Cosmology and Astroparticle Physics* 2020.01 (Jan. 2020), pp. 017–017. ISSN: 1475-7516. DOI: 10.1088/1475-7516/2020/01/017. URL: http://dx.doi.org/10.1088/1475-7516/2020/01/017.

[60] Reginald Christian Bernardo and Kin-Wang Ng. "Charting the nanohertz gravitational wave sky with pulsar timing arrays". In: *International Journal of Modern Physics D* 34.04 (Feb. 2025). ISSN: 1793-6594. DOI: 10.1142/s0218271825400139. URL: http://dx.doi.org/10.1142/S0218271825400139.

[61] Fredrick A. Jenet and Joseph D. Romano. *Understanding the gravitational-wave Hellings and Downs curve for pulsar timing arrays in terms of sound and electromagnetic waves*. 2015. arXiv: 1412.1142 [gr-qc]. URL: https://arxiv.org/abs/1412.1142.